Durham E-Theses

Investigating Pattern Triggered Immunity in Arabidopsis thaliana Upon Botrytis cinerea Infection and the Role of SUMOylation in This Signalling Pathway

CONVEY, KATHERINE,ANNE

Investigating Pattern Triggered Immunity in *Arabidopsis thaliana* Upon *Botrytis cinerea* Infection and the Role of SUMOylation in This Signalling Pathway

Katherine Convey
Supervisor: Dr. Ari Sadanandom
Co-Supervisor: Dr. Elaine Fitches
Master of Research
Department of Biosciences, Durham University
Submitted: March 2023

Abstract

Fungal disease in agriculture poses a significant risk to global food security. The development of crops that are resistant to fungal infection is central to addressing this challenge. *Botrytis cinerea* is a pathogenic fungus that causes grey mould disease in over 200 crop species, causing mass economic and agricultural losses. During *B. cinerea* infection in *Arabidopsis thaliana*, chitin from the fungal cell wall is sensed by a transmembrane protein called CERK1. CERK1 transduces a signal to the rest of the cell to initiate pattern triggered immunity (PTI) defences against the invading fungal pathogen. SUMOylation is a type of post-translational modification that is involved in many types of stress response and has been shown to also play a role in immunity during fungal infection. The goal of this research project was to gain a deeper understanding of plant PTI and to shed light on the potential role of SUMOylation in this signalling pathway during *B. cinerea* infection. After discovering that CERK1 constructs that were to be used in this project contained unintended mutations, CERK1 was re-cloned and SUMO-site mutations were re-inserted. Using the new CERK1 wild type (CERK1^{WT}) and the CERK1 double SUMO-site mutant (CERK1^{2KR}) constructs in co-immunoprecipitation assays with SUMO1, it was determined that both CERK1^{WT} and CERK1^{2KR} are SUMOylated upon chitin elicitation. Using fungal spore infection assays, it was confirmed that CERK1 is an essential protein for plant immunity upon *B. cinerea* infection due to greater lesion development in the CERK1 knockout transgenic line than in wild type plants. It remains unclear whether SUMOylation of CERK1 is essential for initiating an immune response to *B. cinerea* infection, and this is a recommended route for further investigation into this research.

Table of Contents

List of Figures

List of Tables

List of Abbreviations

6xHis	6xhis affinity tag
aa	Amino acid
Amp R	Ampicillin resistance
APS	Ammonium persulfate
BIK1	Botrytis-induced kinase 1
BlpR	Phosphinothricin acetyltransferase
bom	Basis of mobility region
bp	Base pair
CaMV	*Cauliflower mosaic virus*
cDNA	Complementary DNA
CDS	Coding sequence
CERK1	Chitin elicitor receptor kinase1
CERK1^{KR}	CERK1 with 1 lysine to arginine SUMO-site mutation
CERK1^{2KR}	CERK1 with 2 lysine to arginine SUMO-site mutations
CERK1^{3KR}	CERK1 with 3 lysine to arginine SUMO-site mutations
cerk1-2 K/O	CERK1 knockout *Arabidopsis* line
cerk1-CM	CERK1^{WT} re-complemented *cerk1-2* K/O *Arabidopsis* line
cerk1-3KR	CERK1^{3KR} re-complemented *cerk1-2* K/O *Arabidopsis* line
CmR	Chloramphenicol acetyltransferase
Col-0	Columbia-0, wild type *Arabidopsis*
CTAB	Cetrimonium bromide
DeSI	DeSUMOylating isopeptidases
desi3a-1 K/O	DeSI knockout *Arabidopsis* line
dNTPs	Deoxyribonucleotide triphosphates
DPI	Days-post-infection or days-post-infiltration, depending on context
EDTA	Ethylenediaminetetraacetic acid
ETI	Effector triggered immunity
EYFP	Enhanced yellow fluorescent protein
FLS2	Flagellin-sensitive 2
gDNA	Genomic DNA
GFP	Green fluorescent protein
HA	Human Influenza Hemagglutinin epitope tag
HR	Hypertensive response
HRP	Horseradish peroxidase
IB	Immunoblot
IP	Immunoprecipitation

K/O	Knockout
Kan R	Kanamycin resistance
KCl	Potassium chloride
KH$_2$PO$_4$	Monopotassium phosphate
KR	Lysine to arginine
Lac	Lactose
LB	Left border
LB	Lysogeny broth
LYK5	Lysm-containing receptor-like kinase 5
LysM-RLK	Lysine motif-containing receptor-like kinase
MAPK	Mitogen-activated protein kinase
MAPKKK5	MAPK kinase kinase 5
MAS	Mannopine synthase
MCS	Multiple cloning site
MgCl$_2$	Magnesium chloride
mgfp5	Green fluorescent protein tag
NaCl	Sodium chloride
NB-LRR	Nucleotide-binding leucine-rich repeat
NEM	N-ethylmaleimide
NP-40	Nonyl phenoxypolyethoxylethanol
Ori	Origin of replication
OSC	Octopine synthase terminator
p103	pEarlyGate 103
p104	pEarlyGate 104
P201	pEarlyGate 201
PAMPs	Pathogen-associated molecular patterns
PCR	Polymerase chain reaction
PDA	Potato dextrose agar
PRRs	Pattern-recognition receptors
PTI	Pattern triggered immunity
PTM	Post-translational modification
PVDF	Polyvinylidene fluoride
PVPP	Polyvinylpolypyrrolidone
pVS1 oriV	Origin of Replication for *Pseudomonas* plasmid PVS1
pVS1 RepA	Replication Protein from *Pseudomonas* plasmid PVS1
pVS1 StaA	Stability Protein from *Pseudomonas* plasmid PVS1
qPCR	Quantitative polymerase chain reaction
R proteins	Resistance proteins

RB	Right border
RBOHD	Respiratory burst oxidase homologue protein d
RLCK	Receptor-like cytoplasmic kinase
ROS	Reactive oxygen species
SAE1	SUMO activating enzyme 1
SAE1	SUMO activating enzyme 2
SCE1	SUMO conjugating enzyme 1
SDS	Sodium dodecyl sulphate
SDS-PAGE	Sodium dodecyl sulphate polyacrylamide gel electrophoresis
SNPs	Single nucleotide polymorphisms
SUMO	Small ubiquitin-like modifier
TAE	Tris base, acetic acid
TAIR	The *Arabidopsis* information resource
TBST	Tris-buffered saline and Tween20
TEMED	Tetramethylethylenediamine
TMV	*Tobacco mosaic virus*
Tris	Trisaminomethane
ULP	Ubiquitin-like protease
WT	Wild type

Note: Capitalized and italicized refers to gene e.g., *CERK1*

Capitalized and not italicized refers to protein e.g., CERK1

Non-capitalized and italicized refers to transgenic *Arabidopsis* line e.g., *cerk1*

Statement of Copyright

Acknowledgements

I want to thank my supervisor Dr. Ari Sadanandom for his guidance and supervisory style that helped me develop into an independent scientist. My mentors Dr. Prakash Bhagat and Dr. Srayan Ghosh for their proofreading help, invaluable scientific input, and technical advice throughout my project. Navi Mukkawar and Ed Winstanley for their support, friendship and company on many Starbucks runs. I want to thank everyone in the Sadanandom Lab including Dr. Sumesh Kakkunnath, Catherine Gough, Lisa Clark, Dr. Dipan Roy and Dr. Cunjin Zhang for sharing knowledge, materials, advice and help throughout my research project. This lab group feels like a family, and I will miss our group lunches, Christmas dinners and laughter together in the lab. I also want to thank my advisory committee, Dr. Marc Knight and Dr. Peter Etchells for their continuous support and helpful advice. Thank you to my boyfriend Jack, my sister Alexandra, my mom Jennifer, and my dad Steve, for their proofreading help, unwavering support, and encouragement throughout this experience. A special thank you to my dad for inspiring my love of science.

1.0. Introduction

1.1. Background

Crop loss due to fungal infection poses a significant risk to global food security, and this threat will increase in prevalence and severity as climate fluctuations intensify and global food demand grows (Fisher et al. 2012). Crop epidemics caused by fungi have had devastating consequences throughout history, and the possibility of such catastrophes has not decreased over time. In fact, the threat of emerging fungal diseases is actually increasing due to expansion of global trade, transportation logistics and global warming (Fisher et al. 2012). Fungal diseases destroy a third of all food crops each year, causing vast economic loss and contributing to global poverty (Fisher et al. 2012; Stop neglecting fungi 2017; Fausto et al. 2019). The most economically-damaging fungi infect a broad range of host crops, including some of the most important caloric crops globally (Fausto et al. 2019). They are as follows: *Magnaporthe oryzae*, which infects rice and wheat, *Botrytis cinerea*, which infects a broad host range of crops, and *Puccinia spp*, which infects wheat (Shah et al. 2012; Fausto et al. 2019). Since these crops contribute to most of the world's caloric intake, mitigating crop loss caused by these fungi will be essential as the population continues to rise (Fones et al. 2020). Additionally, climate change is predicted to alter the emergence and geographical distribution of pathogenic fungal diseases. Factors such as higher minimum temperature and increased variability in rainfall patterns will likely cause shifts in distribution and diversity of pathogens in a given region, leading to novel threats in that area (Launay et al. 2014). Host crop availability, meaning what crops can be grown where, will also change with a changing climate and this will

have downstream consequences for fungal infection as new host plants become available (Fones et al. 2020). Finally, the trend towards simplification of large-scale agriculture by means of increased field size, decreased crop diversity, and heavy reliance on fewer cereal and oil crops increases susceptibility to disease and poses a significant threat to food security (Fones et al. 2020).

1.2. *Botrytis cinerea*

1.2.1. Lifecycle and Infection

Botrytis cinerea is one of the most prevalent and devastating pathogenic fungi affecting crop species. It infects various tissues in over 200 species including fruits, vegetables, protein, oil, and fibre crops pre- and postharvest, causing annual threats to food security and serious financial loss worldwide (WILLIAMSON et al. 2007; Shah et al. 2012; Sarven et al. 2020; Shao et al. 2021). *B. cinerea* belongs to the *Sclerotiniaceae* family of the class Leotiomycetes (Cheung et al. 2020). Also called grey mould, *B. cinerea* is a necrotrophic fungus, meaning it kills host cells shortly after infection and acquires nutrients from the dead or dying tissue (Shao et al. 2021). Unlike other species in the genus *Botrytis,* which are restricted to infecting a single or small range of hosts, *B. cinerea* is a generalist and can infect and cause grey mould diseases in many species of dicotyledons and some monocotyledons (Cheung et al. 2020). It has a strong tendency to evolve fungicide resistance, uses multiple avenues of infection and has a high reproductive output, therefore making it a highly successfully pathogen (Cheung et al. 2020). The life cycle of *B. cinerea* is primarily asexual, with major routes of transmission being conidia spores from mature conidiophores, as well as mycelia from sclerotia, and infected tissues and

seeds. *B. cinerea* can also undergo a heterothallic sexual cycle, where fertilization of sclerotia with microconidia from an opposite mating type (also called spermatia) forms apothecia, which then produce ascospores. The sexual cycle is predicted to contribute to genetic variation of *B. cinerea*, but it occurs very rarely in nature (WILLIAMSON et al. 2007; Cheung et al. 2020). During the asexual cycle, infection of host plants occurs at damaged tissues or natural openings usually in floral organs of fruiting plants. Conidia production allows the fungus to spread quickly, often using stigmatic fluid as a nutrient and adhesive for airborne conidia to germinate and develop hyphae. Mycelia then grow along the pollen grain pathway and can enter the carpel and ovaries (McNICOL et al. 1985). During this phase, *B. cinerea* exists briefly as a biotroph, but eventually enters an aggressive necrotrophic phase during fruit maturity. This is likely triggered by increased levels of volatile organic compounds, sugar, and nitrogen in ripening fruit tissue (Neri et al. 2015). During the necrotrophic phase, mycelia undergo rapid growth that can be seen on the plant surface as grey conidia masses. Virulence factors including oxalic acid, cell wall degrading enzymes and analogues of plant hormones are secreted to disrupt the plant's metabolism, cell structure and immune system. Virulence factors cause fruit decay and produce symptoms such as softening flesh and brown, leathery skin (Xiao 2006; Cheung et al. 2020). After the tissue is dead, *B. cinerea* continues to grow saprophytically (absorbing nutrients from the dead tissue) in the form of mycelia and sclerotia. Sclerotia are small hardened mycelia and have a melanized surface, β-glucan matrix and nutrient reserves which allow them to remain viable in soil for up to a year, resistant to environmental stress (Figure 1.1, Araújo et al. 2005; Cheung et al. 2020).
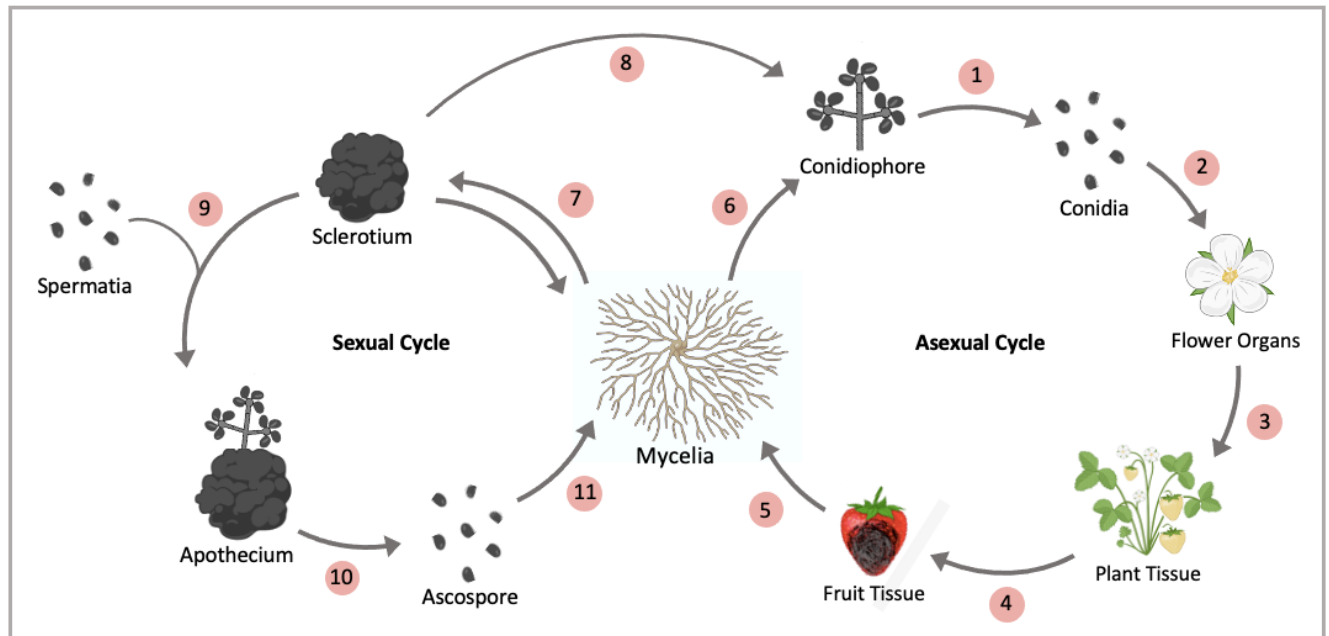
Figure 1.1. *Botrytis cinerea* life cycle. **(1)** During the asexual cycle, mature conidiophores produce conidia which disperse into the environment and act as a primary route of transmission. **(2)** Conidia primarily enter the plant through damaged tissue or natural opening in floral organs. Stigmatic fluid is used as an adhesive and nutrient source for airborne conidia to germinate and develop hyphae. **(3)** Infection is established, and mycelia grow biotrophically to other tissues in plant. **(4)** Necrotrophic phase commences during fruit maturity and mycelia growth can be seen on fruit surface. Virulence factors are excreted from the fungus and cause fruit tissue to decay. **(5)** Mycelia continue to grow saprophytically on dead tissue. **(6)** Mycelia can produce new conidiophores to disperse conidia to new plants/regions. **(7)** Mycelia can condense into small, hardened sclerotium which can last in soil for up to a year. **(8)** Sclerotium can produce conidiophores for another cycle of infection when environmental conditions are suitable. **(9)** During the sexual cycle, sclerotium are fertilized by spermatia, which are conidia from an opposite mating type. **(10)** Fertilized sclerotium form apothecium which produce ascospores. **(11)** Dispersal of ascospores into the environment to find new plant hosts and begin asexual cycle. Figure generated by author using PowerPoint, using Cheung et al. 2020 as reference.

1.2.2. Disease Management

Currently, the most abundantly used disease management approach for *B. cinerea* and

other necrotrophic fungi is single-target chemical fungicide application. This method is costly,

causes environmental pollution, disrupts ecosystems, and poses risks to human health (Sarven

et al. 2020). Excessive use of fungicides also provokes the evolution of new resistant

populations, and there is evidence that *B. cinerea* has already developed resistance to many

widely used fungicides (Fones et al. 2020; Sarven et al. 2020; Shao et al. 2021). Another

method of disease management is breeding single plant resistance genes into cultivars. This is a slow process, taking 10-20 years from initial discovery of a resistance marker to the release of a new cultivar. The use of single resistance genes in monoculture crops also promotes the evolution of resistant pathogen populations able to overcome plant resistance (Fones et al. 2020). Biological control using antagonistic yeasts has been used to prevent grey mould post-harvest, however the effectiveness of this method is inconsistent. Finally, cultural control by removing excess leaves and shoots can work to reduce the spread of infection, however this practice is unrealistic for commercial farming (Cheung et al. 2020). A more efficient and desirable approach to disease management is the production of genetically resistant crop species through transgene cloning or gene editing, as it is much faster and there is more opportunity to manipulate multiple plant resistance pathways and "stack" plant resistance genes (Fones et al. 2020). This requires a thorough understanding of infection mechanisms and molecular interactions between the pathogen and host. Knowledge of plant targets and immune signalling proteins is essential, as these will be the target of genetic manipulation for production of disease-resistant crops.

1.3. The Plant Immune System

Plants have evolved a sophisticated immune system consisting of two lines of defence to combat infection and disease. The first line of defence is called pattern-triggered immunity (PTI) and the second line is called effector-triggered immunity (ETI) (Petutschnig et al. 2014; Yamada et al. 2016). During PTI, the plant recognizes specific molecules secreted from an invading organism called pathogen-associated molecular patterns (PAMPs). PAMPs are highly

conserved and essential to the life of each pathogen. Examples of these materials excreted

from bacteria include flagellin, peptidoglycan and lipopeptides. Examples of PAMP molecules

excreted from fungi are chitin, chitosan, and ß-glucan (Desaki et al. 2018). Plants use pattern-

recognition receptors (PRRs), which are transmembrane proteins located on the plasma

membrane, to recognize exterior PAMPs and trigger PTI within the cell. PTI responses consist

of increased cytosolic Ca^{2+} levels, ion fluxes, production of reactive oxygen species (ROS),

callose deposition in the cell wall, mitogen-activated protein kinase (MAPK) signalling cascades

and expression of immune-related genes (Crabill et al. 2010; Bi et al. 2018; Wang et al. 2021;

Yamaguchi and Kawasaki 2021). These immune responses aim to prevent the establishment of

the pathogen within the plant cell. Pathogens have co-evolved to combat and overcome plant

PTI using effector molecules. Effector molecules target and inhibit plant PRR proteins and

downstream immune signalling proteins to ultimately suppress PTI (Yamada et al. 2016). As a

second line of defence, plants can initiate ETI by sensing effector proteins using disease

resistance proteins (R proteins). R proteins are part of the nucleotide-binding leucine-rich

repeat (NB-LRR) protein family, and after sensing effector proteins, activate an accelerated and

amplified PTI response, resulting in disease resistance and programmed cell-death at the

infection site called the hypersensitive response (HR) (Crabill et al. 2010; Yamada et al. 2016).

Natural selection drives pathogens to evolve new effector proteins which in turn drives plants

to evolve R proteins to defend against these new effectors. This is described as the molecular

arms race, and it helps explain the multitude of different effector and R proteins present in

plant and pathogen species (Jones and Dangl 2006).

1.3.1. *Arabidopsis* PTI Response During Fungal Infection

Chitin, a main component of the fungal cell wall, is the main PAMP molecule active during a fungal infection. It is recognized by and binds to a cell surface PRR, which is a lysine motif-containing receptor-like kinase (LysM-RLK). This is a specialized protein able to elicit an immune signal in response to the PAMP (Desaki et al. 2018). LysM-RLKs have 3 distinct domains: an extracellular domain with a lysine motif, allowing it to sense and bind the PAMP, a transmembrane domain, and an intracellular kinase domain, allowing signal transduction via phosphorylation of downstream proteins (Miya et al. 2007). In *Arabidopsis*, two LysM-RLK proteins called CHITIN ELICITOR RECEPTOR KINASE 1 (CERK1) and LYSM-CONTAINING RECEPTOR-LIKE KINASE 5 (LYK5) are ubiquitously expressed in the plant and work together to sense chitin. Chitin fragments initially bind to the lysM region of LYK5 and CERK1 dimers, which then form a complex to initiate the immune response (Cao et al. 2014). Following activation by chitin, CERK1 phosphorylates a protein called PBL27, which is a downstream receptor-like cytoplasmic kinase (RLCK) protein. PBL27 initiates MAPK signalling by phosphorylating MAPK kinase kinase 5 (MAPKKK5) which in turn activates MAPK kinase 4/5 and MAPK 3/6 (Shinya et al. 2014; Yamada et al. 2016; Liu et al. 2018). Eventually, the MAPK signalling cascade activates transcription factors responsible for inducing the expression of defence-related genes (Wan et al. 2008b). WRKY transcription factors are among the over 100 transcription factors found to be responsive to chitin and have been previously implicated in plant defence. These transcription factors change the expression of over 900 genes in *Arabidopsis*, including pathogenesis-related proteins and disease resistance proteins which all work to prevent fungal establishment in plant tissues (Wan et al. 2008b). BOTRYTIS-INDUCED KINASE 1 (BIK1) is

another RLCK protein that is activated by CERK1 and has been shown to phosphorylate

RESPIRATORY BURST OXIDASE HOMOLOGUE PROTEIN D (RBOHD) to generate a burst of ROS

and trigger callose deposition in the cell wall in response to chitin. BIK1 has not been shown to

be involved in MAPK signalling cascades during fungal infection (Liu et al. 2018). Interestingly,

the bacterial PTI signalling cascade mirrors the fungal system. Although different PRR and RLCK

proteins are used, they are very similar structurally and both pathways use the MAPK signalling

cascade to elicit an immune response (Figure 1.2). Despite their similarity, more detail is known

about the bacterial immune pathway. The specific mechanisms by which LYK5, CERK1, and

PBL27 transduce the chitin PAMP signal to elicit a fungal immune response is not perfectly

understood. However, it is very likely based on literature in plant immunity that post-

translational modification of these proteins is essential.
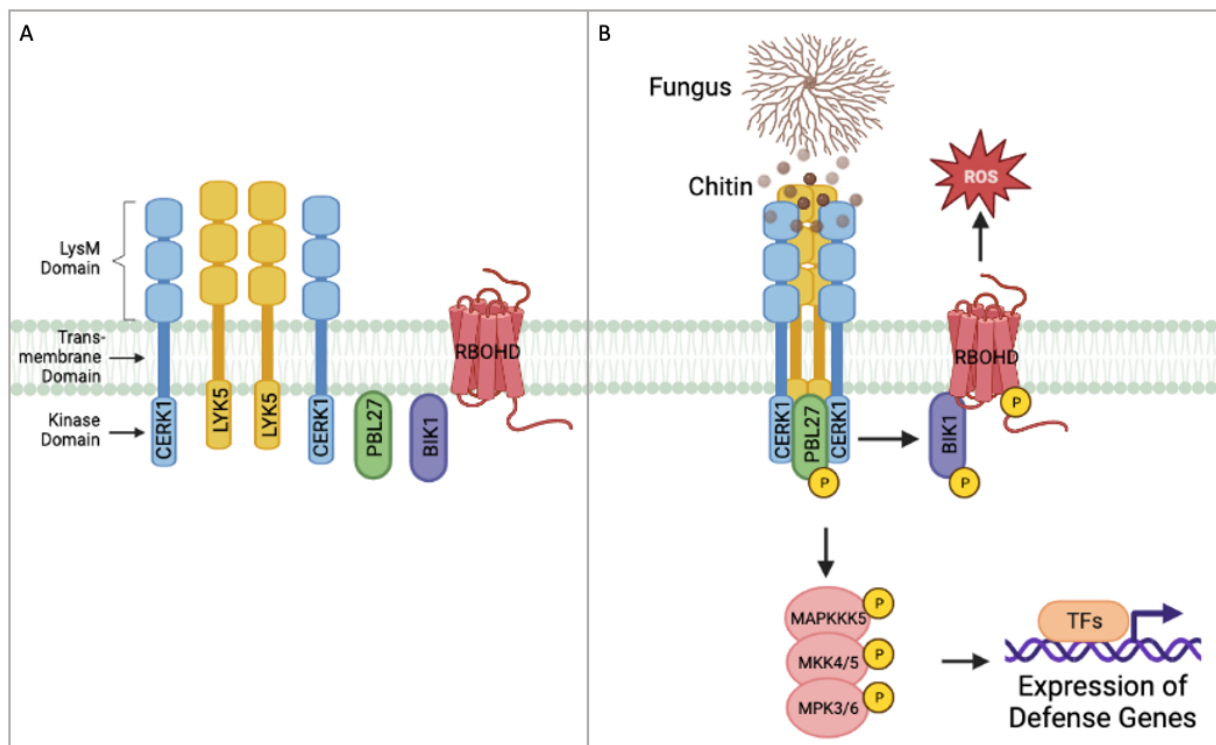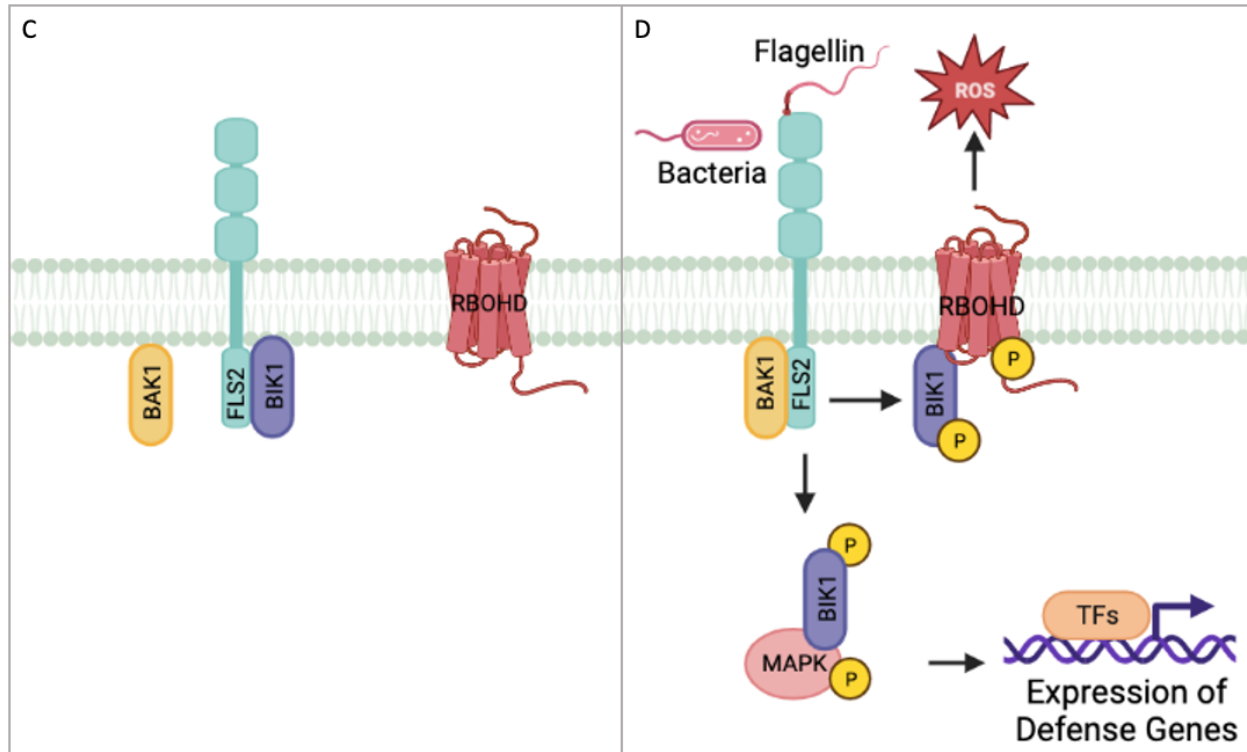
Figure 1.2. Schematic model of **(A & B)** Fungal PTI signalling pathway and **(C & D)** bacterial PTI signalling pathway. **(A)** standby positions of LysM-RLK proteins CERK1 and LYK5 and RLCK proteins PBL27 and BIK1 on the plasma membrane in the absence of chitin. **(B)** In the presence of chitin, LYK5 and CERK1 bind chitin and form a complex. Activated CERK1 phosphorylates PBL27, which in turn phosphorylates downstream MAPK proteins which activate transcription factors (TFs) for the expression of defence genes. Activated CERK1 also phosphorylates BIK1, which phosphorylates RBOHD which produces ROS. **(C)** Standby positions of LysM-RLK protein FLS2 and RLCK proteins BIK1 and BAK1 on the plasma membrane in the absence of flagellin. **(D)** In the presence of flagellin, BAK1 forms complex with FLS2, and FLS2 phosphorylates and releases BIK1. BIK1 can then activate MAPK signalling to activate transcription factors (TFs) for the expression of defence genes, and to phosphorylate RBOHD which produces ROS. CERK1: Chitin Elicitor Receptor Kinase 1; LYK5: Lysm-Containing Receptor-Like Kinase 5; BIK1: Botrytis-Induced Kinase 1; RBOHD: Respiratory Burst Oxidase Homologue Protein D; MAPK: Mitogen-Activated Protein Kinase; MAPKKK5: MAPK Kinase Kinase 5; MKK4/5: MAPK Kinase 4/5; MPK3/6: MAPK 3/6; TFs: Transcription Factors; FLS2: Flagellin Sensitive 2; BAK1: BRI1-Associated Receptor Kinase 1; P: Phosphorylation; ROS: Reactive Oxygen Species. Figures created by author using BioRender.com.

1.4. SUMOylation, a Post-Translational Modification

At all stages of the plant life cycle and in all cellular functions, proteins are subjected to post-translational modifications (PTMs), which is the addition or removal of small molecules to adjust protein activity, stability, localization and protein interactions (Zhang and Zeng 2020).

9

PTMs include phosphorylation, acetylation, glycosylation, redox modification, ubiquitination and SUMOylation. Specifically in plant immunity, PTM of immune proteins such as PRRs and R proteins increases the speed, complexity, specificity, and reversibility of signalling pathways and plant immune responses (Zhang and Zeng 2020). SUMOylation is a PTM similar to ubiquitination and involves the attachment of SUMO (Small Ubiquitin-Like Modifier) proteins to lysine residues in target proteins via an isopeptide bond. SUMOylation is a player in most physiological processes including development, homeostasis, abscisic acid signalling, stress response, and immunity (Castaño-Miquel et al. 2013; Morrell and Sadanandom 2019). SUMO is therefore critical to the functioning of all eukaryotic cells and is conserved across eukaryotic organisms (Morrell and Sadanandom 2019). In *Arabidopsis*, there are 8 SUMO isoforms, but only the expression of SUMO1, 2, 3, and 5 has been verified. SUMO1 and SUMO2 have been shown to have the highest expression (Morrell and Sadanandom 2019). The effect of SUMOylation on a protein is target dependent and can change based on the location and the number of SUMO substrates on the target protein. This adds to the complexity of the SUMO system and the variety of molecular consequences following SUMOylation (Morrell and Sadanandom 2019).

1.4.1. The SUMO Cycle

SUMOylation is a cyclical process with SUMO changing between conjugated and non-conjugated forms in response to stimuli (Morrell and Sadanandom 2019). The attachment of SUMO to target substrates is catalysed by three enzymes: E1-activating enzyme, E2-conjugating enzyme and E3-ligase enzyme (Castaño-Miquel et al. 2017). First, a Ubiquitin-like

protease (ULP) cleaves amino acids from immature SUMO, exposing a C-terminal diglycine motif. Mature SUMO is then activated by E1 activating enzyme, which is a heterodimer of SUMO activating enzyme 1 and 2 (SAE1/2) (Castaño-Miquel et al. 2013; Morrell and Sadanandom 2019). E1-activating enzyme then catalyses an ATP-dependent reaction resulting in the formation of a high-energy thioester bond between the C-terminal glycine of SUMO and the catalytic cysteine residue in SAE2 (Castaño-Miquel et al. 2013; Morrell and Sadanandom 2019). During the conjugation step, activated SUMO is transferred from SAE2 to a cysteine residue in the E2 conjugating enzyme called SUMO conjugating enzyme 1 (SCE1) by a transesterification reaction (Castaño-Miquel et al. 2013; Morrell and Sadanandom 2019). The resulting SUMO-SCE1 thioester complex directly catalyses the formation of an isopeptide bond between the C-terminal glycine of SUMO and ε-amino group of a lysine residue in the target substrate (Castaño-Miquel et al. 2013; Morrell and Sadanandom 2019). SUMO E3 ligases interact with SCE1 and help transfer SUMO from SCE1 to the target substrate, however SUMOylation of a target substrate can occur without E3 ligases (Morrell and Sadanandom 2019). In an additional catalytic step, E4 ligases can be utilized to form polySUMO chains to a single target substrate. This process can then be reversed by deconjugating SUMO proteases which cleave the isopeptide bond between SUMO and the target substrate, allowing free SUMO to be available for another conjugation cycle (Figure 1.3). These SUMO proteases include ULPs, the same proteases responsible for generating mature SUMO at the start of the cycle (Castaño-Miquel et al. 2013; Morrell and Sadanandom 2019). This process is dynamic and provides rapid flexibility in protein regulation (Orosa et al. 2018). Due to the high versatility, SUMOylation of plants offer novel opportunities to improve agricultural productivity (Zhang and Zeng 2020).

SUMOylation is highly substrate-specific, but unlike the large enzyme system of ubiquitination

to provide specificity, there are only a few enzymes involved in SUMOylation (Orosa et al. 2018;

Zhang and Zeng 2020). In contrast, a large number of SUMO proteases have been identified,

suggesting that the de-conjugation step of the SUMO-cycle is what provides substrate-

specificity (Orosa et al. 2018; Morrell and Sadanandom 2019).
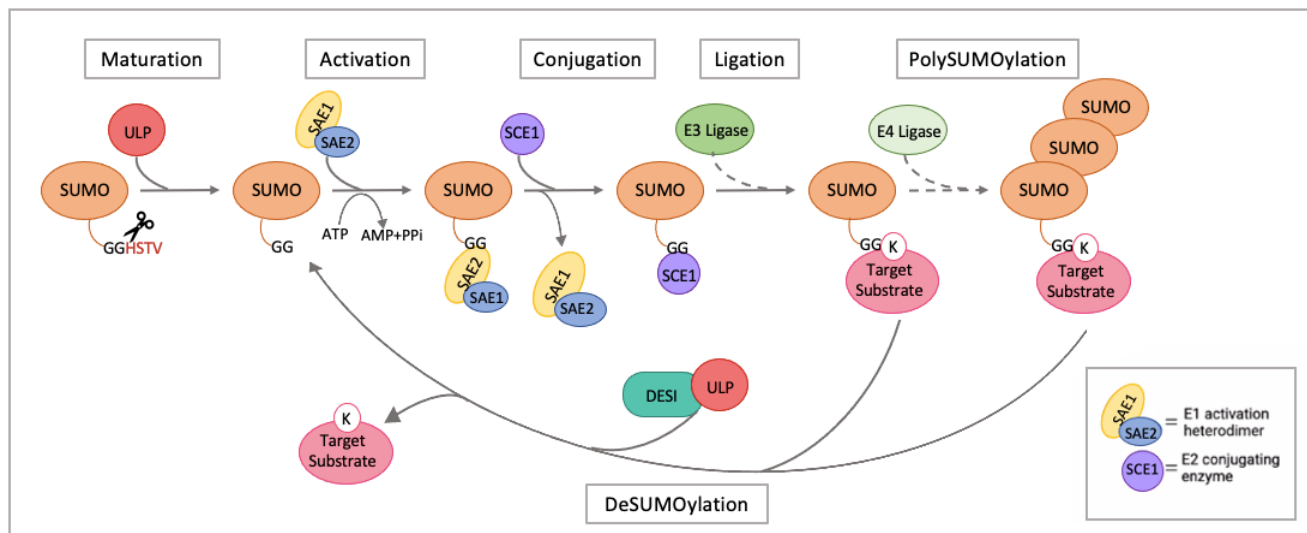
Figure 1.3. The SUMO Cycle. **(Maturation)** ULPs cleave amino acids from SUMO C-terminal, leaving a diglycine motif. **(Activation)** E1 activating enzyme made up of SAE1 and SAE2 catalyse an ATP dependent reaction to form a thioester bond between SUMO C-terminal glycine and SAE1. **(Conjugation)** SUMO is transferred to SCE1 by a transesterification reaction. **(Ligation)** SUMO-SCE1 complex is directly ligated to a lysine residue in the target substrate via an isopeptide bond. E3 ligases sometimes interact with SCE1 to facilitate the isopeptide bond formation. **(PolySUMOylation)** E4 ligases sometimes catalyse the formation of polySUMO chains to a single target substrate. **(DeSUMOylation)** Deconjugating SUMO proteases cleave isopeptide bonds between SUMO and the target substrate, producing free, mature SUMO to be utilized in another conjugation cycle. SUMO: Small Ubiquitin-Like Modifier; ULP: Ubiquitin-Like Protease; SAE1: SUMO Activating Enzyme 1; SAE2: SUMO Activating Enzyme 2; ATP: Adenosine Triphosphate; AMP: Adenosine Monophosphate; PPi: Inorganic Pyrophosphate; SCE1: SUMO Conjugating Enzyme 1; DeSI: DeSUMOylating Isopeptidase. Figure created by author using PowerPoint and Morrell and Sadanandom 2019 as a reference.

1.4.2. De-Conjugation by SUMO Proteases

The SUMO-cycle is reversible and flexible due to SUMO proteases that possess de-

conjugation activity and work to cleave SUMO from target proteins (Orosa et al. 2018).

Proteases are very substrate-specific and there is little overlap in their roles in plant development and immunity. For this reason, it is theorized that the specificity of the SUMO system is achieved via DeSUMOylating-proteases (Orosa et al. 2018). SUMO proteases belong to the cysteine protease family of proteolytic enzymes, and within this family are 2 main categories: the Ubiquitin-Like Proteases (ULPs) and the DeSUMOylating Isopeptidases (DeSIs) (Morrell and Sadanandom 2019). There are at least seven ULP SUMO proteases within the *Arabidopsis* proteome which all localize to the nucleus. There are eight putative DeSI proteases in *Arabidopsis* based on sequence similarity to human DeSI, and one in particular called DeSI3a that has been functionally characterized and found to localize in the cell membrane (Orosa et al. 2018; Morrell and Sadanandom 2019). This study is particularly interested in DeSI3a protease because of its localization in the cell membrane, where CERK1 and other signalling proteins in the fungal PTI pathway reside. Orosa and colleagues found that FLS2, the bacterial PRR protein, and DeSI3a co-localize on the plasma membrane (Orosa et al. 2018). In addition, Orosa and colleagues and Yates found increased expression of defence genes when *desi3a-1* knockout (K/O) *Arabidopsis* were exposed to flagellin treatment (the bacterial PAMP molecule) compared to Columbia-0 wild type *Arabidopsis* (Col-0) (Orosa et al. 2018; Yates 2018). Yates also found that *desi3a-1* K/O plants had increased immunity upon infection with *Pseudomonas syringae* than Col-0 (Yates 2018). These results suggest that DeSI3a protease plays a negative role in plant defence during bacterial infection by repressing defence gene expression. Since DeSI3a plays a negative role during bacterial pathogen defence, then it is justified to explore the possibility of this also being the case for the fungal pathway. Yates observed increased defence gene expression in *desi3a-1* K/O plants compared to Col-0 upon chitosan treatment,

however this experiment was only repeated once and *desi3a-1* K/O immunity upon fungal infection was not tested (Yates 2018). A part of this study is to determine if *desi3a-1* K/O transgenic *Arabidopsis* has increased immunity upon *B. cinerea* infection compared to Col-0.

1.5. SUMOylation During Fungal Infection

It is well established that SUMOylation is essential to plant immunity upon fungal infection in various crop species. The following examples are to illustrate this point. Fraire-Velázquez and colleagues identified SUMO1 as an early expressed gene during *Colletotrichum lindemuthianum*, the fungus causing anthracnose, infection in bean plants (Fraire-Velázquez and Lozoya-Gloria 2003). When measuring compatible (plant susceptibility) and incompatible (plant resistance) interactions, they found much higher gene expression of SUMO1 in incompatible interactions, meaning SUMO1 expression increased as a part of plant resistance (Fraire-Velázquez and Lozoya-Gloria 2003). Li and colleagues found that in a susceptible cultivar of wheat to the powdery mildew fungus *B. graminis*, a gene called *Triticum aestivum* susceptibility (*TaS3*), which is an ortholog of the SUMO protease ELS1, was found to be highly expressed (Li et al. 2013). In cultivars highly resistant to the fungus, *TaS3* was expressed at very low levels. This finding suggests that SUMO deconjugation conferred susceptibility to this fungus, and therefore that SUMOylation is likely important for resistance (Li et al. 2013). SUMOylation was also shown to provide enhanced resistance to *Phytophthora sojae*, a soil-borne oomycete, in soybean during another study by Li and colleagues (Li et al. 2019). SUMO and SUMO-conjugating proteins were found to have high expression in the root cells of resistant soybean when inoculated with the fungus, suggesting a positive relationship between

immunity and SUMOylation (Li et al. 2019). In other research, Stocks and colleagues used

genomic studies to identify resistance genes to Ash Dieback Disease caused by the fungus

Hymenoscyphus fraxineus in Danish Ash trees (Stocks et al. 2019). They identified the SUMO-

conjugating enzyme, SCE1, in close proximity to single nucleotide polymorphisms (SNPs)

conferring resistance to the disease. This indicated a positive role of SUMOylation in the

defence against Ash Dieback (Stocks et al. 2019). SUMOylation has also been shown to be an

essential PTM during infection specifically by *B. cinerea.*   In a study by Castaño-Miquel and

colleagues, the researchers developed transgenic *Arabidopsis* in which SUMOylation was

inhibited by interrupting SUMO E1-activating and E2-conjugating enzyme interactions (Castaño-

Miquel et al. 2017). They discovered that when SUMO1 conjugation was inhibited, plants had

enhanced susceptibility to fungal infection by *B. cinerea*. Leaf lesions appeared sooner and

spread more quickly in plants with impaired SUMOylation compared to Col-0 plants and plants

with enhanced SUMOylation (hyper-SUMOylation). At 15 days post-infection with the fungus,

plants with impaired SUMOylation were dead while Col-0 plants and hyper-SUMOylated plants

were able to survive the infection (Castaño-Miquel et al. 2017). These studies along with others

emphasize the role of SUMOylation as an essential mechanism in the immunity of model and

crop species in necrotrophic fungal attacks, and highlights the potential for improved crop

productivity via manipulation of SUMO conjugation and deconjugation machinery (Sharma et

al. 2021). However, to accomplish this we must understand where and how SUMOylation

occurs in the fungal immune pathway.

1.6. SUMOylation of PRR Proteins During Pathogen Infection

It is clear from the overwhelming evidence that SUMOylation is vital for plant resistance to necrotrophic fungal infection, however there is very little knowledge about the mechanisms by which SUMO accomplishes this. Orosa and colleagues recently discovered a mechanism for SUMO-mediated resistance during bacterial infection (Orosa et al. 2018). They found that SUMOylation of the PRR protein FLAGGELIN-SENSITIVE 2 (FLS2) by SUMO1 is essential for the release and activation of BIK1. Released BIK1 then initiates MAPK signalling and phosphorylates RBOHD, eventually leading to expression of defence genes and production of ROS (Figure 1.4). CERK1 is very similar to FLS2 in structure and function, as both are lysM kinase transmembrane proteins and function to perceive external PAMPs and elicit an immune response in the cell. Since Orosa and colleagues proved that FLS2 SUMOylation in response to flagellin elicitation is essential for the transmission of the immune signal, it is predicted that CERK1 has similar regulation via SUMOylation (Orosa et al. 2018). Using SUMO-site prediction software (Dr. Sadanandom Lab), Yates found three putative SUMOylation sites at lysine residues within the CERK1 protein (Yates 2018). The first putative SUMO-site is at lysine 74 (K74) and lies within the first LysM domain of the protein in the extracellular matrix, the second is at lysine 276 (K276) and resides between the transmembrane domain and the kinase domain, and the third site is at lysine 495 (K495) and resides within the kinase domain (Figure 1.5, Yates 2018). These SUMO-attachment sites become non-functional by mutating the *CERK1* gene so that in the resulting protein, lysine (K) is replaced with arginine (R). Yates was also able to establish that CERK1 K/O transgenic *Arabidopsis* (*cerk1-2* K/O) with reconstituted CERK1 mutated at all three SUMO-sites (*cerk1-3KR*) had lower ROS production when treated with

chitosan than Col-0 and *cerk1-2* K/O *Arabidopsis* reconstituted with wild type CERK1 (*cerk1-CM*). In fact, it had similar ROS levels to *cerk1-2* K/O *Arabidopsis* (Yates 2018). This research suggests that SUMOylation of CERK1 is essential for activation of the oxidative burst immune response, but how this occurs is unknown. Based on this research and the findings by Castaño-Miquel and colleagues, it is predicted that SUMOylation of CERK1 is an essential PTM that in response to chitin elicitation, activates CERK1 and allows signal transduction to downstream proteins to provoke an immune response in the cell (Figure 1.6).
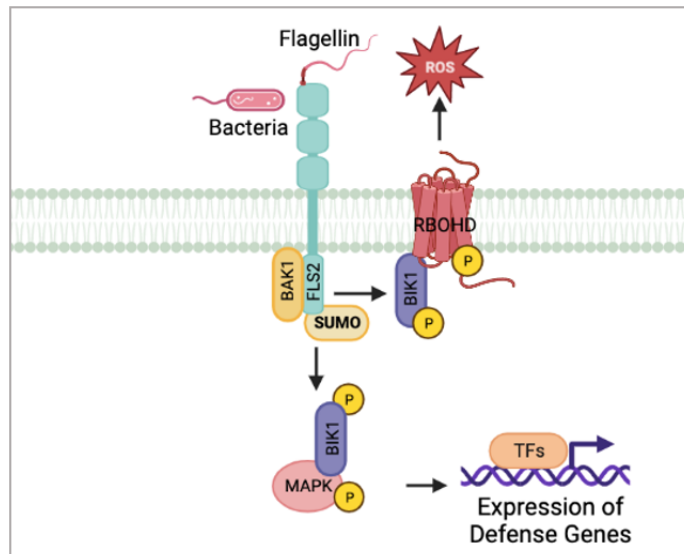
Figure 1.4. SUMO-mediated resistance in the PTI pathway during bacterial infection. SUMOylation of FLS2 upon flagellin elicitation is essential for the activation and release of BIK1. Released BIK1 can then phosphorylate MAPK signalling proteins to induce transcription factors for the expression of defence genes and RBOHD to induce the production of ROS. FLS2: Flagellin Sensitive 2; BIK1: Botrytis-Induced Kinase 1; SUMO: Small Ubiquitin-Like Modifier; RBOHD: Respiratory Burst Oxidase Homologue Protein D; MAPK: Mitogen-Activated Protein Kinase; TFs: Transcription Factors; BAK1: BRI1-Associated Receptor Kinase 1; P: Phosphorylation; ROS: Reactive Oxygen Species. Figure created by author using BioRender.com and Orosa et al. 2018 as a reference.
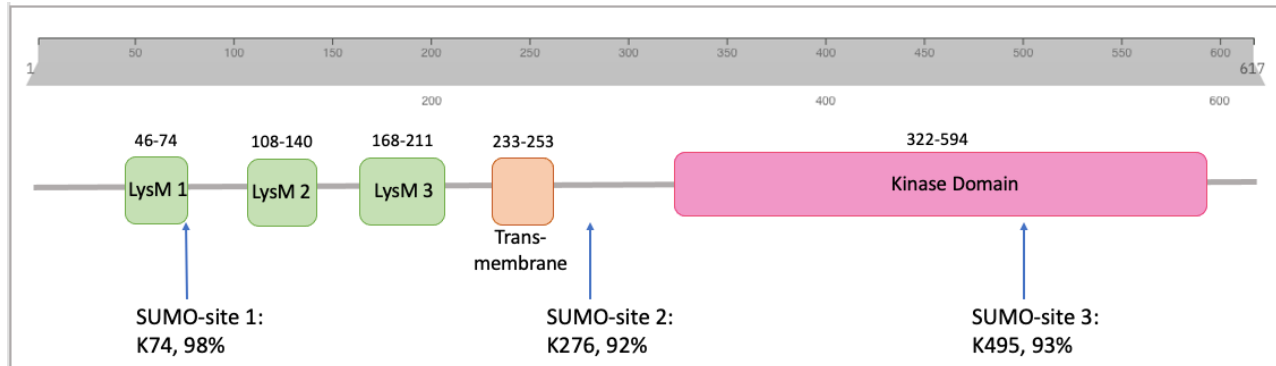
Figure 1.5. Putative SUMOylation sites in CERK1 protein. SUMO-site 1 at lysine 74 (K74) lies in the extracellular matrix within the first LysM protein domain, with a certainty of 98% predicted by the software. SUMO-site 2 at lysine 276 (K276) lies inside the cell between the transmembrane domain and the kinase domain with a certainty of 92% predicted by the software. SUMO-site 3 at lysine 495 (K495) lies within the kinase domain with a certainty of 93% predicted by the software. Figure created by author using PowerPoint and Yates 2018 as a reference.
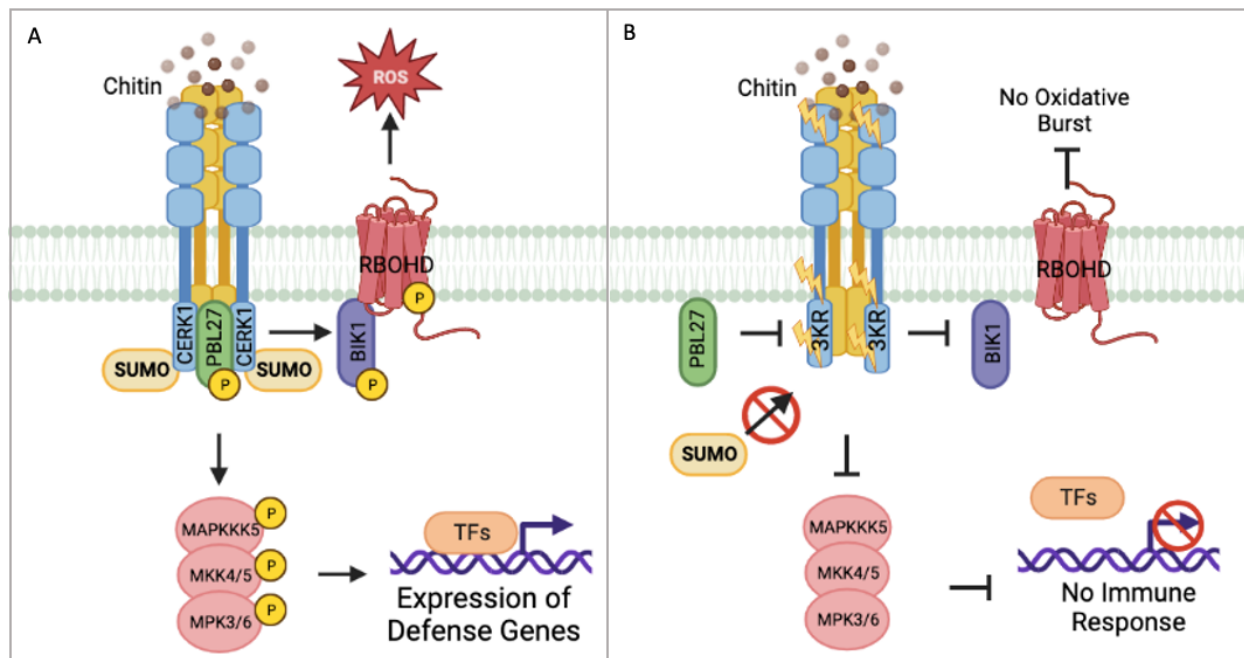
Figure 1.6. Diagram of hypothesized role of SUMO in the fungal PTI pathway. **(A)** CERK1 is SUMOylated, which allows interaction with and activation of LYK5, PBL27 or BIK1 (or all three) in response to chitin. Activation of these signalling proteins allows the progression of MAPK immune signalling, expression of defence genes and generation of ROS. **(B)** When all three CERK1 SUMO-sites are mutated (3KR), SUMO is unable to interact with CERK1, which disables activation of downstream signalling proteins and prevents expression of defence genes and generation of ROS. CERK1: Chitin Elicitor Receptor Kinase 1; LYK5: Lysm-Containing Receptor-Like Kinase 5; BIK1: Botrytis-Induced Kinase 1; RBOHD: Respiratory Burst Oxidase Homologue Protein D; MAPK: Mitogen-Activated Protein Kinase; MAPKKK5: MAPK Kinase Kinase 5; MKK4/5: MAPK Kinase 4/5; MPK3/6: MAPK 3/6; TFs: Transcription Factors; P: Phosphorylation; ROS: Reactive Oxygen Species. Figures created by author using BioRender.com.

1.7. Thesis Objectives and Hypotheses

This thesis aims to explore the role of SUMOylation in the fungal PTI pathway upon *B. cinerea* infection using two approaches. Firstly, the interaction of SUMO1 with CERK1, the main PRR protein for chitin in the model plant *Arabidopsis*, will be explored using co-immunoprecipitation upon chitin elicitation. If WT CERK1 (CERK1^{WT}) is able to interact with SUMO1 while CERK1 3KR mutant lacking functional SUMO-sites (CERK1^{3KR}) is not, then the interaction of CERK1^{3KR} with other PTI signalling proteins, LYK5 and PBL27, will be explored to determine if lack of SUMOylation of CERK1 inhibits the initiation of an immune response.   The second approach for determining the role of SUMO in the fungal PTI pathway is the analysis of *B. cinerea* infection assays. Comparing lesion size development in *cerk1-3KR* and *desi3a-1* K/O transgenic *Arabidopsis* with Col-0, *cerk1-CM*, and *cerk1-2* K/O *Arabidopsis* upon *B. cinerea* infection will reveal immunity conferred by SUMOylation during infection. The working hypotheses for this study are that like FLS2, CERK1 is SUMOylated upon chitin elicitation and that this PTM is essential for the activation of PTI signalling in the cell. Secondly, SUMOylation is a positive regulator of immunity, so *cerk1-3KR* transgenic *Arabidopsis* will have decreased immunity upon *B. cinerea* infection while *desi3a-1* K/O transgenic *Arabidopsis* will have increased immunity upon *B. cinerea* infection.

1.8. Special Note and Thesis Outline

The immunoprecipitation assays were carried out using the *CERK1^{WT}* and *CERK1^{3KR}* constructs from Dr. Sadanandom's laboratory stores. After a few experimental replicates, expression of CERK1 on immunoblots could not be visualized, so constructs were sequenced as

a troubleshooting protocol. It was discovered that the constructs contained unintended and potentially destabilizing mutations. Following this discovery, the transgenic *Arabidopsis* lines that had also been received from Dr. Sadanandom's laboratory stores were genotyped to confirm their identity. Surprisingly, the transgenic plant lines were found to not be transgenic but only Col-0 and *cerk1-2* K/O lines. These results are explained in detail in chapter 3. Following this discovery, the focus of the project was shifted to prioritize re-cloning *CERK1* constructs and re-generating the SUMO-site mutations, which is described in Chapter 4. *CERK1, LYK5* and *PBL27* were successfully cloned and 2 out of the three SUMO-site mutations were successfully inserted (*CERK1^{WT}*, *LYK5^{WT}*, *PBL27^{WT}* and *CERK1^{2KR}*). The triple *CERK1^{3KR}* mutant construct could not be generated due to technical challenges and time constraints. Subcellular localization of cloned constructs, immunoprecipitation assays of CERK1^{WT} and CERK1^{2KR} and co-immunoprecipitation assays with SUMO1 are described in Chapter 5. Evidence that both CERK1^{WT} and CERK1^{2KR} are SUMOylated upon chitin elicitation is shown, but the presence of a contaminating band in the negative control prevents confirmation of this data. Finally, *B. cinerea* infection assays were carried out in chapter 6 using Col-0, *cerk1-2* K/O, and *desi3a-1* K/O as there was not enough time to reproduce the *cerk1-CM* and *cerk1-3KR* transgenic *Arabidopsis* plant lines. *cerk1-2* K/O line was found to have significantly larger lesion development at 5 days-post-infection (DPI) compared to Col-0, but there was no significant difference in lesion size of *desi3a-1* K/O and Col-0. There was also no significant difference in the fungal DNA accumulation at 5 DPI in each genotype.

2.0. Materials and Methods

2.1 Materials

2.1.1. Vectors

Table 2.1. Vectors used in project Including protein tag, antibiotic resistance, and source.

Vector	Protein tag	Promoter	Resistance	Source
pJET 1.2 blunt Cloning Vector	-	T7 Promoter	Ampicillin	Thermo Scientific
Gateway pENTR™ 4 Dual Selection Vector	-	N/A	Kanamycin	Invitrogen
Gateway pEarlyGate 103	C-terminal GFP	35S Promoter	Kanamycin	Dr. Sadanandom lab stocks
Gateway pEarlyGate 201	N-terminal HA	35S Promoter	Kanamycin	Dr. Sadanandom lab stocks
Free-GFP	N/A	35S Promoter	Kanamycin	Dr. Sadanandom lab stocks
P19	N/A	35S Promoter	Kanamycin	Dr. Sadanandom lab stocks
$CERK1^{WT}$ pEarlyGate 104	N-terminal YFP	35S Promoter	Kanamycin	Dr. Sadanandom lab stocks
$CERK1^{3KR}$ pEarlyGate 104	N-terminal YFP	35S Promoter	Kanamycin	Dr. Sadanandom lab stocks
$SUMO1$ pEarlyGate 201	N-terminal HA	35S Promoter	Kanamycin	Dr. Sadanandom lab stocks
$FLS2^{WT}$ pEarlyGate 103	C-terminal GFP	35S Promoter	Kanamycin	Dr. Sadanandom lab stocks
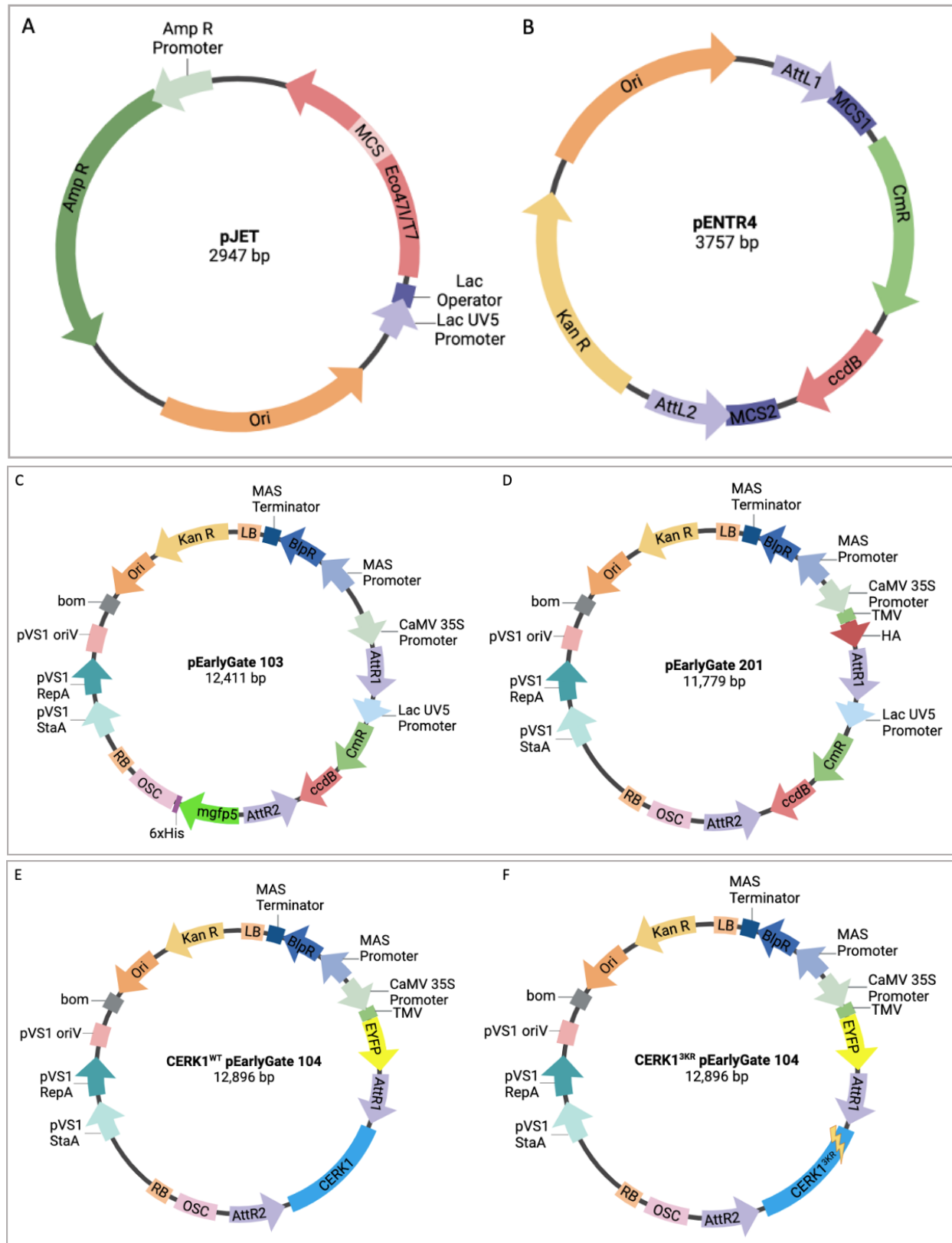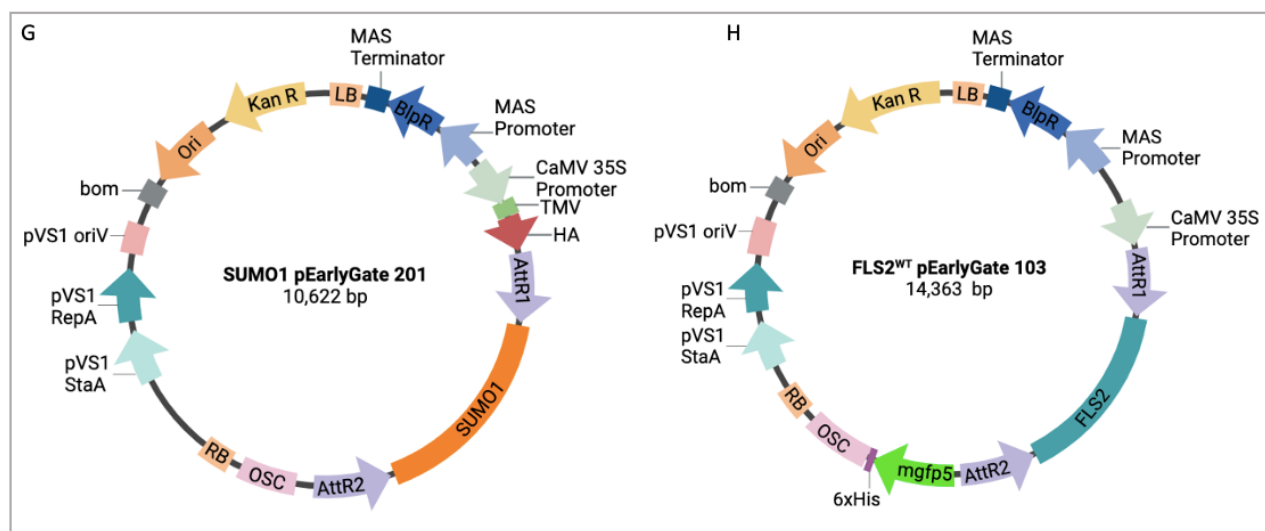
Figure 2.1. Vector maps of vectors used in this project. **(A)** pJET cloning vector. **(B)** pENTR4 entry vector. **(C)** pEarlyGate 103 (p103) expression vector. **(D)** pEarlyGate 201 (p201) expression vector. **(E)** *CERK1^WT* pEarlyGate 104 expression vector. **(F)** *CERK1^3KR* pEarlyGate 104 expression vector. **(G)** *SUMO1* pEarlyGate 201 expression vector. **(H)** *FLS2^WT* pEarlyGate 103 expression vector. Amp R: Ampicillin Resistance; Ori: Origin of Replication; Lac UV5 Promoter: *E. coli* Lactose UV5 Promoter; Lac Operator: *E. coli* Lactose Operator; Eco47I/T7: Mutant Eco47I Restriction Endonuclease; MCS: Multiple Cloning Site; CmR: Chloramphenicol Acetyltransferase; ccdB: ccdB bacterial toxin; Kan R: Kanamycin Resistance; bom: basis of mobility region; pVS1 oriV: Origin of Replication for *Pseudomonas* plasmid PVS1; pVS1 RepA: Replication Protein from *Pseudomonas* plasmid PVS1; pVS1 StaA: Stability Protein from *Pseudomonas* plasmid PVS1; RB: Right Border repeat from Nopaline C58 T-DNA; OSC: Octopine Synthase Terminator; 6xHis: 6xHis affinity tag; mgfp5: Green Fluorescent Protein tag; Att2: recombination site 2 for Gateway LR reaction; Att1: recombination site 1 for Gateway LR reaction; CaMV 35S promoter: Constitutive Promoter from *Cauliflower mosaic virus*; MAS promoter: Mannopine Synthase Promoter; BlpR: Phosphinothricin Acetyltransferase; MAS terminator: Mannopine Synthase Terminator; LB: Left Border repeat from Nopaline C58 T-DNA; TMV: translational enhancer from *Tobacco mosaic virus*; HA: Human Influenza Hemagglutinin epitope tag. EYFP: Enhanced Yellow Fluorescent Protein. Vector maps created by author using BioRender.com

2.1.2. Primers*

Table 2.2. Primers used in project listing primer sequence, product size and restriction enzyme site (highlighted in yellow) embedded in sequence when applicable. All primers obtained from Integrated DNA technologies (IDT).

Primer Name	Sequence	Product Size (bp)	Restriction enzyme
CERK1 Exon 5 Forward	5'-ATA AGC GTG GAC AAA TCT GTT-3'	713 (gDNA) 460 (cDNA)*	-

---

* gDNA refers to genomic DNA and cDNA refers to complementary DNA which only contains the coding sequence of the gene and excludes introns. For this reason, the gDNA product size is larger than the cDNA product size.

CERK1 Exon 8 Reverse	5'-CTT TGC TCG GAA TTT CTG GTC-3'		-
CERK1 Exon 10 Forward	5'-GGA GAA GTG TCT GCA AAA GTA G-3'	723 (gDNA) 380 (cDNA)	-
CERK1 Exon 12 Reverse	5'-CTA CCG GCC GGA CAT AAG ACT G-3'		-
CERK1 Forward	5' CCATGGGAATGAAGCTAAAGATTTCTCTAATCGCT '3	1,851	NcoI
CERK1 Reverse	5' GATATCTCCGGCCGGACATAAGACT '3		EcoRV
LYK5 Forward	5' GGTACCGAATGGCTGCGTGTACACTC '3	1,992	KpnI
LYK5 Reverse	5' CTCGAGTGGTTGCCAAGAGAGCCGG '3		XhoI
PBL27 Forward	5' CCATGGGAATGAGTGGGTGTTTGCCTT '3	1,539	NcoI
PBL27 Reverse	5' GATATCTGTCATTTGTACTATCAAAGCTGCC '3		EcoRV
Attb1	5' ACAAGTTTGTACAAAAAAGCAGGCT '3	N/A	
Attb2	5' ACCACTTTGTACAAGAAAGCTGGGT '3	N/A	
CERK1 K74R Forward	5' CAGTAACATTAGAGACAAAGATAGAATC '3	1,851	
CERK1 K74R Reverse	5' GATTCTATCTTTGTCTCTAATGTTACTG '3		
CERK1 K267R Forward	5' TTCCGTTGTCTACTAGGGCTGATCATG '3	1,851	
CERK1 K267R Reverse	5' CATGATCAGCCCTAGTAGACAACGGAA '3		
CERK1 K495R Forward	5' AGTGTCTGCAAGAGTAGTTGTATATG '3	1,851	
CERK1 K495R Reverse	5' CATATACAACTACTCTTGCAGACACT		
Botrytis cinerea Actin Forward	5' CCCAATCAACCCAAAGTCCAACAG '3	275	
Botrytis cinerea Actin Reverse	5' CAAATCACGACCAGCCATGTC '3		
Arabidopsis Ubiquitin F	5'-ATGCAGATCTTTGTTAAGACTCTC-3'	301	
Arabidopsis Ubiquitin R	5'-TCAACCACCACGGAGCCTGA-3'		

2.1.3. Bacterial Strains

Table 2.3. Bacteria used in this project including strain and antibiotic resistance

Organism	Strain	resistance
Agrobacterium tumefaciens (*Agrobacterium*)	GV3101 (with pMP90)	Gentamycin and Rifamycin

Escherichia coli	DH5α	N/A

2.1.4. Plant Lines

Table 2.4. *Arabidopsis thaliana* plant lines used in this project including selection media and source.

Name	Selection	Source
Col-0	N/A	Dr. Sadanandom lab stocks
cerk1-2 K/O	BASTA	Dr. Sadanandom lab stocks
cerk1-CM1	BASTA	Dr. Sadanandom lab stocks
cerk1-CM2	BASTA	Dr. Sadanandom lab stocks
cerk1-3KR-2-5	BASTA	Dr. Sadanandom lab stocks
cerk1-3KR-3-6	BASTA	Dr. Sadanandom lab stocks
desi3a-1 K/O	BASTA	Dr. Sadanandom lab stocks

2.1.5. *Botrytis cinerea*

Botrytis cinerea strain H/A5 was kindly donated by the James Hutton institute plant

pathology group.

2.1.6. Antibodies

Primary antibody solutions were prepared from laboratory stocks, stored at -80°C and

frozen in working concentration at -20°C. GFP primary antibody was used up to 8 times and HA

primary antibody was used up to 4 times before discarding. Secondary antibodies were

prepared for each experiment and discarded after use. Table 2.5 shows the working

concentration and suppliers of all antibodies used.

Table 2.5. Antibodies used in this project including host, working concentration and supplier.

Antibody		Host	Working concentration	Supplier
Primary	Anti-GFP	Rabbit	1:5000	Abcam
	Anti-HA	Rat	1:3000	Sigma-Aldrich
Secondary	Anti-Rabbit-HRP		1:20,000	Abcam

	Anti-Rat-HRP		1:10,000	Sigma-Aldrich

2.1.7. Enzymes

Table 2.6. Enzymes and co-reaction buffers used in this project and supplier.

Enzyme	Reaction Buffer	Supplier
REDTaq® ReadyMix™ PCR Reaction Mix	N/A	Sigma-Aldrich
Q5® Hot Start High-Fidelity DNA Polymerase	Q5® High GC Enhancer, Q5® Reaction Buffer	New England BioLabs
SYBR® Green JumpStart™ Taq ReadyMix™	N/A	Sigma-Aldrich
T4 DNA Ligase	T4 Ligation Buffer	New England BioLabs
Gateway™ LR Clonase™ II Enzyme mix	N/A	Invitrogen
Restriction Enzymes: NcoI EcoRV XhoI KpnI DpnI BspHI	CutSmart® Buffer	New England BioLabs

2.1.8. Antibiotics

Antibiotic stocks were prepared in a laminar flow hood, filter sterilized and aliquoted into 1.5mL Eppendorf tubes. Stocks were stored at -20°C. Table 2.7 describes the solvent and working concentration of each antibiotic used.

Table 2.7. Antibiotics used in this project, solvent they were dissolved in and working concentration.

Antibiotic	Solvent	Working concentration µg/mL
Ampicillin	Autoclaved water	100
Kanamycin	Autoclaved water	50
Gentamycin	Autoclaved water	25
Rifamycin	100% methanol + few drops of NaOH to dissolve	50

2.1.9. Buffers, Media, Solutions, and Chemicals

Table 2.8. Buffers, media, solutions, and chemicals used in this project, their composition, preparation, and pH where applicable. Concentrations indicate chemicals dissolved in pure water unless otherwise specified.

Buffer/Media/Solution/Chemical		Composition and preparation & Source	pH
Buffers	Plant DNA extraction buffer	0.2M Tris pH 8.5, 0.25M NaCl, 0.025M EDTA, 0.5% SDS.	
	TAE buffer	Varying concentrations, Sigma-Aldrich.	
	Original SDS protein extraction buffer	0.05M Tris pH 8.5, 0.05M NaCl, 0.1% SDS, 0.001M EDTA, 0.5% NP-40, 0.5% Sodium Deoxycholate, 1 tablet per 10mL of buffer proteinase inhibitor, 0.05 NEM. Mix ingredients on ice, dissolve NEM in ethanol and add to buffer right before tissue grinding.	
	Modified KCl protein extraction buffer	0.05M Tris pH 8.5, 0.15M NaCl, 0.08M KCl, 0.001M EDTA, 1% NP-40, 0.5% Sodium Deoxycholate, 1 tablet per 10mL of buffer proteinase inhibitor, 0.05 NEM. Mix ingredients on ice, dissolve NEM in ethanol and add to buffer right before tissue grinding.	
	1x Running buffer	25mM Tris, 192mM Glycine, 0.1% SDS.	
	1x Transfer buffer	25mM Tris, 192mM Glycine, 20% methanol.	
	1x Tris-buffered saline and Tween20 (TBST)	20mM Tris, 137mM NaCl, 0.1% Tween20.	7.6
	4x Laemmli dye	200mM Tris-HCl (pH 6.8), 8% SDS, 40% glycerol, 588mM β-mercaptoethanol, 50mM EDTA, 0.8mg/mL Bromophenol Blue.	
	Fungal DNA extraction buffer	2% CTAB, 1.4M NaCl, 0.02% β-mercaptoethanol, 20mM EDTA (pH 8), 100mM Tris (pH 8). Mix ingredients and adjust pH to 5 with HCl and make up rest of volume with water.	5
Media	Agar lysogeny broth (LB)	25g/L LB broth Miller Granulated (Fisher Scientific), 15g/L Microagar (Duchefa Biochemie). Autoclaved.	

	Liquid LB	25g/L LB broth Miller Granulated (Fisher Scientific). Autoclaved.	
	Potato dextrose agar (PDA)	39g/L Potato Dextrose agar (Oxoid). Autoclaved.	
	Agar	0.6g/L Microagar (Duchefa Biochemie). Autoclaved.	
	Agarose gel	0.01g/mL agarose, (Severn Biotech Ltd). Heated to dissolve.	
	Advance F2 + Sand soil	Levington.	
Solutions/ chemicals	Ethanol	70mL/L ethanol.	
	Magnesium chloride (MgCl$_2$)	10 mM, Sigma-Aldrich. Autoclaved.	
	Polyvinylpolypyrrolidone (PVPP)	Sigma-Aldrich.	
	TWEEN20	VWR Chemicals.	
	3',5'-Dimethoxy-4'hydroxy-acetophenone (Acetosyringe)	0.1g dissolved in 1mL Dimethyl Sulfoxide (DMSO). VWR Chemicals.	
	Trisaminomethane (Tris)	1.5M, mixed on spinner and pH brought to 8.8 with HCl for resolving gel. 1M mixed on spinner and pH brought to 6.8 for stacking gel. pH brought to 8.5 for protein lysis buffer.	8.8, 6.8, 8.5
	Sodium chloride (NaCl)	5M, VWR Chemicals. Autoclaved.	
	Potassium chloride (KCl)	2M, Sigma-Aldrich. Autoclaved.	
	Ethylenediaminetetraacetic acid (EDTA)	0.5M, VWR Chemicals. Autoclaved	
	nonyl phenoxypolyethoxylethanol (NP-40)	10%, IGEPAL CA-630, Sigma-Aldrich.	
	Sodium deoxycholate	10%, Sigma-Aldrich.	
	N-Ethylmaleimide (NEM)	1M, Sigma-Aldrich.	
	Acrylamide	30%, Sigma-Aldrich.	
	Tetramethylethylenediamine (TEMED)	Sigma-Aldrich.	
	Sodium dodecyl sulphate (SDS)	10%, Melford. Autoclaved.	
	Ammonium persulfate (APS)	10%, Sigma-Aldrich.	
	Dextrose	0.1M, Sigma-Aldrich. Autoclaved.	
	Monopotassium phosphate (KH$_2$PO$_4$)	0.1M, Sigma-Aldrich. Autoclaved.	5
	Chloroform/isoamyl alcohol mixture (24:1 ratio)	Invitrogen.	

	Cetrimonium bromide (CTAB)	2%, Sigma-Aldrich.	
	Beta-mercaptoethanol	0.2%, Sigma-Aldrich.	
	Chitooctaose 8HCl	Stock solution of 100μM made by dissolving in DMSO, working concentration of 1μM made by diluting stock solution with water. Biosynth.	

2.1.10. DNA Kits

Table 2.9. DNA extraction kits used in this project, usage, and source.

Kit	Use	Source
ZR Plasmid Miniprep	Isolate plasmids from bacterial cultures.	Zymo Research
Monarch® DNA Gel Extraction Kit	Isolate DNA band from agarose gel.	New England Biolabs

2.2. DNA Analysis and Manipulation

2.2.1. Genomic DNA Extraction

One 2–3-week-old *Arabidopsis* leaf was placed in a 1.5 Eppendorf tube with 150μL of

DNA extraction buffer. The leaf tissue was homogenized with a micro pestle until tissue and

buffer became a liquid solution. The sample was centrifuged at 16,242 ×g for 5 minutes, and

the supernatant was transferred into a new Eppendorf tube. One hundred microlitres of

isopropanol was added and mixed by inverting the tube. The mixture was allowed to stand for

5 minutes, then centrifuged at 16,242 ×g for 10 minutes. Following centrifugation, the

supernatant was removed, leaving the pellet remaining. Five hundred microlitres of 70%

ethanol was then added, and the mixture was pipetted up and down to dislodge and mix the

pellet. The mixture was then centrifuged at 16,242 ×g for 5 minutes, the supernatant was

removed, and the pellet was centrifuged for an additional 1 minute. Additional supernatant

was removed. The Eppendorf tube containing the pellet was inverted upside down and left to

dry for 10 minutes. Fifty microlitres of 10mM Tris pH 8.5 was added and mixed by pipetting up

and down to dislodge the pellet. The concentration of the isolated DNA was measured using a

Nanodrop spectrophotometer (NanoDrop One, Thermo Scientific) machine and stored at -20°C.

2.2.2. Taq Polymerase PCR

One microlitre of genomic DNA was mixed with 1μL of 10μM forward primer, 1μL of

10μM reverse primer, 5μL of RedTaq mix and 2μL deionized water on ice. The mixture was run

in a thermocycler at 95°C for 6 minutes, and 30 cycles of the following: 95°C for 30 seconds,

55°C for 30 seconds, and 72°C for 30 seconds. After 30 cycles, the samples were heated at

72°C for 5 minutes, then stored at 10°C.

2.2.3. Agarose Gel Electrophoresis

For 50mL of 1% gel, 0.5g of agarose was mixed with 50mL of 1X TAE buffer and heated

in a microwave to dissolve for 1 minute. Half of a microlitre of ethidium bromide (VWR

Chemicals) was added to the mixture for DNA visualization. The gel was poured into a mould

containing wells and left to set for 30 minutes. The solid gel was then placed in an

electrophoresis tank containing 1X TAE buffer and 4μL of 1Kb Hyperladder (Meridian

Biosciences) was added to the first well to measure DNA band size. PCR amplified samples

were loaded into remaining wells. Samples were run at 125 volts for 30-45 minutes and then

visualized under UV light using the G: BOX F3 (Syngene).

Ten microlitres of 50mg/mL kanamycin was added to 10mL of LB liquid media and inoculated with *E. coli* culture containing the construct over a flame. The culture was grown overnight at 37°C with shaking at 4 ×g. The culture was then centrifuged at 2,795 ×g for 5 minutes and the supernatant was removed. The plasmid was then isolated from the culture using the Zymo Research Plasmid Miniprep kit following the manufacturer's instructions. The concentration of the isolated plasmid was measured using a nanodrop spectrophotometer (Thermo Scientific) and stored at -20°C.

2.2.5. DNA Sequencing and Analysis

The isolated plasmid was adjusted to recommended concentrations (150 ng/μL) and sent for sequencing along with 3.2μM AttB sequencing primers (Table 2.2). Sequencing data of constructs was aligned with coding sequences (CDS) from The *Arabidopsis* Information Resource (TAIR) database (https://www.arabidopsis.org/) using Clustal Omega multiple sequence alignment tool (https://www.ebi.ac.uk/Tools/msa/clustalo/).

2.2.6. Q5 PCR Gene Amplification

CERK1, *LYK5* and *PBL27* coding sequences were amplified from Col-0 *Arabidopsis* cDNA using *CERK1*, *LYK5* and *PBL27* forward and reverse primers respectively (Table 2.2). PCR amplification reaction was mixed on ice and contained the following components for a 50μL reaction:

2μL of 10mM deoxyribonucleotide triphosphates (dNTPs, Invitrogen)

2.5μL of 10μM forward primer

2.5μL of 10μM reverse primer

3μL of template Col-0 cDNA

10μL of 5X Q5 reaction buffer

10μL of 5X Q5 high GC enhancer

0.5μL of Q5 high fidelity DNA polymerase

22.5μL nuclease-free water

The reaction mixture was run in a thermocycler at 95°C for 6 minutes, and 30 cycles of the following: 95°C for 30 seconds, 65°C for 30 seconds, and 72°C for 2 minutes. After 30 cycles, samples were heated at 72°C for 5 minutes then stored at 10°C. Gel loading dye (New England Biolabs, 6X concentration) was added to amplified reaction mixture and run through agarose gel (section 2.2.3).

2.2.7. DNA Agarose Gel Extraction

Amplified PCR products run through agarose gel were extracted using a razor blade under UV light to visualize DNA bands. Gel fragments were placed in 1.5mL Eppendorf tubes and weighed. Gel extraction was carried out using the Monarch® DNA Gel Extraction Kit as per manufacturer's instructions. The concentration of isolated DNA was measured using a nanodrop spectrophotometer (Thermo Scientific) and stored at -20°C.

2.2.8. T4 Ligation

pJET cloning vector: 5μL of 10-20ng/μL DNA, 1μL pJET entry vector, 10μL ligase reaction buffer, 1μL T4 ligase and 3μL of nuclease-free water were mixed on ice. The reaction was left overnight at 16°C and transformed into DH5α competent *E. coli*.

pENTR entry vector: 250ng of linearized pENTR4 entry vector and 500ng of DNA were mixed with 2μL reaction buffer and 1μL T4 ligase enzyme. Nuclease-free water was added to make up a 20μL reaction. Reaction was left overnight at 16°C and transformed into DH5α competent *E. coli*.

2.2.9. Colony PCR

Single positive colonies growing on LB agar plates containing antibiotics were mixed with 5μL of nuclease-free water. Three microlitres of this mixture was added to 1μL of 10μM forward primer, 1μL of 10μM reverse primer and 5μL of RedTaq mix on ice. The mixture was run in a thermocycler at 95°C for 6 minutes, and 30 cycles of the following: 95°C for 30 seconds, 58°C for 30 seconds, and 72°C for 1 minute and 30 seconds. After 30 cycles, samples were heated at 72°C for 5 minutes, then stored at 10°C.

2.2.10. Restriction Enzyme Digestion

Twenty microlitres of vector was mixed with 5μL of 10X CutSmart buffer, 1μL each of restriction enzymes and 3μL of nuclease-free water. Reactions were placed at 37°C overnight for full digestion.

2.2.11. LR Clonase Reaction

One microgram of pENTR4 vector containing the coding sequence of each gene of interest was first linearized with a restriction enzyme outside of the coding sequence region (BspHI) so that any unreacted vector could not grow on LB containing kanamycin. Restriction digests was carried out according to restriction enzyme digestion protocol (section 2.2.10.) using 1 μg of pENTR entry vector and up to 50μL of nuclease-free water. The enzyme was then inactivated by incubating the mixture at 80°C for 20 minutes. One microlitre of 25ng/μL linearized entry vector was mixed with 1μL of 50ng/μL destination vector, 1μL of LR clonase II enzyme and 1μL of nuclease-free water on ice. The mixture was incubated at room temperature for 1 hour, then 0.5μL of proteinase K solution (Invitrogen) was added, and the mixture was incubated for another 10 minutes at 57°C. The mixture was then transformed into DH5α competent *E. coli*.

2.2.12. Site-Directed Mutagenesis

CERK1 pENTR4 entry vector was subjected to site-directed mutagenesis reactions using primers designed to cause single nucleotide substitutions at specified sites. PCR amplification reaction was mixed in Eppendorf tube on ice and contained the following components for a 50μL reaction:

1μL of 10mM dNTPs (Invitrogen)

2.5μL of 10μM forward primer

2.5μL of 10μM reverse primer

1μL of template *CERK1* pENTR4 entry vector

10μL of 5X Q5 reaction buffer

10μL of 5X Q5 high GC enhancer

0.5μL of Q5 high fidelity DNA polymerase

22.5μL nuclease-free water

The reaction mixture was divided into 4 PCR tubes each containing 12.5μL. Tubes were spread out in thermocycler in order of increasing temperature for gradient PCR. The reaction mixtures were run in thermocycler at 95°C for 6 minutes, then 27 cycles of the following: 95°C for 30 seconds, 50-72°C (temperature gradient across thermocycler) for 30 seconds, and 72°C for 2 minutes. After 27 cycles, samples were heated at 72°C for 5 minutes, then stored at 10°C. 6x gel loading dye (New England Biolabs) was added to 4μL of amplified reaction mixture and run through agarose gel (section 2.2.3). Reactions that showed amplified product of ~1.8 kb (size of *CERK1* CDS) in the agarose gel were used. The remaining 8.5μL of amplified product was digested with 0.5μL DpnI restriction enzyme and 1μL CutSmart buffer overnight at 37°C, and then transformed into DH5α competent *E. coli*.

2.3. Microbiology Methods

2.3.1. *E. coli* Growth

E. coli liquid cultures were grown in LB media with 50μg/mL Kanamycin or 100μg/mL Ampicillin overnight at 37°C with 4 ×g shaking. *E. coli* plated on LB agar media containing 50μg/mL kanamycin or 100μg/mL Ampicillin was grown overnight at 37°C.

2.3.2. *Agrobacterium* Growth

Agrobacteria liquid cultures were grown in LB media containing 50μg/mL Kanamycin, 50μg/mL Rifamycin and 25μg/mL Gentamycin overnight at 28°C with 4 ×g shaking. *Agrobacteria* plated on LB agar media containing 50μg/mL Kanamycin, 50μg/mL Rifamycin and 25μg/mL Gentamycin was grown for two days at 28°C.

2.3.3. *E. coli* Transformation

One to five microlitres of DNA construct to be transformed and 200μL of DH5α competent *E. coli* stored at -80°C were thawed on ice and then mixed in a 1.5mL Eppendorf tube. The mixture was incubated on ice for 20minutes. The mixture was then heat shocked in 42°C water for 1 minute and transferred back to ice for 5 minutes. Eight hundred microlitres of liquid LB was added to the mixture over a flame, then placed at 37°C with 4 ×g shaking for 2 hours. After 2 hours, the mixture was centrifuged at 6,151 ×g for 2 minutes and 700μL of supernatant was removed. Remaining liquid was mixed with the pellet to resuspend cells and plated on LB agar media containing 50μg/mL kanamycin or 100μg/mL Ampicillin over a flame by evenly spreading the mixture around petri dish with a streaking stick. Plates were placed at 37°C to grow overnight.

2.3.4. *Agrobacterium* Transformation

Five hundred nanograms of DNA construct to be transformed and 200μL of competent GV3101 *Agrobacterium* cells stored at -80°C were thawed on ice and then mixed in a 1.5mL Eppendorf tube. The mixture was flash frozen in liquid nitrogen and then placed in 37°C water

for 3 minutes. After 3 minutes, the mixture was placed on ice for 5 minutes. One millilitre of liquid LB was added to the mixture over a flame, then placed at 28°C with 4 ×g shaking for 2-4 hours. The mixture was then centrifuged at 1,538 ×g for 2 minutes and 900μL of supernatant was removed. The remaining liquid was mixed with the pellet to resuspend cells and plated on LB agar media containing 50μg/mL Kanamycin, 50μg/mL Rifamycin and 25μg/mL Gentamycin over a flame by evenly spreading the mixture around petri dish with a streaking stick. The petri dish was placed at 28°C to grow for 2 days.

2.4. Plant growth

2.4.1. *Nicotiana benthamiana* Growth

N. benthamiana plants were grown at 28°C with 16 hours of light and 8 hours of dark and watered regularly.

2.4.2. *Arabidopsis thaliana* Growth

Arabidopsis seeds were sown in wet Levington Advance F2 + Sand soil and placed at 4°C for three days for stratification. Plants were then transferred to Panasonic MLR Plant Growth Chambers programmed to long day growing: 16 hours of light at 22°C and 8 hours of dark at 20°C with a constant humidity of 70%. After 2 weeks, seedlings were transferred into individual pots in a 24-pot tray and watered 2-3 times a week.

2.5. Protein Analysis

2.5.1. Agroinfiltration

Expression clones containing genes of interest as well as free-GFP as a positive control, and p19 RNA silencing suppressor were transformed into GV3101 competent *Agrobacteria* (section 2.3.4.) and grown overnight in liquid LB and antibiotics according to section 2.3.2. 750μL of each culture was mixed with 250μL 100% glycerol over a flame and flash frozen in liquid nitrogen. These glycerol stocks were stored at -80°C for future use. The remaining 9.25mL of each culture was centrifuged at 2,264 ×g for 10 minutes. After discarding the supernatant, the pellet was washed by resuspending in 10mL of 10mM $MgCl_2$ and centrifuging again at 2,264 ×g. This washing process was repeated. After the second wash, cells were resuspended in 10mL of $MgCl_2$ and the optical density at a wavelength of 600nm (OD_{600}) was measured using a spectrophotometer (GeneQuant 1300). Samples containing each construct of interest as well as free-GFP were mixed with the culture containing p19 and diluted with $MgCl_2$ so that the final OD_{600} of both construct and p19 was 0.1. Acetosyringone solution was added to each culture to yield of final concentration of 200μM acetosyringone. Cultures were then placed in the dark for 2 hours. Each culture was infiltrated into the underside of 3-4 lower leaves of a 4-5-week-old *N. benthamiana* plant with a blunt end syringe. Plants were then left to grow in conditions described in section 2.4.1 for 48 hours.

2.5.2. Tissue Harvesting

After 48 hours, infiltrated leaves of *N. benthamiana* plants were removed and the midrib of each leaf was cut out. Leaves were weighed and compiled to reach a final weight of

2-3 grams per sample. Samples were wrapped in aluminium foil, flash frozen in liquid nitrogen

and stored at -80°C.

2.5.3. Protein Extraction

The protein lysis buffer was prepared on ice and 1 tablet of proteinase inhibitor per

10mL of buffer was added. All equipment including mortar and pestle, liquid nitrogen spoon

and surrounding area were wiped liberally with 70% ethanol. In 4°C cold laboratory, liquid

nitrogen was spooned into the mortar and frozen leaf tissue sample was added. Tissue was

broken with the pestle in the liquid nitrogen, and then ground to a power when the liquid

nitrogen had evaporated. Another spoonful of liquid nitrogen was added, and the sample was

ground again with the pestle. This process was repeated one more time, and when the final

spoonful of liquid nitrogen had evaporated, a capful of PVPP was added to prevent oxidization

of the sample. Next, protein lysis buffer was added in a 1g:1mL tissue sample to buffer ratio.

The sample was covered with aluminium foil and left to thaw slowly in the cold laboratory for

approximately 1 hour. After 1 hour, the lysis buffer was mixed into the sample with the pestle

to form a thick paste. After another 20 minutes of thawing, the sample was a "smoothie"

consistency and was poured into pre-cooled 2mL Eppendorf tubes. The sample was then

centrifuged at 20,768 ×g for 10 minutes at 4°C, and the supernatant was transferred into a new

pre-cooled 2mL tube. The sample was centrifuged again at 20,768 ×g for 10 minutes at 4°C.

The supernatant was transferred to a new pre-cooled 2mL tube and placed on ice in the cold

laboratory. For 2mL of protein extract, 50μL was removed and placed in new 1.5mL tube. 18μL

of 4X Laemmli buffer was added, and this sample was flash frozen. This would be the protein input sample. The remaining protein extract was used for immunoprecipitation.

2.5.4. Immunoprecipitation

Twenty-five microlitres of Anti-GFP beads or anti-HA beads were added to ~2mL of protein extract and inverted 4 times to mix. The sample was then left on ice positioned diagonally for 15 minutes. After 15 minutes, the sample was placed on a rotator and spun for 15 minutes. Meanwhile, a MACS magnetic column was arranged in the μMACS separator on the MACS MultiStand magnetic stand in the cold laboratory (all Miltenyi Biotec). The column was calibrated with 500μL of protein lysis buffer. After 15 minutes, the protein extract sample was removed from the rotator and pipetted into the column. The column was left for 15 minutes for the sample to flow through. After the sample had emptied out of column, 500μL of protein lysis buffer was added and left to flow through for 5 minutes. This step was repeated two more times for a total of 3 washes. The apparatus was then moved to room temperature and a 1.5mL Eppendorf tube was placed under the column. The column was eluted with 20μL 1x Laemmli dye (heated to 98°C). After the 20μL had flown through the column, 60μL more 98°C 1x Laemmli dye was added. The column was pressed down from the top to create a vacuum if the sample got stuck. The immunoprecipitation sample in the Eppendorf tube was then flash frozen in liquid nitrogen and stored at -80°C. The column was reused 3-4 times by rinsing with deionized water, running 2mL of deionized water through the column 1mL at a time, running 2mL of 1% SDS through the column 1mL at a time and finally running 2mL of 100% ethanol through the column 1mL at a time.

Two glass plates with a 1.5mm gap (front plate and back plate) were pressed together and set into a casting frame. The frame containing glass plates was then set into a casting stand. 8% polyacrylamide gels were made by hand and were composed of a resolving gel and a stacking gel. The resolving gel was poured first and 2mL of 100% isopropanol was immediately poured on top to ensure level setting of the gel and to prevent oxidation. After 15 minutes, the gel had set, and the isopropanol was removed. The stacking gel was immediately poured over the resolving gel, and a 10-well 1.5mm comb was placed in the top. The gel was allowed to set for another 15 minutes. The composition of each gel are as follows:

Resolving gel

4.6mL deionized water

2.7 mL 30% acrylamide

2.5mL 1.5M Tris, pH 8.8

0.1mL 10% SDS

0.1mL 10% APS

0.006mL TEMED

Stacking gel

2.1mL deionized water

0.5mL 30% acrylamide

0.38mL 1M Tris, pH 6.8

0.3mL 10% SDS

0.3mL 10% APS

0.003mL TEMED

The glass plates containing the gel were removed from the stand and frame and assembled into the electrophoresis gasket with the front plate facing inward. The gasket was then placed in the electrophoresis tank and 1x running buffer was added to fully submerge the gel. Once submerged, the comb was removed. Eight microlitres of PageRuler Plus Pre-Stained Protein Ladder (Thermo Fisher Scientific) was loaded into the first lane. Immunoprecipitation and input samples were prepared by thawing from -80°C on ice, and then placing in a 98°C heating block for ~30 seconds right before loading into gel. Thirty microlitres of immunoprecipitation sample and 10μL of input sample were pipetted into wells, and the electrophoresis tank was set to run at 80 volts for the first 30 minutes, or until the protein samples had run through the stacking gel. After 30 minutes, the voltage was turned to 100V for about 2 hours.

2.5.6. Protein Transfer

A polyvinylidene fluoride (PVDF) membrane (Immobilon-PSQ, Sigma-Aldrich) was cut to 7x9cm and activated by incubating with 100% methanol for 5 minutes on shaker at low speed. The membrane was then removed from the methanol and placed in 1x transfer buffer on shaker at low speed. After 2.5 hours, the glass plates containing the gel was removed from the electrophoresis tank and gasket, and the front plate was gently lifted. The stacking gel layer was cut away and the remaining gel was carefully lifted into 1x transfer buffer and placed on shaker at low speed for 5 minutes. The transfer cassette components were placed in large tub containing 1x transfer buffer and fully submerged. The transfer cassette sandwich was assembled in the following order:

Clear side of cassette frame

1 black sponge

1 blue sponge

2 sheets of blotting paper

PVDF membrane

Resolving gel

2 sheets of blotting paper

1 blue sponge

1 black sponge

Black side of cassette frame

The clamp was then closed firmly shut and the cassette was placed in the conductor unit within the Mini-Protean Tetra gel tank (BIO-RAD) along with an ice pack and more 1x transfer buffer to fully submerge the cassette. The transfer was run at 25V in the 4°C cold laboratory overnight.

2.5.7. Immunoblotting

Following the overnight transfer, the PVDF membrane was removed from the transfer cassette and placed in 1x TBST buffer on shaker for 5 minutes at medium speed. Blocking buffer was prepared by mixing skim milk powder with 1xTBST buffer to a final concentration of 5%. The membrane was then placed in blocking buffer and set on rocker for 1-2 hours at low speed with the active side of the membrane facing upwards. The membrane was then removed from blocking buffer and washed for 5 minutes in 1xTBST buffer on shaker at medium speed. The membrane was then placed in 1x TBST buffer containing the correct primary

antibody (Table 2.5) and 0.25% skim milk and incubated on a rocker at low speed in the cold laboratory overnight. The following morning, the membrane was removed from primary antibody and washed with 1xTBST buffer 6 times for 5 minutes each on shaker at high speed. The membrane was then placed in 1xTBST buffer containing the correct secondary antibody (Table 2.5) and left to incubate on rocker for 1 hour at low speed. The membrane was removed from the secondary antibody and washed 10 times in 1xTBST for 5 minutes each on shaker at high speed.

2.5.8. Protein Visualization

After the final wash, 1xTBST buffer was removed from the membrane. Peroxide solution and luminol enhancer solution (Bio-Rad Clarity Western ECL Substrate Kit) were mixed in a 1:1 ratio, 2mL total for 1 membrane. This mixture was poured over the membrane and swirled over the surface of the membrane for 2 minutes. The membrane edges were blotted on tissue paper for about 30 seconds to remove excess liquid, then placed onto a layer of transparent copier film in a light-proof cassette. Another layer of copier film was placed on top of the membrane, and any air bubbles between the film and the membrane were removed. The copier film was taped securely into the cassette, and the cassette was closed tightly. The membrane in the cassette was taken to the dark laboratory and exposed to Fujifilm X-ray film (Fisher) for 30 seconds to 1 hour depending on exposure time required. The exposed X-ray film was then placed in Protec Optimax 2010 X-Ray film processor to develop. The resulting immunoblots were photographed and converted to greyscale.

2.6. *Botrytis cinerea* Infection Assay

2.6.1. *Botrytis cinerea* Growth and Maintenance

Botrytis cinerea strain HA/5 was re-streaked onto petri dishes containing PDA in a flume hood in the fungal pathology laboratory. The petri dishes were sealed with Parafilm (StarLab) and placed in the dark at 23°C. After two weeks of growth, sterile forceps were used to cut a small square in the PDA in a region that contained *B. cinerea* spores (brown fluffy regions, Figure 2.2). This PDA square was then placed onto the surface of new PDA plate and sealed with parafilm. This process was repeated very 2 weeks.
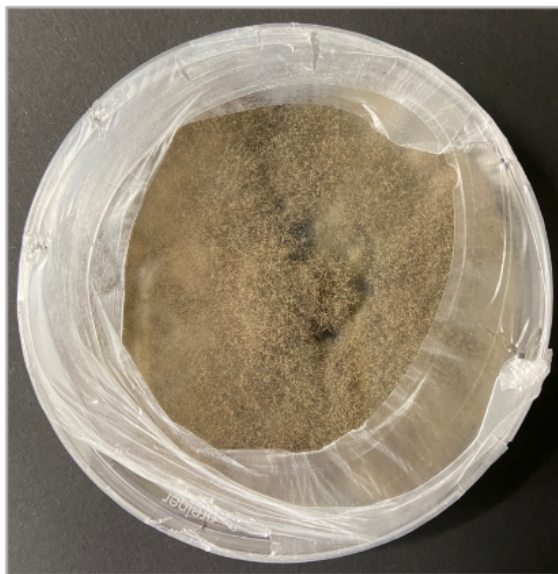
Figure 2.2. *Botrytis cinerea* strain H/A5 grown for 3 weeks at 23°C in the dark on PDA. Brown furry regions are conidiophores (spores). Picture taken by author.

2.6.2. Spore Suspension Preparation

Eight to ten millilitres of sterile 0.02% Tween20 was poured onto the surface of 2–3-week-old *B. cinerea* cultures on PDA plates. A sterile L spreader was used to spread the Tween20 around the plate and scrape the surface to release the spores into the solution. The liquid was then poured into a 50mL falcon tube, and the process was repeated with 2-3 plates

total, pooling liquid into the same falcon tube. The falcon tube was then vortexed for 1 minute.

Circular sterile filter paper was folded twice to create a cone shape and fitted into a fresh 50mL

falcon tube. The spore suspension was poured into the filter paper slowly to filter out mycelial-

hypha fragments. The filtered spore suspension was centrifuged at 25,155 ×g for 10 minutes

and the supernatant was removed. The spore pellet was resuspended in 1mL of sterile water.

The spore concentration was measured by placing 10μL of suspension onto the grid section of a

5x5 haemocytometer (Hecht Assistent®, Germany) and covering with a cover slip. The

haemocytometer was placed onto the stage of an optical microscope and viewed under X400

magnification. Spores were counted in all 16 squares of section A, B, C, D and E (Figure 2.3).

The total number of spores in each section was calculated by adding up the spore count in each

of the smaller 16 squares, and then the average was calculated by adding the total number of

spores in each section together and then dividing by 5. This average spore count was then

multiplied by 10^4 to obtain the concentration of spores/mL. The concentration of spores was

then diluted to 3.0×10^6/mL. One millilitre of spore suspension was then mixed with 1.1mL of

0.1M sterile dextrose, and 0.73mL of 0.1M sterile KH_2PO_4 (pH 5), bringing the final spore

suspension concentration to 1.06×10^6. The mixture was left to incubate at room temperature

for 1 hour.
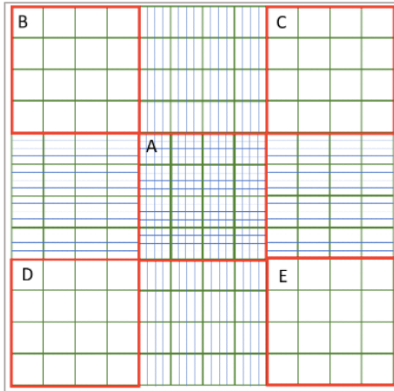
Figure 2.3. Haemocytometer. Spore concentration calculated by counting the spores in each square and using the formula: spores/mL= $\left[\frac{A+B+C+D+E}{5}\right] \times 10^4$. Figure taken from bitesizebio.com.

2.6.3. *B. cinerea* Infection Assay

Leaves of similar size and developmental stage of 4–5-week-old *Arabidopsis* plants were removed and placed on a square petri dish containing 0.6% agar. Five leaves of each genotype were placed in a row on a single plate, and an additional leaf from each genotype was placed below as a water control. This was repeated with two more plates for a total of 15 leaves per genotype. Ten microlitres of spore suspension was dropped onto one side of each leaf, and 10μL of control solution made up of 1 mL of sterile water, 1.1mL of 0.1M sterile dextrose, and 0.73mL of 0.1M sterile KH_2PO_4 (pH 5) was pipetted onto control leaves. Plates were sealed with micropore tape (3M) and placed in the dark at 23°C. Photographs of leaves were taken at 3-, 4- and 5-days post infection (DPI). At 5 DPI, Leaves were pooled into samples of 5 leaves each, wrapped in aluminium foil, flash frozen in liquid nitrogen and stored at -80°C.

2.6.4. Lesion Size Data Analysis

ImageJ software was used to measure the total area of each leaf and total area of each lesion of respective leaves from photographs taken at 5DPI. Lesion % of total leaf area was

then calculated for all 15 leaves of each genotype. The experiment was repeated 3 times to obtain a total count of 60 leaves per genotype. Outliers were removed from dataset using the interquartile range (IQR) method. Quartile 1 (Q1) and quartile 3 (Q3) were calculated using excel, and the IQR was calculated by subtracting Q1 from Q3. The upper bound of the dataset was calculated by the formula Q3 + (1.5*IQR) and the lower bound of the dataset was calculated by the formula Q1 – (1.5*IQR). Any data points above the upper bound or below the lower bound were removed from the dataset.

2.6.5. Fungal DNA Extraction

A frozen *B. cinerea* assay leaf sample was placed in a mortar and pestle, along with a spoonful of liquid nitrogen. The sample was ground into a fine powder with the pestle once the liquid nitrogen had evaporated. One millilitre of CTAB extraction buffer was added to the sample and left to thaw for 10 minutes. Once thawed, the sample was mixed with the pestle and poured into 2mL Eppendorf tubes. The sample was incubated at 60°C for 1 hour with intermittent mixing on a vortex, then centrifuged at 16,242 ×g for 5 minutes. The supernatant was transferred to a new 1.5mL Eppendorf tube. Two hundred microlitres of chloroform/isoamyl alcohol mixture (24:1 ratio) was added per 1mL of sample and mixed with a vortex. The sample was centrifuged again at 16,242 ×g for 5 minutes. The supernatant was collected, and this process was repeated with another 200μL of chloroform/isoamyl alcohol. The final supernatant was collected (aqueous layer) and 0.7mL of 100% isopropanol was added per 1mL of sample. The sample was mixed and left for 30 minutes at -20°C for DNA to precipitate. The sample was then centrifuged at 4,709 ×g for 5 minutes, and the supernatant

was removed. The DNA pellet was washed by adding 0.5mL of 70% ethanol and pipetting up and down to dislodge and mix the pellet. The sample was centrifuged again at 4,709 ×g for 5 minutes. The supernatant was removed, and the DNA sample was left to dry by placing the open tube upside down on a tissue for 1 hour. When the pellet was completely transparent, the DNA was resuspended with 50μL of ultrapure water. The concentration of the DNA was measured using a nanodrop spectrophotometer.

2.6.6. Quantitative PCR (qPCR)

PCR reactions were prepared in a 96-well PCR plate on ice in dark lighting. A single PCR reaction consisted of the following components:

5μL 1x SYBR Green JumpStart Taq ReadyMix

0.5μL 10mM forward primer

0.5μL 10mM reverse primer

3μL nuclease-free water

1μL 100ng/μL DNA

B. cinerea Actin was amplified to measure fungal DNA accumulation and *Arabidopsis ubiquitin* was used as a reference. Each reaction had three technical replicates. Samples were run in StepOnePlus Real-Time PCR System (Applied Biosystems) under the following conditions: 95°C for 20 seconds then 25 cycles consisting of the following steps: 95°C for 30 seconds, and 55-65°C for 30 seconds. Following 25 cycles, samples were heated at 72°C for 2 minutes, then stored at 10°C.

<u>2.6.7. qPCR Data Analysis</u>

The average Ct (take-off) value of each sample was obtained using the Ct values of 3 technical replicates of each sample. Average Ct vales of *B. cinerea Actin* for each genotype was subtracted by the average Ct value of *Arabidopsis Ubiquitin* of the corresponding sample. This value was the change in Ct (ΔCT). The formula $2^{-\Delta CT}$ was used to obtain the relative gene copy number of *B. cinerea Actin* compared to *Arabidopsis Ubiquitin*, and therefore the relative fungal DNA accumulation (or relative fungal load) in each sample.

2.7. Confocal Microscopy

Leaf samples of $0.5cm^2$ were cut from *N. benthamiana* leaves with a razor at 2 DPI and mounted on a microscope slide (VWR Chemicals) with water. Samples were then covered with 22x22mm cover slips (Menzel Glaser) and secured with micropore tape. The slide was placed on the stage of a Zeiss LSM 880 confocal microscope, 64x objective oil lens was used for viewing and an argon laser was used to excite GFP at 488nm. Images were processed with ImageJ.

3.0. Checking and Validating Constructs and Plant Lines

3.1 Introduction

The primary materials received at the start of this project from Dr. Sadanandom's laboratory stores were two CDS constructs for the co-immunoprecipitation assays and five transgenic *Arabidopsis* line seeds for the *B. cinerea* infection assays. The CDS constructs were *CERK1^{WT}* in p104 pEarlyGate vector (*CERK1^{WT}* p104) and *CERK1^{3KR}* in p104 pEarlyGate vector (*CERK1^{3KR}* p104). The transgenic seeds were *CERK1* knockout *(cerk1-2 K/O)*, *CERK1* complement line 1 *(cerk1-CM1)*, *CERK1* complement line 2 *(cerk1-CM2), CERK1* 3KR line 2-5 *(cerk1-3KR-2-5),* and *CERK1* 3KR line 3-6 *(cerk1-3KR-3-6).* As previously mentioned in section 1.8, the immunoprecipitation assays were carried out using the *CERK1^{WT}* p104 and *CERK1^{3KR}* p104 constructs. After a few experimental replicates, expression of CERK1 on immunoblots could not be visualized, so constructs were sequenced as a troubleshooting protocol. It was discovered that the constructs contained potentially destabilizing mutations, so the transgenic *Arabidopsis* lines that had also been received as materials were genotyped to confirm their identity as a precautionary measure. The transgenic plant lines were found to not be transgenic but only Col-0 and *cerk1-2* K/O lines. The next steps of this research project were then shifted to prioritize re-cloning *CERK1^{WT}* and re-inserting the SUMO-site mutations via site-directed mutagenesis to carry out co-immunoprecipitation assays. Ideally, once constructs had been cloned, transgenic *Arabidopsis* plant lines could be remade for *B. cinerea* infection assays. However, there was not enough time to remake transgenic *Arabidopsis* lines due to the time constraints of this project.

3.2. Results

3.2.1. Transient Expression of *CERK1*^{WT} p104 and *CERK1*^{3KR} p104 Constructs in *N. benthamiana*

CERK1^{WT} p104 and *CERK1*^{3KR} p104 expression clones were transformed into

Agrobacteria and infiltrated into the underside of 4-week-old *N. benthamiana* plants. 2 days

post infiltration, leaf tissue was harvested, and total protein was extracted. The GFP-tagged

CERK1 proteins were then purified with immunoprecipitation using anti-GFP beads. Purified

samples were then run through SDS-PAGE along with total protein input samples. Separated

protein in gel was then transferred to a PVDF membrane and immunoblotted with anti-GFP.

The protein was visualized using chemiluminescence and X-ray paper. Plants infiltrated with

the free-GFP expression clone were used as a positive control for protein extraction and

immunoblotting. CERK1 protein is 67.3kDa and GFP is 27kDa, so the CERK1-GFP fusion protein

should be 94.3kDa. CERK1^{WT} and CERK1^{3KR} protein expression was not visualized on

immunoblots after multiple attempts, while high expression of the GFP positive control a (band

at 27kDa in the GFP input lane) was visualized (Figure 3.1.)

Figure 3.1. Immunoblot lacking visible expression of CERK1^{WT} and CERK1^{3KR}. Total protein from *N. benthamiana* leaves infiltrated with *CERK1^{WT}* p104 and *CERK1^{3KR}* p104 was extracted 2 days post infiltration. 50μL of total protein was preserved as input, and the rest was purified by immunoprecipitation using anti-GFP beads (IP: α GFP). IP and Input samples were then separated on an SDS-PAGE gel, transferred to a PVDF membrane, and immunoblotted with anti GFP (IB: α GFP). CERK1 = 67.3 kDa, GFP = 27 kDa, CERK1-GFP = 94.3kDa. Experiment was repeated several times with the same result.

3.2.2. Sequencing *CERK1* Constructs

As a troubleshooting protocol to determine why proteins were not being expressed on immunoblots, *CERK1^{WT}* p104 and *CERK1^{3KR}* p104 constructs were subjected to sequencing to check that no mutations were present. *E. coli* cultures containing constructs were grown overnight from frozen glycerol stocks and plasmids were isolated using the ZR Plasmid Miniprep kit. Plasmids were then sequenced using AttB primers which span the gateway cloning region and CDS (Table 2.2). The resulting sequencing data was aligned with the *CERK1* CDS from the TAIR *Arabidopsis* online database. *CERK1^{WT}* p104 contained a nucleotide change of A to G at 1459 base pairs (bp) which translated into an amino acid change of glutamic acid to glycine at position 467 (Figure 3.2). *CERK1^{3KR}* p104 contained a nucleotide change of G to A at 249 bp,

53

which translated into an amino acid change of aspartic acid to asparagine at position 64 (Figure

3.3, A). *CERK1³ᴷᴿ* p104 also contained a deletion at 1037 bp, which translated into a protein

with a shifted reading frame and premature stop codon at position 326 (Figure 3.3, B). Finally,

CERK1³ᴷᴿ p104 contained only two of the three nucleotide changes that translated into K to R

SUMO-site mutations and did not contain a nucleotide change of A to G at bp 827, which would

have translated into the K276R SUMO-site mutation (Figure 3.3, C).
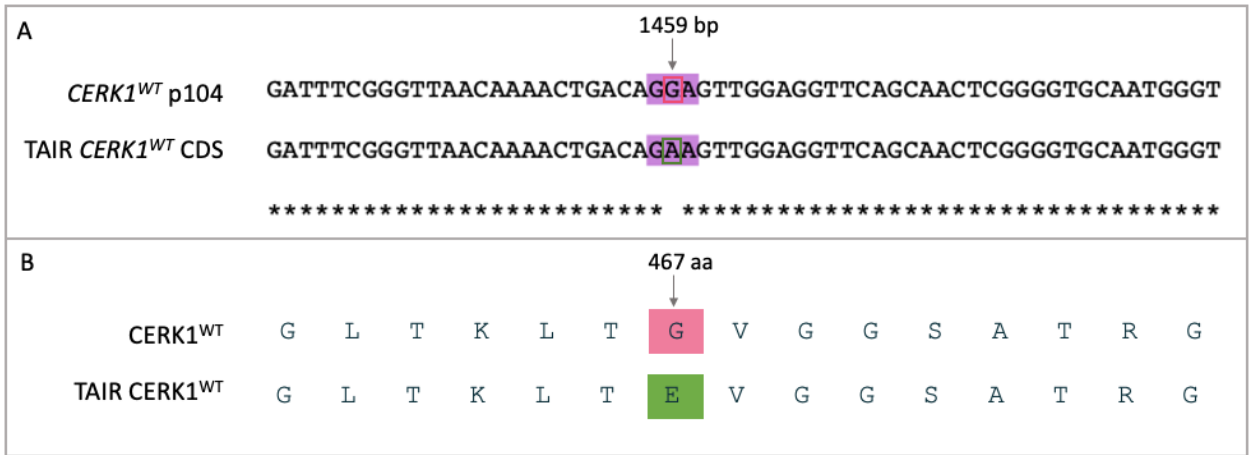
Figure 3.2. Nucleotide and amino acid sequence alignment of *CERK1ᵂᵀ* p104 with *CERK1* CDS **(A)** Nucleotide sequence alignment of *CERK1ᵂᵀ* p104 with *CERK1* CDS (AT3G21630.1) from TAIR online database (https://www.arabidopsis.org/) shows nucleotide change of A to G at 1459 bp. **(B)** This nucleotide change translated to an amino acid change from glutamic acid (E) to glycine (G) at position 467.
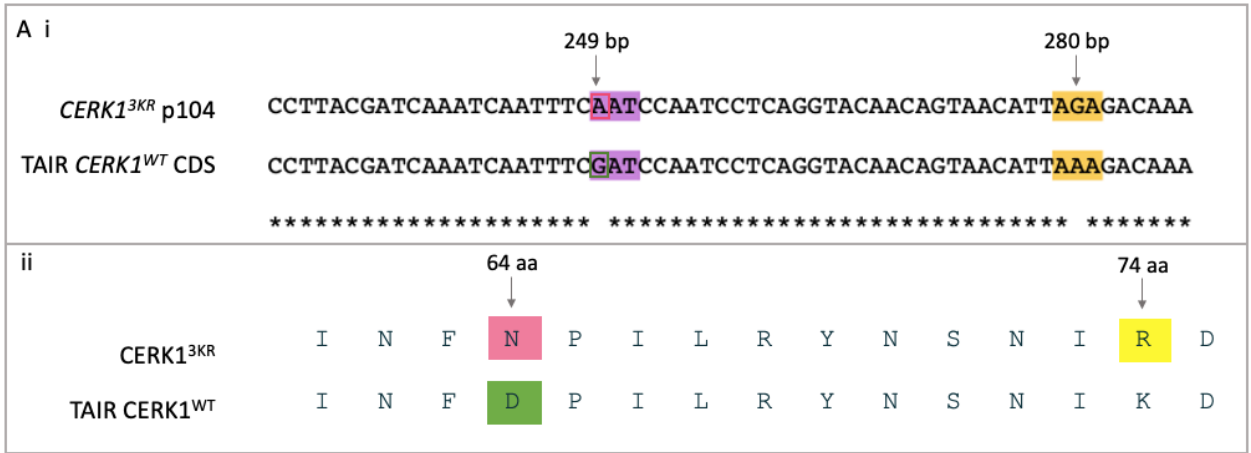
Figure 3.3. Nucleotide and amino acid sequence alignment of *CERK1³ᴷᴿ* p104 with *CERK1* CDS (AT3G21630.1) from TAIR online database (https://www.arabidopsis.org/) **(A, i)** Nucleotide change of G to A at 249 bp (Purple) and nucleotide change of A to G at 280 bp (yellow) **(A, ii)** Nucleotide changes translate into amino acid change from aspartic acid (D) to asparagine (N) at amino acid 64 and lysine (K) to arginine (R) (K74R SUMO-site mutation). **(B, i)** Deletion of T at 1037 bp. **(B, ii)** Deletion causes reading frame shift in translated amino acid sequence at position 326, leading to a premature stop codon at position 341. **(C, i)** Lack of A to G nucleotide change at 827 bp. **(C, ii)** Sequence translates to protein that does not contain lysine (K) to arginine (R) amino acid change at position 276. Resulting protein lacks K276R SUMO-site mutation. Figures generated using Clustal Omega multiple sequence alignment tool and PowerPoint.

3.2.3. Genotyping Transgenic *Arabidopsis*

Transgenic *Arabidopsis* seeds that were to be used in experiments for the duration of this project were subjected to genotyping analysis to confirm their identity. Transgenic seeds included *CERK1* knockout *(cerk1-2 K/O)*, *CERK1* complement line 1 *(cerk1-CM1)*, *CERK1* complement line 2 *(cerk1-CM2), CERK1* 3KR line 2-5 *(cerk1-3KR-2-5),* and *CERK1* 3KR line 3-6

(cerk1-3KR-3-6). Two sets of primers were used to amplify *CERK1* exon 5-8 and *CERK1* exon 10-12 (Table 2.2). Based on the size of the amplified bands, it was possible to determine if the plant lines were transgenic or not.   The expected results are that the 5-8 exon primer set amplifies a region of 713 bp in Col-0 and *cerk1-2* K/O, and a region of 713 bp and 460 bp in the *CERK1* complement lines. The 10-12 exon primer set amplifies a region of 723 bp in Col-0, and 380 bp in the complement lines (Table 3.1). Both primer sets amplify a smaller band in the CERK1 complement lines because they contain a copy of the *CERK1* CDS which lacks introns and is therefore smaller than the *CERK1* genomic sequence.   The 10-12 exon primer set does not amplify a band in the *cerk1-2* K/O because this region includes the T-DNA insert, which is too large to be amplified (Figure 3.4). Figure 3.5 shows the amplified products run through agarose gel. The Col-0 sample produced a band of 713 bp when amplified with the exon 5-8 primer set and a band of 723 bp when amplified with the exon 10-12 primer set. The *cerk1-2* K/O sample produced a band of 723 bp when amplified with the exon 5-8 primer set, and no band when amplified with the exon 10-12 primer set, indicating the presence of the T-DNA insertion between exon 10 and 11. The *cerk1-CM1* sample produced a band of 713 bp when amplified with the exon 5-8 primer set and a band of 723 bp when amplified with the exon 10-12 primer set, which are the band sizes expected for Col-0. The *cerk1-CM2*, *cerk1-3KR-2-5* and *cerk1-3KR-3-6* samples all produced a band of 723 bp when amplified with the exon 5-8 primer set, and no band when amplified with the exon 10-12 primer set, which are the results expected for the *cerk1-2* K/O (Figure 3.5).

Table 3.1. Genotyping primers and predicted amplicon size for Col-0 and each transgenic *Arabidopsis* line.

	Col-0	*Cerk1-2* K/O	CERK1 Complement & CERK1 3KR

Primer set 1: exon 5-8	713 bp	713 bp	713 bp & 460 bp
Primer set 2: exon 10-12	723 bp	No band	380 bp
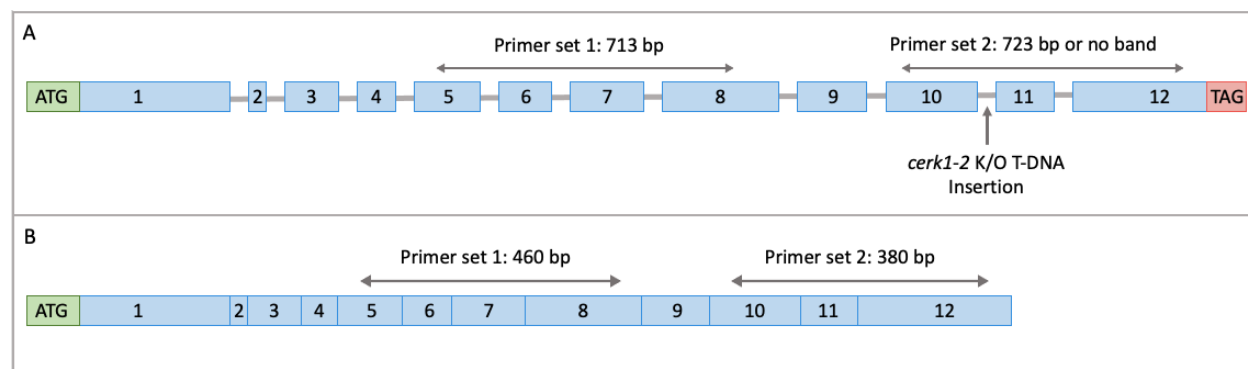
Figure 3.4. Schematic diagram of regions that each genotyping primer is designed to amplify in CERK1 gene and CDS, and predicted band size. **(A)** *CERK1* gene containing introns causes primer set 1 to amplify a region of 713 bp, and primer set 2 to amplify a region of 723 bp or no band when the T-DNA insertion in present. **(B)** *CERK1* CDS does not contain introns and causes primer set 1 to amplify a region of 460 bp and primer set 2 to amplify a region of 380 bp. Image adapted from (Miya et al. 2007) by author in PowerPoint.
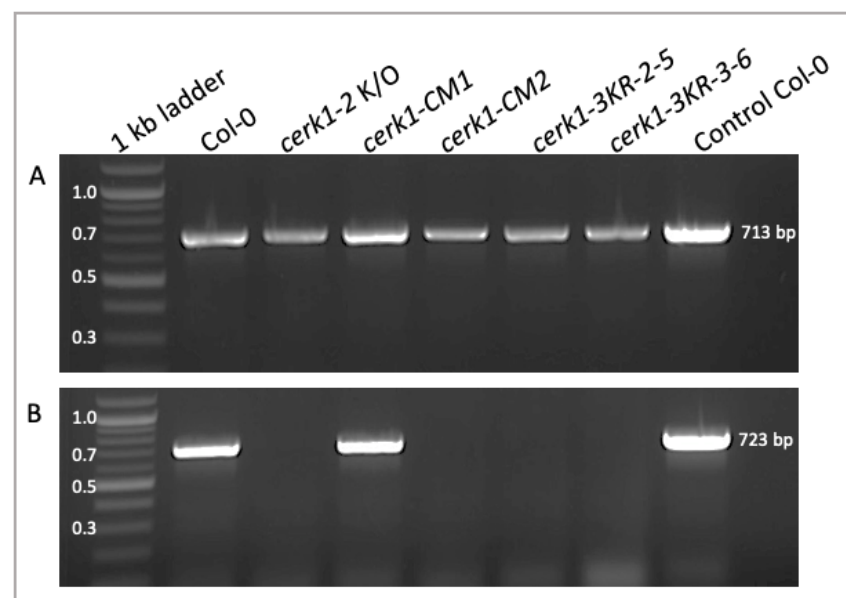
Figure 3.5. Amplified DNA from Col-0 and transgenic *Arabidopsis* samples run through 1% agarose gel. **(A)** Primer set 1 amplified a region in *CERK1* from exon 5 to exon 8. **(B)** Primer set 2 amplified a region in *CERK1* from exon 10 to exon 12. This experiment was repeated with the same results.

3.3. Discussion

3.3.1. *CERK1^{WT}* p104 and *CERK1^{3KR}* p104 Constructs Contained Potentially Destabilizing Mutations

CERK1^{WT} and CERK1^{3KR} did not show expression on immunoblots while the GFP positive control did show expression. CERK1 is a transmembrane protein and is embedded in the cellular membrane, making protein extraction difficult. The SDS in the lysis buffer is a strong detergent that can solubilize the membrane to extract membrane-bound proteins. However, it also can denature protein 3D structure and is not suitable for sensitive or unstable proteins (Lewis 1997). It was discovered in section 3.2.2. that both *CERK1^{WT}* p104 and *CERK1^{3KR}* p104 contained missense mutations leading to amino acid changes. In *CERK1^{WT}* p104, the change of A to G at nucleotide 1459 translated into a missense mutation of glutamic acid to glycine at amino acid 467. This change replaced a negatively charged amino acid to a neutral amino acid within the kinase domain of the protein (Figure 3.6a). In *CERK1^{3KR}* p104, the substitution of G to A at nucleotide 249 caused a missense mutation in the first lysM domain, replacing negatively charged aspartic acid to neutral asparagine. It is possible that these mutations disrupted a hydrogen or ionic bond in the tertiary structure of the protein, affecting protein stability and or function. Additionally, the deletion of a T residue at nucleotide 1037 in *CERK1^{3KR}* p104 caused a frameshift mutation at amino acid 326, leading to a premature stop codon at amino acid 341 (Figure 3.6b). This truncation occurred at the beginning of the kinase domain, so it is likely to significantly affect protein stability and function. Either these proteins were unable to fold correctly and localize properly to the cell membrane due to the mutations, or they managed to localize to the membrane but were more vulnerable to denaturation by the strong SDS

detergent in the lysis buffer which prevented them from showing expression on the immunoblot. Confocal microscopy of tissue samples infiltrated with *CERK1^{WT}* p104 and *CERK1^{3KR}* p104 would help determine if the proteins were able to express and localize to the membrane, however, this experiment was not done because priority was placed on re-cloning *CERK1* to create a construct without any mutations. Finally, *CERK1^{3KR}* p104 did not contain all three SUMO-site K to R mutations. Sequence data shows lack of an A to G substitution at nucleotide 827, which yielded a protein with a lysine residue at amino acid 276 instead of the intended replacement with arginine. It is clear from this information that these constructs could not be used. *CERK1^{WT}* would be re-cloned, and K to R SUMO-site mutations would be reintroduced via site-directed mutagenesis.
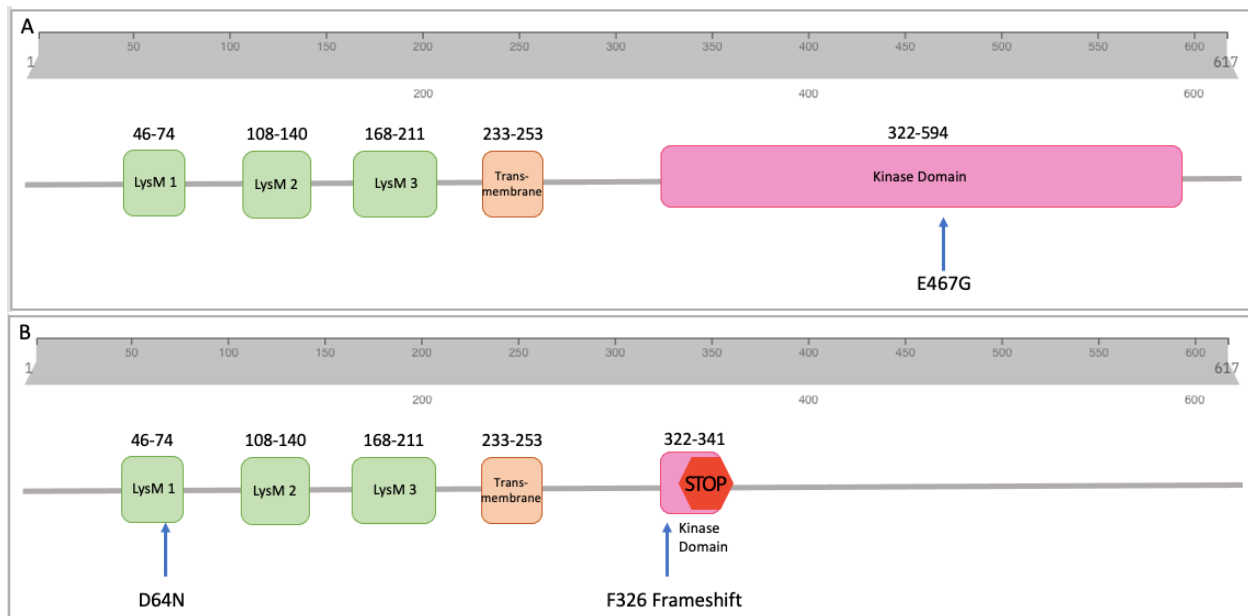
Figure 3.6. Visualization of mutations in *CERK1* p104 constructs in relation to protein domains. **(A)** CERK1^{WT} contained a mutation causing the change of glutamic acid to glycine at amino acid 467 (E467G) within the kinase domain of the protein. **(B)** CERK1^{3KR} contained a mutation causing the change of aspartic acid to asparagine at amino acid 64 (D64N) in the first LysM domain of the protein as well as a deletion causing a frameshift mutation at amino acid 326, causing a premature stop codon at amino acid 341 in the kinase domain. Figure created by author in PowerPoint.

3.3.2. Genotyping Analysis Revealed Non-Transgenic *Arabidopsis* Plant Lines

The results from the genotyping analysis suggest that each transgenic plant line that was to be used for *B. cinerea* infection assays in this project were not truly transgenic. The *cerk1-CM1* line showed the same banding pattern as Col-0, suggesting that it did not contain *CERK1* CDS. *cerk1-CM1* was created by incorporating *CERK1^{WT}* p104 expression clone into the *cerk1-2* K/O line. Since the CDS does not contain introns, it is therefore smaller than the genomic version of the gene and produces a smaller band when amplified.   In the true *CERK1* complement, 5-8 exon primers should have amplified a band of 460 bp (*CERK1* CDS) in addition to the 713 bp genomic DNA band and in the 10-12 region would have only amplified a band of 380. The 10-12 primer set would have been unable to amplify the genomic band of 723 bp due to the presence of the T-DNA insert. Since the *cerk1-CM1* sample produced genomic-sized bands and not the smaller CDS bands when amplified by both primer sets, it can be concluded that the *cerk1-CM1* line is Col-0 and not in fact transgenic. *cerk1-CM2* as well as *cerk1-3KR-2-5* and *cerk1-3KR-3-6* samples produced the same band pattern as *cerk1-2* K/O. True complement lines would have produced a band at 713 bp and 460 bp when amplified by the exon 5-8 primer set, and a band at 380 bp when amplified by the exon 10-12 primer set. These samples instead produced only one band at 713 when amplified by exon 5-8 primer set and no band when amplified by exon 10-12 primer set, suggesting that no *CERK1* CDS was present in samples. It can be concluded from these results that each of these plant lines were *cerk1-2* K/O lines and were not transgenic. It is unclear why these plant lines which were labelled as transgenic were not, but possible explanations include multiple handling by different people over years and mislabelling of samples.

4.0. Cloning and Site-Directed Mutagenesis

4.1. Introduction

To understand the role of SUMOylation in the fungal PTI pathway, co-immunoprecipitation assays were to be carried out with CERK1^{WT} and SUMO1 as well as CERK1^{3KR} (SUMO-site triple mutant) and SUMO1 to determine 1: if CERK1 is SUMOylated during an immune response and 2: if SUMOylation is inhibited when the SUMO-sites in CERK1 are mutated. If these results were determined, then further co-immunoprecipitation assays would be performed with CERK1^{3KR}, PBL27^{WT} and LYK5^{WT} to determine if lack of SUMOylation in CERK1^{3KR} prevented the interaction with signalling proteins in the PTI pathway. In order to achieve these research goals, functioning *CERK1^{WT}*, *CERK1^{3KR}*, *LYK5^{WT}* and *PBL27^{WT}* constructs had to be created. Following the discovery that the *CERK1* constructs received as materials for the study had unintended mutations (section 3.2.2.), the first course of action was to re-clone *CERK1^{WT}* and reproduce CERK1^{3KR}. *LYK5* and *PBL27* genes were cloned as well, as they would potentially be used later in the project. The purpose of this chapter is to describe the process of cloning *CERK1*, *LYK5* and *PBL27*, and the site-directed mutagenesis of *CERK1*. *CERK1*, *LYK5* and *PBL27* were successfully cloned, and all three single CERK1^{KR} SUMO-site mutants as well as one double CERK1^{2KR} SUMO-site mutant were generated. The triple CERK1^{3KR} SUMO-site mutant was not successfully generated, so the project progressed using CERK1^{2KR} as a substitute.

4.2. Results

4.2.1. Cloning *CERK1*, *LYK5* and *PBL27*

CERK1, *LYK5* and *PBL27* CDS were amplified from Col-0 *Arabidopsis* cDNA using primers

in table 2.2, and PCR products were run through 1% agarose gel. *CERK1* CDS is 1,851 bp, *LYK5*

CDS is 1,992 bp and *PBL27* CDS is 1,539 bp (Figure 4.1). DNA of each CDS was extracted from

the agarose gel, and a T4 ligation reaction was carried out to insert each CDS into the pJET

cloning vector (Figure 4.2). Following colony PCR to confirm the insertion of each CDS in pJET,

positive colonies were grown overnight at 37°C and plasmids were isolated from the culture.

pJET cloning vectors were then digested with the restriction enzymes matching the specific

restriction enzyme cut site that had been added to the beginning and end of each CDS via

primers during PCR amplification (Table 2.2.). *LYK5* was digested with KpnI and XhoI, *PBL27* was

digested with NcoI and EcoRV, and *CERK1* was digested with NcoI and EcoRV. In addition, 2

separate digestions of empty pENTR4 entry vector were performed with each respective

restriction enzyme set. Digested fragments were run through 1% agarose gel, and CDS

fragments were isolated from the gel. (Figure 4.3). To isolate the empty pENTR4 entry vector,

the larger fragment was isolated from the gel, discarding the ccbd toxic gene (Figure 4.3, A & B).

To isolate *LYK5*, the smaller fragment at 2 kb was extracted (Figure 4.3, C). To isolate *PBL27*,

the small fragment at 1.5 kb was extracted (Figure 4.3, D) and finally to isolate *CERK1*, the small

fragment at 1.8 kb was extracted (Figure 4.3, E). Extracted CDS fragments and linearized

pENTR4 were purified from the agarose gel, then each CDS was ligated overnight with

linearized pENTR4 in separate reactions and transformed into DH5α competent *E. coli*.

Following colony PCR to confirm the insertion of each CDS into pENTR4, positive colonies were

grown overnight at 37°C and plasmids were isolated from the culture (Figure 4.4). Constructs

were sequenced to confirm that the whole CDS of each gene was present and that no

unintended mutations had occurred (Appendix, Figures 8.1, 8.2, 8.3). As there were no

mutations present in the constructs, the CDS in pENTR4 entry vectors were then transferred

into pEarlyGate expression vectors using the LR Gateway cloning reaction. *CERK1* was cloned

into pEarlyGate 103 (p103), and *LYK5* and *PBL27* were cloned into both p103 and pEarlyGate

201 (p201). The resulting expression clones are from here on referred to as *CERK1*^{WT} p103,

LYK5^{WT} p103, *PBL27*^{WT} p103, *LYK5*^{WT} p201, and *PBL27*^{WT} p201, and plasmid maps are shown in

figure 4.5.
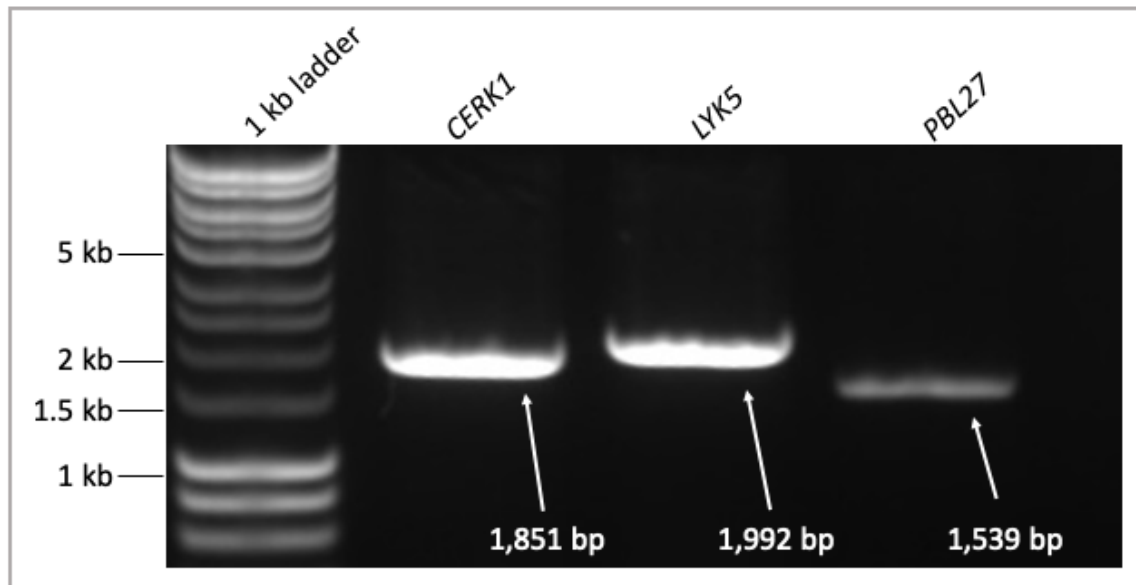
Figure 4.1. *CERK1* (1,851 bp), *LYK5* (1,992 bp) and *PBL27* (1,539 bp) CDS amplified from *Arabidopsis* Col-0 cDNA using primer sets in table 2.2 and run through 1% agarose gel.
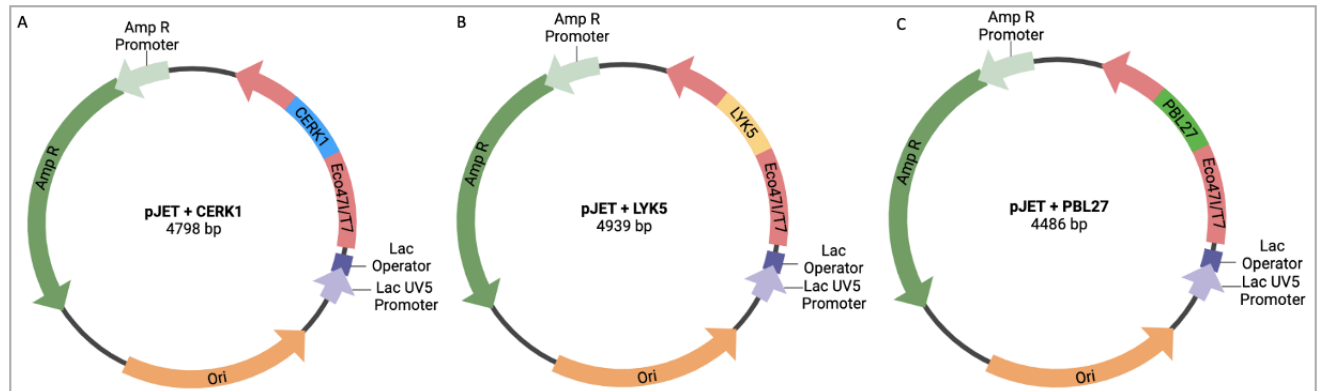
Figure 4.2. pJET cloning vectors containing CDS of *CERK1*, *LYK5* and *PBL27*. CDS inserted into multiple cloning sites. **(A)** *CERK1* pJET. **(B)** *LYK5* pJET. **(C)** *PBL27* pJET. Amp R promoter: Ampicillin Resistance Promoter; Amp R: Ampicillin Resistance; Ori: Origin of Replication; Lac UV5 Promoter: *E. coli* Lactose UV5 Promoter; Lac Operator: *E. coli* Lactose Operator; Eco47I/T7: Mutant Eco47I Restriction Endonuclease. Figure created by author using BioRender.com.
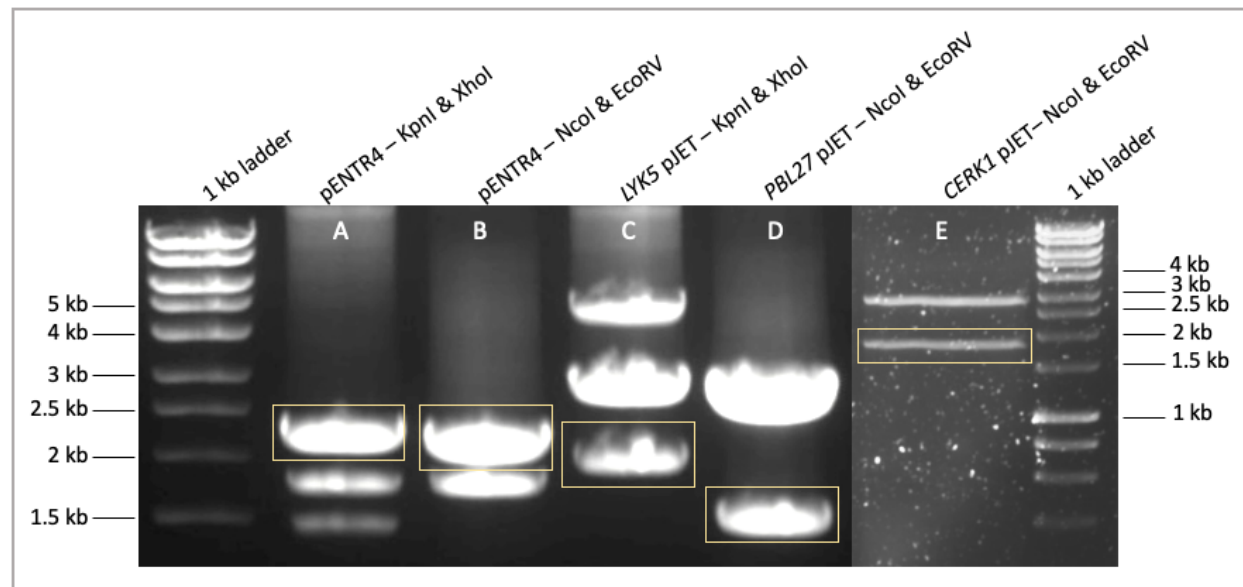
Figure 4.3. Restriction enzyme digested pENTR4 entry vectors and pJET cloning vectors run through 1% agarose gel. **(A)** pENTR4 empty vector digested with enzymes KpnI and XhoI. Larger band in yellow box is linearized pENTR4. **(B)** pENTR4 empty vector digested with enzymes NcoI and EcoRV. Larger band in yellow box is linearized pENTR4. **(C)** *LYK5* pJET digested with enzymes KpnI and XhoI. Smaller band in yellow box is *LYK5* CDS. **(D)** *PBL27* pJET digested with enzymes NcoI and EcoRV. Smaller band in yellow box is *PBL27* CDS. **(E)** *CERK1* pJET digested with enzymes NcoI and EcoRV. Smaller band in yellow box is *CERK1* CDS.

64
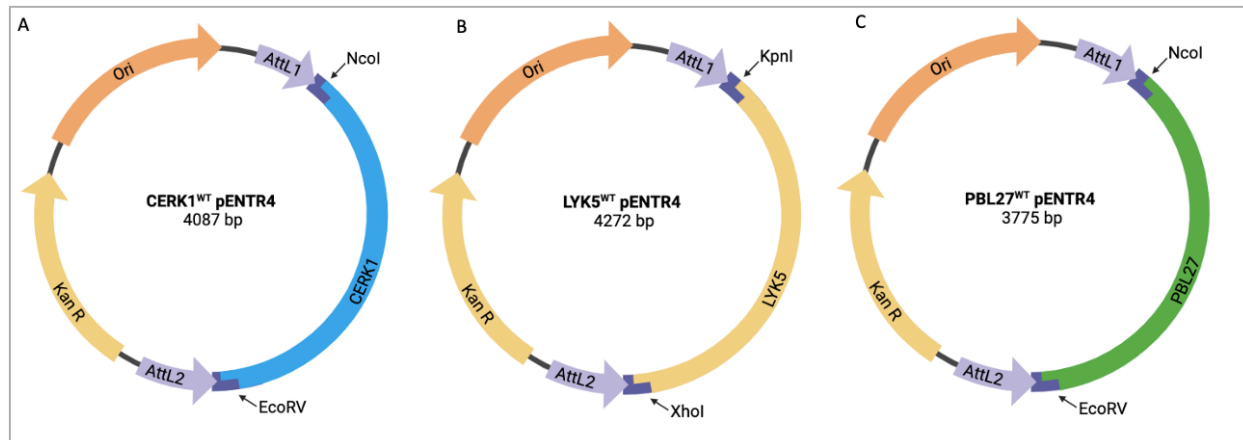
Figure 4.4. pENTR4 entry vectors containing CDS of *CERK1*, *LYK5* and *PBL27*. **(A)** *CERK1* pJET and empty pENTR4 were digested with NcoI and EcoRV, then ligated together with T4 ligase to produce *CERK1^{WT}* pENTR4. **(B)** *LYK5* pJET and empty pENTR4 were digested with KpnI and XhoI, then ligated together with T4 ligase to produce *LYK5^{WT}* pENTR4. **(C)** *PBL27* pJET and empty pENTR4 were digested with NcoI and EcoRV, then ligated together with T4 ligase to produce *PBL27^{WT}* pENTR4. Ori: Origin of Replication; Kan R: Kanamycin Resistance; AttL1: recombination site 1 for Gateway LR reaction; AttL2: recombination site 2 for Gateway LR reaction. Figure created by author using BioRender.com.
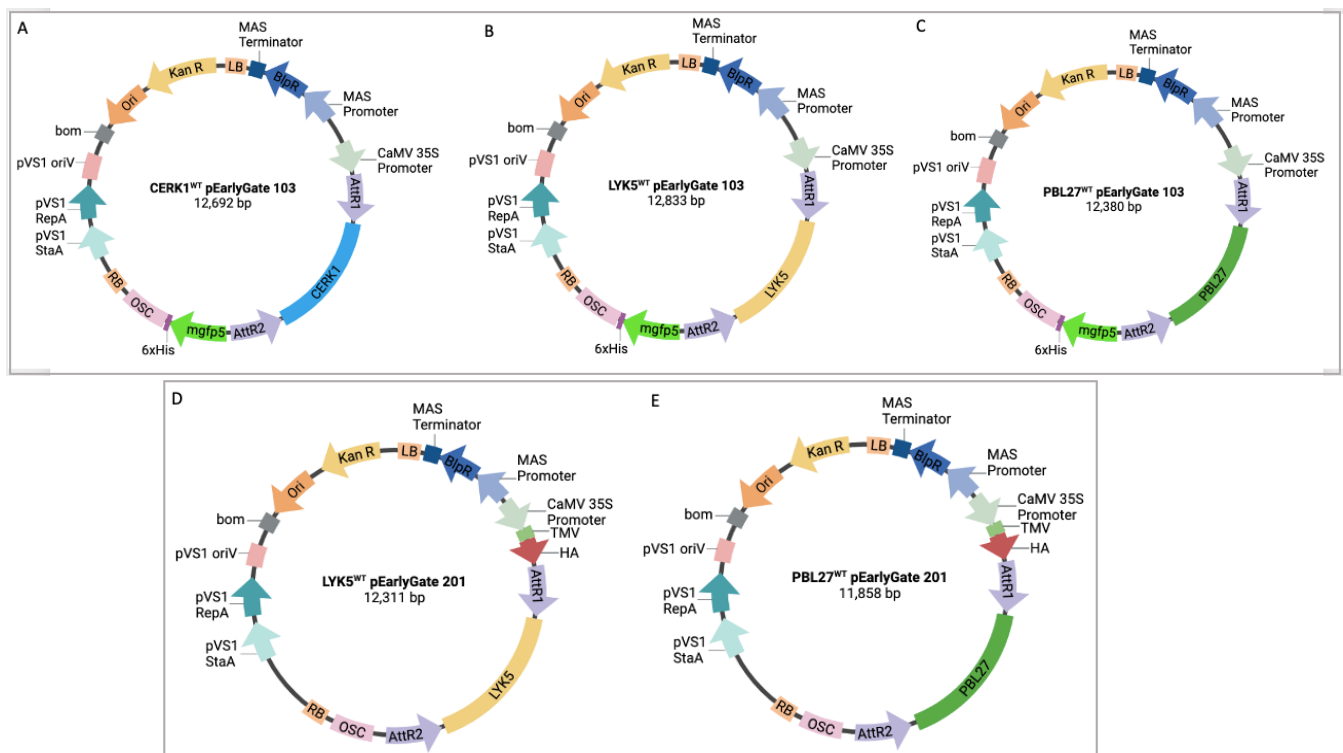
Figure 4.5. Expression vectors containing CDS of genes following LR Clonase reaction. **(A)** *CERK1^{WT}* p103. **(B)** *LYK5^{WT}* p103. **(C)** *PBL27^{WT}* p103. **(D)** *LYK5^{WT}* p201. **(E)** *PBL27^{WT}* p201. Kan R: Kanamycin Resistance; Ori: Origin of Replication; bom: basis of mobility region; pVS1 oriV: Origin of Replication for *Pseudomonas* plasmid PVS1; pVS1 RepA: Replication Protein from *Pseudomonas* plasmid PVS1; pVS1 StaA: Stability Protein from *Pseudomonas* plasmid PVS1; RB: Right Border repeat from Nopaline C58 T-

DNA; OSC: Octopine Synthase Terminator; 6xHis: 6xHis affinity tag; mgfp5: Green Fluorescent Protein tag; AttR2: recombination site 2 for Gateway LR reaction; AttR1: recombination site 1 for Gateway LR reaction; CaMV 35S promoter: Constitutive Promoter from *Cauliflower mosaic virus*; MAS promoter: Mannopine Synthase Promoter; BlpR: Phosphinothricin Acetyltransferase; MAS terminator: Mannopine Synthase Terminator; LB: Left Border repeat from Nopaline C58 T-DNA; TMV: translational enhancer from *Tobacco mosaic virus*; HA: Human Influenza Hemagglutinin epitope tag. Figure created by author using BioRender.com.

4.2.2. Site-Directed Mutagenesis of *CERK1*

Site directed mutagenesis PCR was carried out using *CERK1^WT^* pENTR4 entry vector and *CERK1* K74R, *CERK1* K276R and *CERK1* K495R mutagenesis primer sets in separate reactions (Table 2.2). 4μL of each PCR reaction was run through agarose gel to visualize if the mutagenesis reaction was successful. All annealing temperatures used during gradient PCR produced amplified products, so the PCR products that were subjected to the highest annealing temperatures were used for DpnI digestion (Figure 4.6). The remaining 8.5μL of the 55°C PCR reactions were digested with DpnI at 37°C overnight to remove the unmutated DNA template. Digested products were transformed into DH5α competent *E. coli*, and colony PCR was used to confirm transformation of mutated *CERK1^KR^* pENTR4 constructs into bacteria. Positive colonies were grown overnight at 37°C, and plasmids were isolated from the culture. Isolated plasmids were sequenced using Attb sequencing primers (Table 2.2). The site-directed mutagenesis PCR successfully introduced each single nucleotide substitution in *CERK1^WT^* which translated into lysine to arginine (KR) amino acid changes at each predicted SUMO-site in the protein. The sequencing data confirms the creation of *CERK1^K74R^*, *CERK1^K276R^*, and *CERK1^K495R^* mutants (Figure 4.7 & 4.8). This process was repeated with the *CERK1^K74R^* pENTR4 construct using *CERK1* K276R mutagenesis primers, successfully introducing a second substitution at nucleotide 827 into the *CERK1^K74R^* mutant, creating the double mutant *CERK1^K74R/K276R^* (Figure 4.9). Many attempts

were made to introduce a third substitution at nucleotide 1,484 in *CERK1*$^{K74R/K276R}$ to generate the triple 3KR mutant. However, when PCR amplification products were run through agarose gel, no or very faint bands were produced, indicating lack of successful amplification of mutagenesis product. When PCR reactions that produced these faint bands were digested with DpnI, transformed into DH5α competent *E. coli*, isolated from bacteria and sequenced, the plasmid did not contain the third intended mutation. Efforts were abandoned after 4-5 attempts when sequencing data of the potential 3KR mutant only showed the introduction of K74R and K276R mutations (Figure 4.10). *CERK1*$^{K74R/K276R}$ would be used as a substitute for *CERK1*^{3KR} and was cloned into the p103 expression vector to yield *CERK1*^{2KR} p103 (Figure 4.11.).
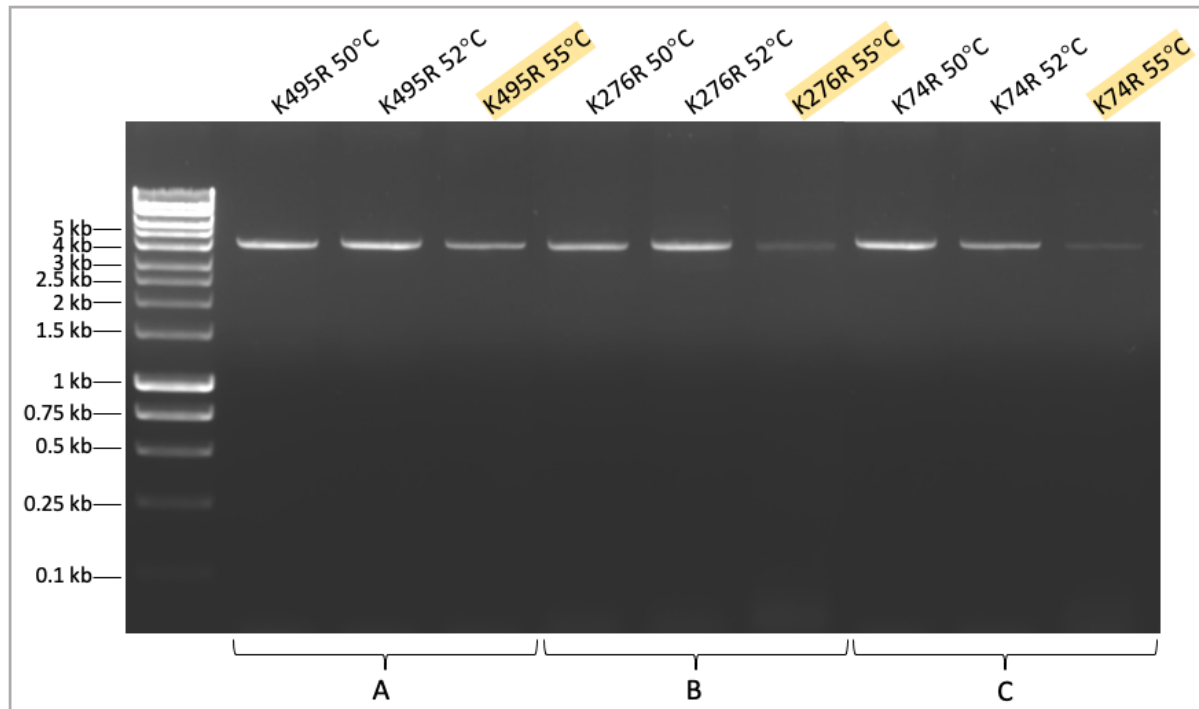
Figure 4.6. Site-directed mutagenesis PCR reactions using CERK1^{WT} pENTR4 as template DNA and single SUMO-site mutagenesis primers run through 1% agarose gel. Annealing temperatures ranged from 50°C to 55°C in gradient PCR. **(A)** *CERK1* K495R mutagenesis primers used to generate *CERK1*^{K495R}. **(B)** *CERK1* K276R mutagenesis primers used to generate *CERK1*^{K276R} **(C)** *CERK1* K74R mutagenesis primers used to generate *CERK1*^{K74R}. The 55°C PCR amplification product of each mutagenesis reaction was used for DpnI digestion and transformation into DH5α competent *E. coli.*

Figure 4.7. Sequence alignment of mutated *CERK1* pENTR4 entry vectors. **(A)** A to G substitution at nucleotide 221 to generate the *CERK1^K74R^* mutant. **(B)** A to G substitution at nucleotide 827 to generate the *CERK1^K276R^* mutant. **(C)** A to G substitution at nucleotide 1,484 to generate the *CERK1^K495R^* mutant. Figure generated by author using Clustal Omega multiple sequence alignment tool and PowerPoint.

Figure 4.8. Amino acid sequence alignment of mutated CERK1^WT. **(A)** K74R mutation highlighted in yellow. **(B)** K276R mutation highlighted in pink. **(C)** K495R mutation highlighted in blue.
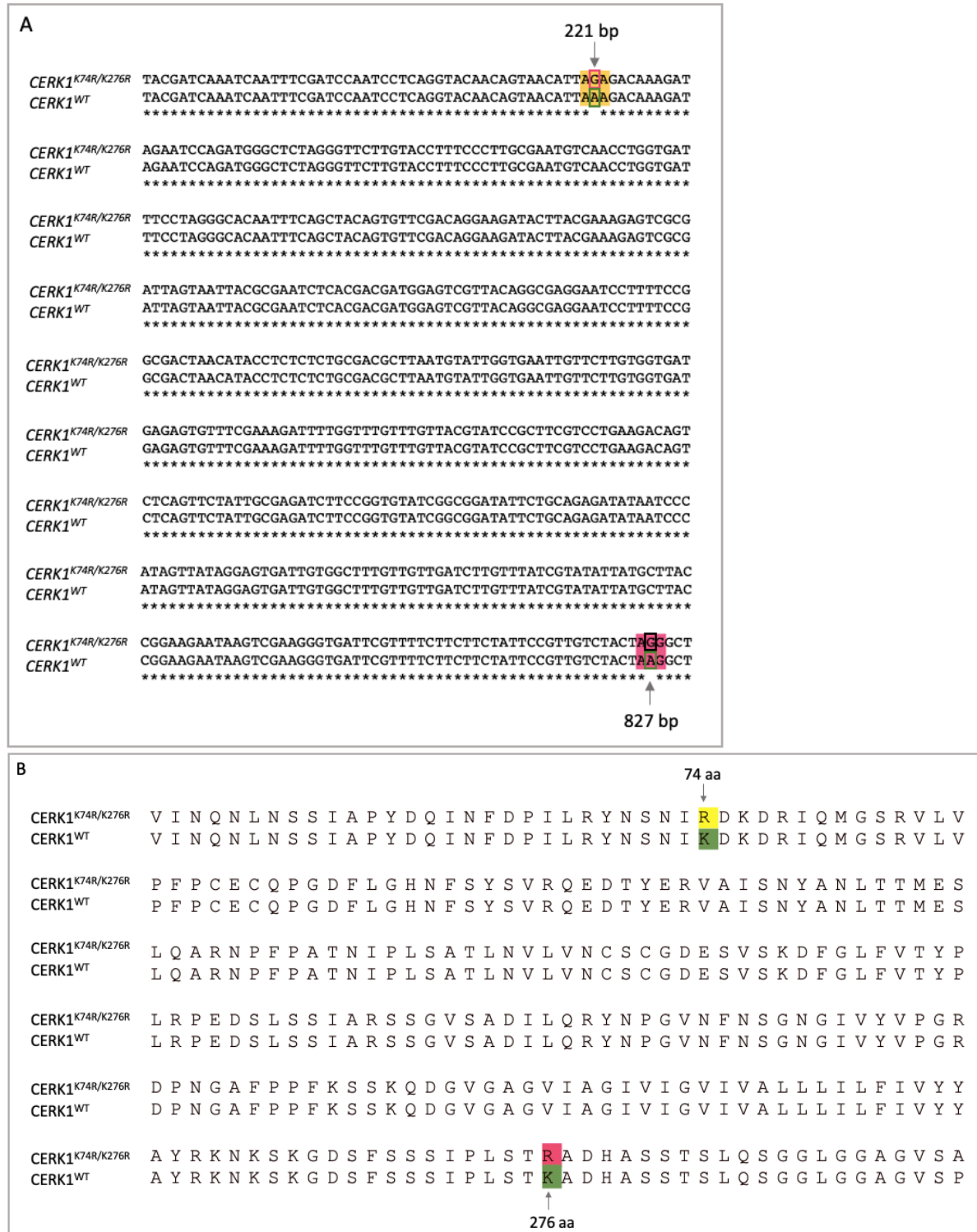
Figure 4.9. Sequence alignment of *CERK1^{K74R/K276R}* double mutant. **(A)** Nucleotide sequence alignment of mutated *CERK1^{K74R}* after second round of site-directed mutagenesis to introduce K276R mutation. A to G substitution at nucleotide 221 for K74R mutation is highlighted in yellow, and A to G substitution at nucleotide 827 for K276R mutation is highlighted in pink. **(B)** Amino acid sequence alignment of CERK1^{K74R/K276R} double mutant. K74R mutation highlighted in yellow, and K276R mutation highlighted in

pink. Figure generated by author using Clustal Omega multiple sequence alignment tool and PowerPoint
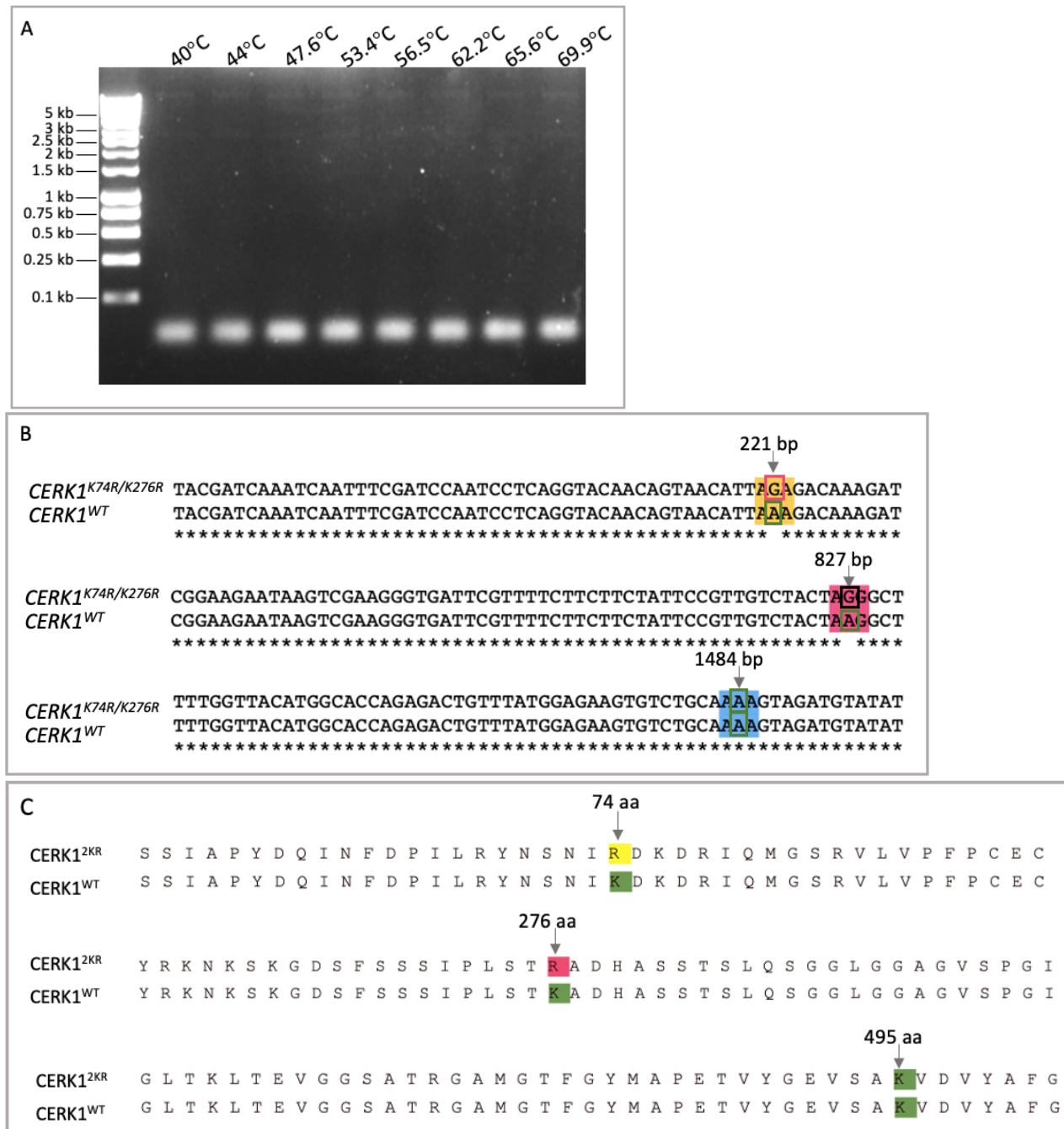
Figure 4.10. Attempted site-directed mutagenesis to produce *CERK1^3KR* mutant. **(A)** Site-directed mutagenesis PCR amplification products, using *CERK1^K74R/K276R* as template DNA and *CERK1* K495R mutagenesis primers, run through 1% agaraose gel. Gradient PCR was used with annealing temperatures ranging from 40°C to 70°C. **(B)** Nucleotide sequence alignmnet of *CERK1^K74R/K276R* after third round of site-directed mutagenesis to introduce K495R mutation. A to G substitution at nucleotide 221 for K74R mutation is highlighted in yellow, and A to G substitution at nucleotide 827 for K276R mutantion is highlighted in pink. Lack of A to G substitution at nucleotide 1,484, highlighted in blue. **(C)** Amino acid sequence alignmnet of attempted CERK1^3KR triple mutant. K74R mutation highlighted in yellow, K276R

70

mutation highlighted in pink, and lack of K495R mutation highlighted in green. Figure generated by author using Clustal Omega multiple sequence alignment tool and PowerPoint
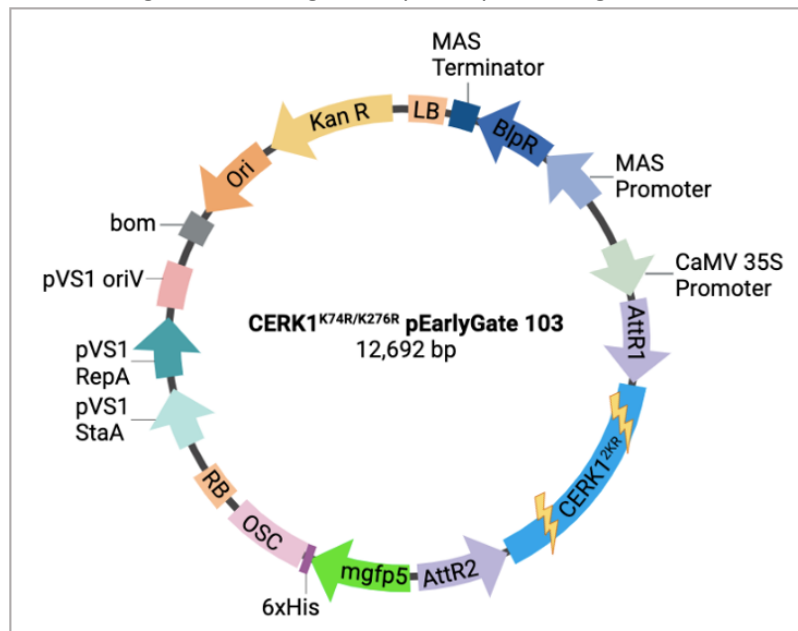
Figure 4.11. *CERK1^{K74R/K276R}* pEarlyGate 103 (*CERK1^{2KR}* p103) expression clone. Kan R: Kanamycin Resistance; Ori: Origin of Replication; bom: basis of mobility region; pVS1 oriV: Origin of Replication for *Pseudomonas* plasmid PVS1; pVS1 RepA: Replication Protein from *Pseudomonas* plasmid PVS1; pVS1 StaA: Stability Protein from *Pseudomonas* plasmid PVS1; RB: Right Border repeat from Nopaline C58 T-DNA; OSC: Octopine Synthase Terminator; 6xHis: 6xHis affinity tag; mgfp5: Green Fluorescent Protein tag; AttR2: recombination site 2 for Gateway LR reaction; AttR1: recombination site 1 for Gateway LR reaction; CaMV 35S promoter: Constitutive Promoter from *Cauliflower mosaic virus*; MAS promoter: Mannopine Synthase Promoter; BlpR: Phosphinothricin Acetyltransferase; MAS terminator: Mannopine Synthase Terminator; LB: Left Border repeat from Nopaline C58 T-DNA. Figure created by author using BioRender.com.

4.3. Discussion

4.3.1. Site-Directed Mutagenesis Successful in Generating Some but not all *CERK1* SUMO-Site Mutants

The *CERK1* single KR SUMO-site mutants (*CERK1^{K74R}* *CERK1^{K276R}* and *CERK1^{K495R}*) as well

as one double KR mutant (*CERK1^{K74R/K276R}*) were successfully generated using site-directed

mutagenesis, however the triple KR mutant (*CERK1^{3KR}*) was not successfully generated. Several

attempts were made to generate this mutant using trouble shooting methods such as designing

new mutagenesis primers, changing the annealing temperature in the PCR reactions, and trying

different combinations of *CERK1^{KR}* single mutants, such as inserting the K74R and K276R

mutations into the single *CERK1^{K495R}* mutant, however unsuccessfully. Mutagenesis primers

contain a single mismatch with the template DNA and annealing temperature in the PCR cycle

changes the primer's affinity for the DNA template. Lower annealing temperatures increase

primer affinity to template DNA, however very low temperatures can cause unspecific binding

of primer and template. Higher annealing temperatures increase the specificity of primer-

template binding, but very high temperatures prevent the primer from binding to the template

containing a mismatch. Primers of different lengths in combination with annealing

temperatures ranging from 40°C to 70°C were tried. These attempts would either produce no

amplified bands or very faint bands when PCR products were run through agarose gel. When a

site-directed mutagenesis PCR reaction produced a faint band in the agarose gel, the PCR

product was used for the rest of the site-directed mutagenesis procedure. However, these

constructs transformed into *E. coli* would either not grow on kanamycin plates, or the few

colonies that did grow did not contain a construct with the intended mutation when

sequenced. It is unclear why these attempts to incorporate the K495R mutation in a single

construct with the other mutations was unsuccessful. A common limitation in site-directed

mutagenesis is the creation of "primer-dimers" during amplification. The mutagenesis primers

are completely complementary and therefore favour self-annealing over annealing to the

template DNA which contains a mismatch with the primers (Zeng et al. 2018). Primer-dimers

were very prominent in the attempted CERK1^{3KR} site-directed mutagenesis PCR reaction (Figure

4.10, A, the bands seen in each lane under 0.1 kb), while no primer dimers were present in the

single CERK1^{KR} site-directed mutagenesis PCR reactions (Figure 4.6). Although the same *CERK1*

K495R mutagenesis primers were used in both PCR reactions, the primers had a higher affinity

for self-annealing when placed in the PCR reaction with *CERK1$^{K74R/K276R}$* than with *CERK1^{WT}*. It is

unclear why the mutated *CERK1* construct caused more primer-dimer formation under the

same reaction conditions, but this is likely the reason that the third KR mutation was

unsuccessfully inserted. Many variations of this site-directed mutagenesis protocol have been

developed for multiple-site mutations in a single PCR reaction that utilize specialized primer

design (Mikaelian and Sergeant 1992; Jensen and Weilguny 2005; Liu and Naismith 2008; Zeng

et al. 2018). It is suggested for future research on this project to utilize these methods to try to

create *CERK1^{3KR}* in a single PCR reaction to reduce time, labour, and likelihood of primer-dimer

formation during the single-step PCR reactions. It is appropriate to note here that the original

CERK1^{3KR} p104 construct received at the start of the project also did not contain all three KR

mutations, but this construct lacked the K276R mutation, not the K495R mutation. There is

likely some reason that the combination of all three mutations in a single construct is difficult to

generate, and it is likely due to the inefficiency of single-site site-directed mutagenesis. Since

the CERK1^{3KR} SUMO-site mutant could not be generated in this research project, CERK1^{2KR} was

used as a substitute since it contained mutations in two out of the three putative SUMO-sites.

CERK1^{2KR} was cloned into p103 expression vector to be used in co-immunoprecipitation assays

with SUMO1, with the prediction that less SUMOylation would occur in this protein because it

only has one viable SUMO-site.

5.0. CERK1 Transient Expression and SUMOylation Analysis

5.1. Introduction

SUMOylation is a critical PTM for controlling protein activity, localization and turnover in a number of cellular processes, such as development and homeostasis under normal conditions as well as defensive roles during stress response (Castaño-Miquel et al. 2013; Rytz et al. 2018; Morrell and Sadanandom 2019). The importance of SUMOylation in defence against biotic stress by pathogens has been described by many studies (Section 1.5), and its importance during *B. cinerea* infection has been specifically described by Castaño-Miquel and colleagues (Castaño-Miquel et al. 2017). Although this study determined the importance of SUMOylation for immunity, the specific mechanisms and protein targets of SUMO during immune signalling remain unclear. Orosa and colleagues discovered a SUMO-dependent stage of the PTI signalling cascade during bacterial infection and proved that SUMOylation of the PRR protein FLS2 was essential for the activation and release of BIK1, a downstream signalling RLCK protein. Therefore, the activation of MAPK signalling and induction of transcription factors to activate expression of defence genes is also SUMO-dependent (Orosa et al. 2018). One of the working hypotheses of this project states that due to similarity to bacterial PTI, fungal PTI also has a SUMO-dependent step and that the interaction of SUMO1 with CERK1 upon *B. cinerea* infection is essential for initiation of downstream immune signalling. This chapter aims to explore this hypothesis by analysing protein expression and subcellular localization of cloned constructs (*CERK1*^{WT} p103, *CERK1*^{2KR} p103, *LYK5*^{WT} p103, *PBL27*^{WT} p103) using confocal microscopy and analysing protein interaction of these proteins with SUMO1 upon chitin elicitation using co-

immunoprecipitation[1]. It is predicted that CERK1 and SUMO interact upon chitin elicitation and SUMO1 will therefore be co-immunoprecipitated with CERK1, while CERK1^{2KR} and SUMO1 will have reduced or no interaction upon chitin elicitation, and therefore reduced or no co-immunoprecipitation.

5.2. Results

5.2.1. Subcellular Localization

Expression clones were transformed into *Agrobacteria*, and positive colonies were grown overnight at 28°C. Cultures were then prepared for agroinfiltration and diluted to an OD$_{600}$ of 0.1. Cultures were infiltrated into 4-week-old *N. benthamiana* plants, and after 48 hours samples were viewed under a confocal microscope to confirm the expression of constructs and to determine protein subcellular localization. CERK1^{WT} and CERK1^{2KR} both localized to the cellular membrane compared to free-GFP which localized in the cytoplasm and nucleus (Figure 5.1). LYK5^{WT} and PBL27^{WT} also localized to the cell membrane.

---

[1] In this section, CERK1^{WT} and CERK1^{2KR} are referring to the re-cloned *CERK1* construct in p103 expression vector described in chapter 4, and not the *CERK1* p104 expression vectors received at the start of the project.
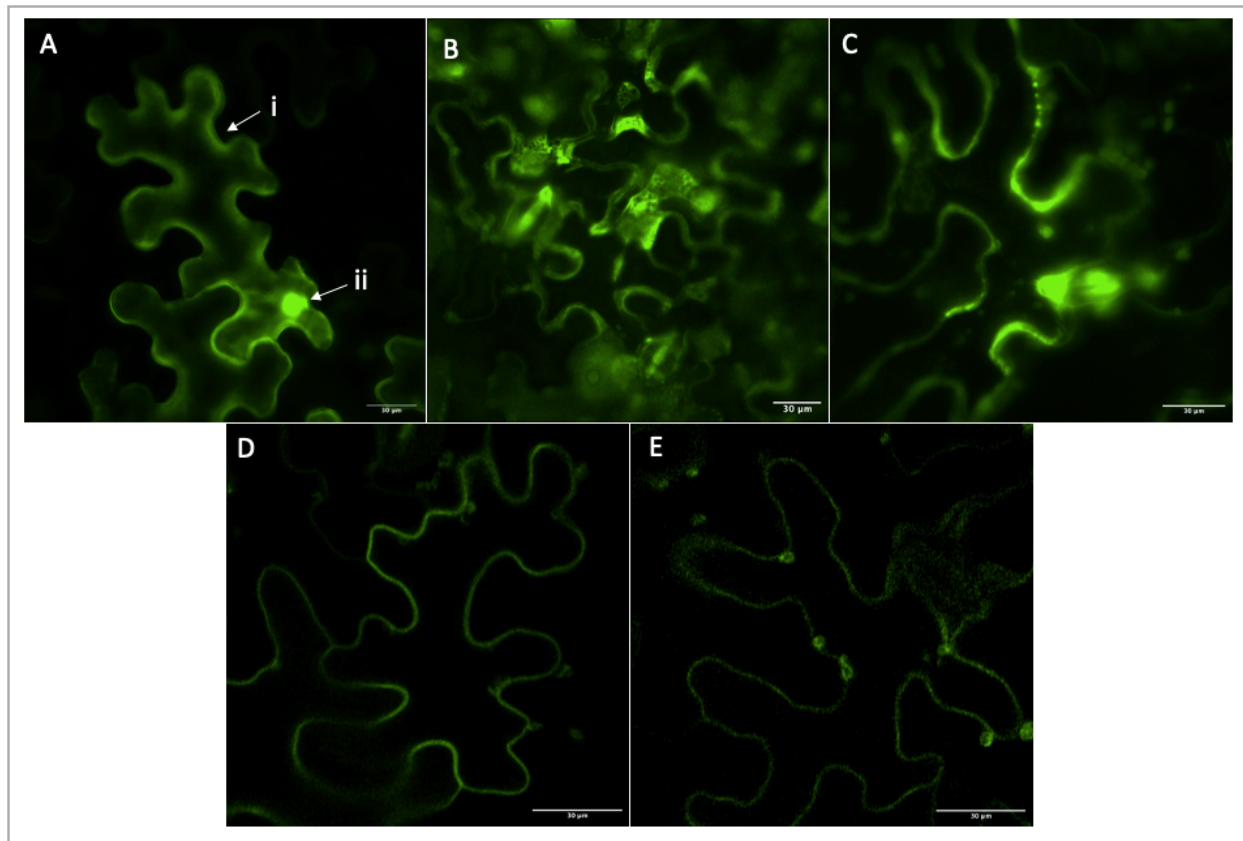
Figure 5.1. Subcellular localization of GFP-tagged constructs in *N. benthamiana* leaf samples infiltrated with *Agrobacteria* containing constructs at an OD_{600} of 0.1 and visualized with a confocal microscope at 2 DPI. **(A)** Free-GFP localized in **(i)** the cytoplasm and **(ii)** the nucleus. **(B)** CERK1^{WT} localized in the cell membrane. **(C)** CERK1^{2KR} localized in the cell membrane. **(D)** LYK5^{WT} localized in the cell membrane. **(E)** PBL27^{WT} localized in the cell membrane. Bar represents 30 μm.

5.2.2. CERK1^{WT} and CERK1^{2KR} Expression

CERK1^{WT} p103 and *CERK1^{2KR}* p103 expression clones were transformed into *Agrobacteria* and infiltrated into the underside of 4-week-old *N. benthamiana* plants. 2 days post infiltration, leaf tissue was harvested, and total protein was extracted. The protein lysis buffer was changed to include KCl and SDS was removed. The GFP-tagged CERK1 proteins were then purified with immunoprecipitation using anti-GFP beads. Purified samples were then run through SDS-PAGE along with total protein input samples. Separated protein in gel was then transferred to a PVDF membrane and immunoblotted with anti-GFP. The protein was visualized using

chemiluminescence on X-ray paper. CERK1^{WT} and CERK1^{2KR} were consistently expressed on immunoblots. CERK1 is 67.3kDa and GFP is 27kDa, so the resulting band on the immunoblot blot representing the CERK1-GFP fusion protein is 94.3kDa. A distinct band around 100kDa was visualized on immunoblots indicating the successful expression, localization, and extraction of CERK1^{WT} and CERK1^{2KR} (Figure 5.2).
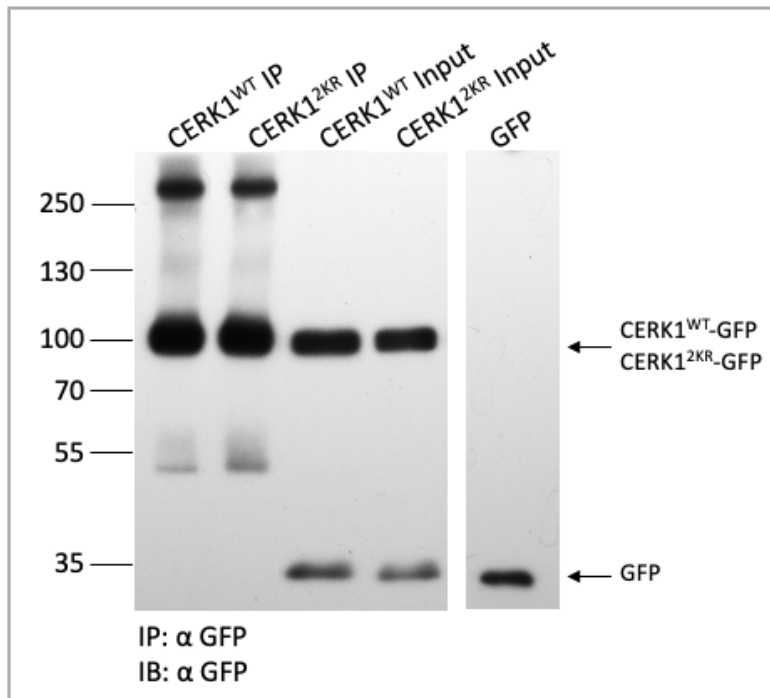
Figure 5.2. Immunoblot showing CERK1^{WT} and CERK1^{2KR} expression. Total protein from *N. benthamiana* leaves transiently expressing CERK1^{WT} and CERK1^{3KR} was extracted. 50μL of total protein was preserved as input, and the rest was purified by immunoprecipitation using anti-GFP beads (IP: α GFP). IP and Input samples were then separated on an SDS-PAGE gel, transferred to a PVDF membrane, and immunoblotted with anti-GFP (IB: α GFP). CERK1 = 67.3kDa, GFP = 27kDa, CERK1-GFP fusion protein = 94.3kDa.

5.2.3. Co-Immunoprecipitation of CERK1^{WT} and SUMO1

Co-immunoprecipitation of CERK1^{WT} with SUMO1 was then performed to determine if CERK1 is SUMOylated upon chitin elicitation. Co-immunoprecipitation of FLS2^{WT} and SUMO1 was used as a positive control for SUMOylated protein, free-GFP was used as a positive control

for the anti-GFP immunoblot and SUMO1 was used as a positive control for the anti-HA

immunoblot. *CERK1*^{WT} p103 was co-infiltrated with *SUMO1* p201 in equal concentrations. 2

days post infiltration, leaves were inoculated with 1μM chitooctaose and left for 30 minutes

before leaf tissue was harvested and total protein was extracted. Protein samples were then

purified with immunoprecipitation using anti-GFP microbeads. The SUMO1 control sample was

immunoprecipitated with anti-HA microbeads. Purified samples were then run through two

separate SDS-PAGE gels along with total protein input samples. Separated protein in gels were

then transferred to PVDF membranes and one was immunoblotted with anti-GFP while the

other was immunoblotted with anti-HA. The protein was visualized using chemiluminescence

on X-ray paper. On the anti-GFP blot, bands around 100kDa were visualized in the CERK1^{WT} and

CERK1^{WT} + SUMO1 sample lanes, and bands between 130kDa and 250kDa were visualized in the

FLS2^{WT} and FLS2^{WT} + SUMO1 sample lanes. A band at 27kDa was visualized in the free-GFP

positive control lane (Figure 5.3, A). On the anti-HA immunoblot, there were bands at

approximately 110kDa and 130kDa in the CERK1^{WT} + SUMO1 sample lane, 230kDa in the FLS2^{WT}

+ SUMO1 sample lane and 15kDa in the SUMO1 positive control lane (Figure 5.3, B). Since

CERK1 is 67.3kDa, GFP is 27kDa, SUMO1 is 15kDa and HA is 1.1kDa, the CERK1-GFP fusion

protein with 1-3 SUMO1 conjugations would range from 110.4kDa to 142.6kDa or more

depending on the possibility of poly-SUMO tail conjugation. FLS2 is 128.8kDa, so the FLS2-GFP

fusion protein with 1-5 SUMO conjugations would range from 171.9kDa to 236.3kDa or more

due to the possibility of poly-SUMO tail conjugation. This same immunoblot was subjected to

longer exposure time on X-ray film before developing. The resulting image showed a band at

approximately 130kDa in the CERK1^{WT} negative control lane and a band at approximately

230kDa in the FLS2^{WT} negative control lane (Figure 5.4). This exact experiment was repeated several times, with conscious effort to ensure there was no mixing of samples during protein extraction, immunoprecipitation and while loading samples into SDS-PAGE gel wells. The same bands were seen in the CERK1^{WT} and FLS2^{WT} negative control lanes each time the experiment was repeated.

Figure 5.3. Immunoblots showing interaction of CERK1^{WT} and FLS2^{WT} with SUMO1. **(A)** Total protein from *N. benthamiana* leaves transiently expressing CERK1^{WT}, FLS2^{WT} and free-GFP as well as co-expressing CERK1^{WT} + SUMO1 and FLS2^{WT} + SUMO1 were extracted following 30 minutes of 1μM chitooctaose treatment. 50μL of total protein was preserved as input, and the rest was purified by immunoprecipitation using anti-GFP beads (IP: α GFP). IP and Input samples were then separated in an SDS-PAGE gel, transferred to a PVDF membrane, and immunoblotted with anti-GFP (IB: α GFP). X-ray exposed to immunoblot for 1 minute. **(B)** Total protein from *N. benthamiana* leaves transiently expressing CERK1^{WT}, FLS2^{WT} and SUMO1 as well as co-expressing CERK1^{WT} + SUMO1 and FLS2^{WT} + SUMO1 were extracted following 30 minutes of 1μM chitooctaose treatment. 50μL of total protein was preserved as input, and the rest was purified by immunoprecipitation using anti-GFP beads (IP: α GFP) for all samples except SUMO1, and anti-HA beads (IP: α HA) for SUMO1. IP and Input samples were then separated in an SDS-PAGE gel, transferred to a PVDF membrane, and immunoblotted with anti-HA (IB: α HA). X-ray exposed to immunoblot for 15 minutes. CERK1 = 67.3kDa, FLS2 =128.8kDa, GFP = 27kDa, CERK1-GFP fusion protein = 94.3kDa, FLS2-GFP fusion protein = 155.8kDa, SUMO1 = 15kDa, HA = 1.1kDa, CERK1-GFP-3 SUMO1-HA = 142.6kDa, FLS2-GFP-5 SUMO1-HA = 236.3kDa
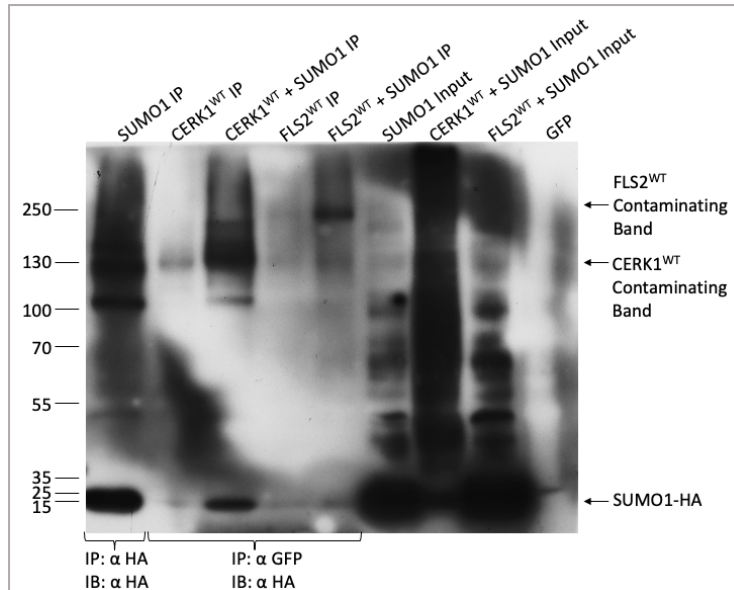
Figure 5.4. Immunoblot showing contaminating bands in CERK1^{WT} and FLS2^{WT} negative control lanes. Total protein from *N. benthamiana* leaves transiently expressing CERK1^{WT}, FLS2^{WT} and SUMO1 as well as co-expressing CERK1^{WT} + SUMO1 and FLS2^{WT} + SUMO1 were extracted following 30 minutes of 1μM chitooctaose treatment. 50μL of total protein was preserved as input, and the rest was purified by immunoprecipitation using anti GFP-beads (IP: α GFP) for all samples except SUMO1, and anti HA-beads (IP: α HA) for SUMO1. IP and Input samples were then separated in an SDS-PAGE gel, transferred to a PVDF membrane, and immunoblotted with anti-HA (IB: α HA). X-ray exposed to immunoblot for 30 minutes. CERK1 = 67.3kDa, FLS2 =128.8kDa, GFP = 27kDa, CERK1-GFP fusion protein = 94.3kDa, FLS2-GFP fusion protein = 155.8kDa, SUMO1 = 15kDa, HA = 1kDa, CERK1-GFP-3 SUMO1-HA = 142.6kDa, FLS2-GFP-5 SUMO1-HA = 236.3kDa

5.2.4. Co-Immunoprecipitation of CERK1^{2KR} and SUMO1

Co-immunoprecipitation of CERK1^{2KR} with SUMO1 was performed to determine if

CERK1^{2KR}, which contains two SUMO-site mutations, is SUMOylated upon chitin elicitation.

Free-GFP was used as a positive control for the anti-GFP immunoblot and SUMO1 was used as a

positive control for anti-HA immunoblot. *CERK1^{WT}* p103 was co-infiltrated with *SUMO1* p201

and *CERK1^{2KR}* p103 was co-infiltrated with *SUMO1* p201 in equal concentrations. 2 days post

infiltration, leaves were inoculated with 1μM chitooctaose and left for 30 minutes before leaf

tissue was harvested and total protein was extracted. Protein samples were then purified with

immunoprecipitation using anti-GFP microbeads, except for the SUMO1 control sample which

was immunoprecipitated with anti-HA microbeads. Purified samples were then run through

two separate SDS-PAGE gels along with total protein input samples. Separated protein in gels

were then transferred to PVDF membranes and one was immunoblotted with anti-GFP, and the

other immunoblotted with anti-HA. The protein was visualized using chemiluminescence on X-

ray paper. In the anti-GFP blot, bands at approximately 100kDa were visualized in the CERK1^{WT},

CERK1^{WT} + SUMO1, CERK1^{2KR} and CERK1^{2KR} + SUMO1 IP sample lanes, as well as a band around

27kDa in the free-GFP positive control lane (Figure 5.5, A). In the anti-HA blot, a band at

approximately 130kDa was visualized in the CERK1^{WT} + SUMO IP sample lane and CERK1^{2KR} +

SUMO sample lane. Similarly to the previous immunoblots, there also appeared to be faint

bands at 130kDa in the CERK1^{WT} and CERK1^{2KR} negative control lanes (Figure 5.5, B). This

experiment was repeated several times, with conscious effort to ensure there was no mixing of

samples during protein extraction, immunoprecipitation and while loading samples into SDS-

PAGE gel wells. The same contaminating bands were seen in the control lanes each time the
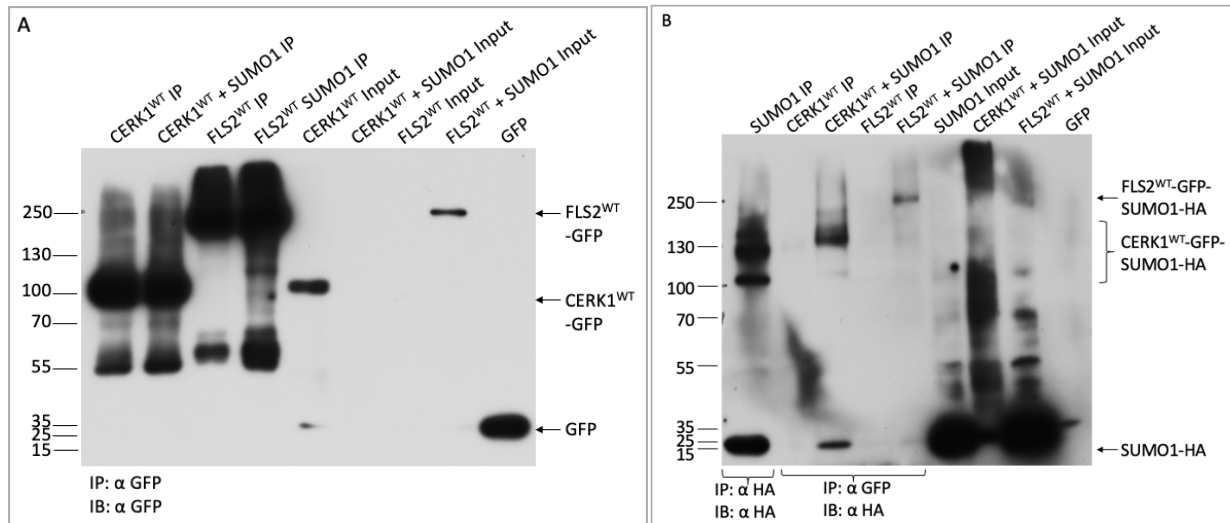
experiment was repeated.
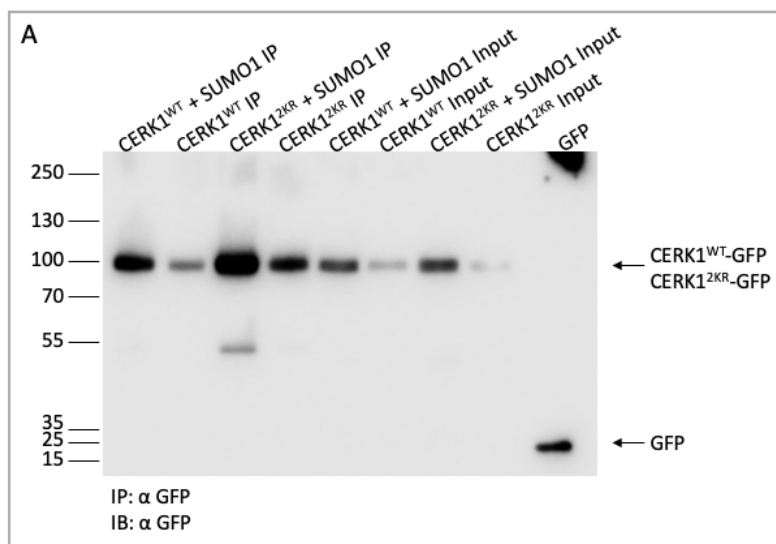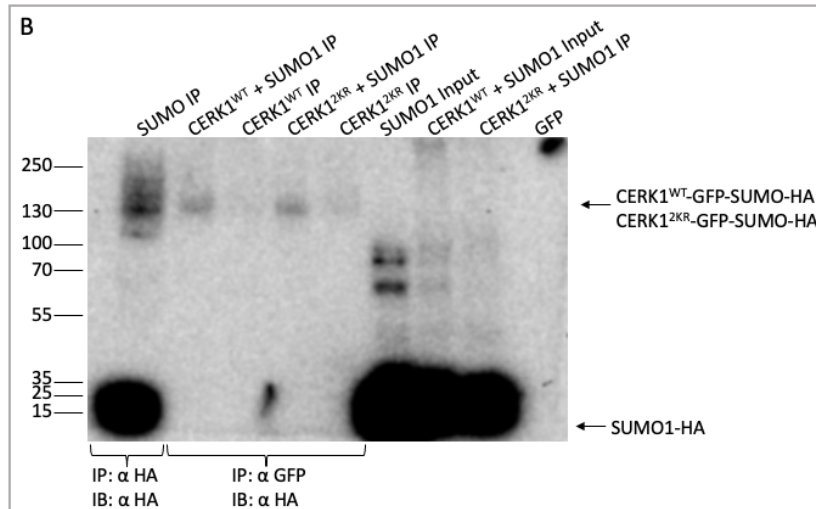
Figure 5.5. Immunoblots showing interaction of CERK1^{WT} and CERK1^{2KR} with SUMO1. **(A)** Total protein from *N. benthamiana* leaves transiently expressing CERK1^{WT} and CERK1^{2KR} and free-GFP as well as co-expressing CERK1^{WT} + SUMO1 and CERK1^{2KR} + SUMO1 were extracted following 30 minutes of 1μM chitooctaose treatment. 50μL of total protein was preserved as input, and the rest was purified by immunoprecipitation using anti-GFP beads (IP: α GFP). IP and Input samples were then separated in an SDS-PAGE gel, transferred to a PVDF membrane, and immunoblotted with anti-GFP (IB: α GFP). X-ray exposed to immunoblot for 5 minutes. **(B)** Total protein from *N. benthamiana* leaves transiently expressing CERK1^{WT}, CERK1^{2KR} and SUMO1 as well as co-expressing CERK1^{WT} + SUMO1 and CERK1^{2KR} + SUMO1 were extracted following 30 minutes of 1μM chitooctaose treatment. 50μL of total protein was preserved as input, and the rest was purified by immunoprecipitation using anti GFP-beads (IP: α GFP) for all samples except SUMO1, and anti-HA beads (IP: α HA) for SUMO1. IP and Input samples were then separated on an SDS-PAGE gel, transferred to a PVDF membrane, and immunoblotted with anti-HA (IB: α HA). X-ray exposed to immunoblot for 1 hour. CERK1 = 67.3kDa, GFP = 27kDa, CERK1-GFP fusion protein = 94.3kDa, SUMO1 = 15kDa, HA = 1kDa, CERK1-GFP-3 SUMO1-HA = 142.6kDa

5.3. Discussion

5.3.1. Protein Localization to the Cellular Membrane

CERK1^{WT} and CERK1^{2KR} appeared to localize in the cell membrane. This makes sense based on literature proving that CERK1 is a transmembrane protein embedded in the phospholipid bilayer. This localization is essential to CERK1 function as a receptor kinase, as the lysM domain in the extracellular matrix functions to receive external signals from chitin, the transmembrane domain allows the protein to span the phospholipid bilayer, and the kinase domain within the cell can initiate signal transduction via phosphorylation to downstream

proteins. Several other studies have found similar cellular localization of CERK1 (Miya et al. 2007; Shinya et al. 2014; Yamada et al. 2016; Erwig et al. 2017). CERK1^{2KR} was also found to localize in the cellular membrane, confirming proper transcription, translation, and localization of *CERK1^{2KR}* p103. Expression of CERK1^{2KR} confirmed that protein formation and stability was not affected by the two amino acid substitutions, which is important information for future investigations in this project because it confirms that the 2KR mutation in CERK1 does not destabilize the protein or prevent it from localizing in the membrane. Showing that the CERK1^{2KR} mutant is expressed in the membrane confirms that any impact on protein function has to do with the specific mutation induced and not with issues in protein expression and localization. LYK5 and PBL27 were also shown to localize to the cellular membrane, corroborating previous literature that also showed membrane localization of these proteins (Shinya et al. 2014; Yamada et al. 2016; Erwig et al. 2017; Giovannoni et al. 2021). LYK5 is a transmembrane receptor protein which works in a complex with CERK1 to bind to chitin upon fungal infection, so localization to the cellular membrane is vital to its function (Erwig et al. 2017; Giovannoni et al. 2021). PBL27 is a plasma membrane-anchored protein and it interacts with both CERK1 and MAPKKK5 at the plasma membrane to conduct the chitin immune signal in the cell via phosphorylation (Shinya et al. 2014; Yamada et al. 2016).

5.3.2. CERK1^{WT} and CERK1^{2KR} Expression and Visualization on Immunoblots

CERK1^{WT} and CERK1^{2KR} were expressed in *N. benthamiana* and were consistently isolated, purified and visualized on immunoblots (Figure 5.2). These constructs were cloned from scratch and sequenced to ensure that they did not contain any mutations that could

destabilize the protein (Section 4.2.1.). In addition to the fact that these constructs didn't

contain any unwanted mutations, the protein lysis buffer was also changed to contain KCl and

SDS was removed. SDS is a strong detergent used in lysis buffers to solubilize the plasma

membrane to extract membrane-bound proteins. However, it can denature more sensitive

proteins, and this was a potential problem when trying to extract protein expressed by the

original constructs received (*CERK1^WT* p104 and *CERK1^3KR* p104) in section 3.2.3. These

constructs contained potentially destabilizing mutations, making them more vulnerable to

denaturing with SDS application. Removing SDS reduced the lysis buffer's strength to solubilize

the membrane but also reduced the probability of denaturing CERK1 in the process. NP-40

remained in the buffer as a detergent, however it is non-ionic and less likely to denature

proteins (Lewis 1997). The addition of KCl increased the salt content of the buffer, which

increases the ionic strength of detergents to solubilize the membrane (Lewis 1997). It is likely

that removal of SDS made the buffer less able to solubilize the membrane but allowed

membrane bound proteins such as CERK1 to remain stable, while the addition of KCl increased

the strength of the remaining detergents (NP-40) to disrupt the membrane, keeping

membrane-bound proteins intact. It is unclear whether the KCl lysis buffer would have been

able to extract protein from the *CERK1^WT* p104 and *CERK1^3KR* p104 constructs from the

membrane in section 3.2.3, because the new lysis buffer was researched and formulated while

re-cloning of *CERK1* was already underway. This experiment was not done in the interest of

time. Once CERK1^WT and CERK1^3KR were consistently visualized on immunoblots, co-

immunoprecipitation assays with SUMO1 could commence.

Figure 5.3 shows evidence that CERK1^{WT} and SUMO1 interact upon chitin elicitation because of the bands visualized at approximately 110kDa and 130kDa in the CERK1^{WT} + SUMO1 IP sample lane in the anti-HA immunoblot (Figure 5.3). This sample was purified with anti-GFP microbeads and immunoblotted with anti-HA antibody, so only HA-tagged proteins interacting with CERK1^{WT} should appear on this immunoblot. The band visualized is therefore likely SUMO-HA that is conjugated to CERK1 *in-vivo*. The band sizes ranging from 110kDa to 130kDa make sense in this context because they represent the CERK1^{WT}-GFP fusion protein with 1, 2, 3 or more SUMO conjugations, which would produce protein complexes with a total size 110.4kDa, 126.5kDa and 142.6kDa respectively. A band of approximately 230kDa visualized in the FLS2^{WT} + SUMO1 IP sample in the anti-HA immunoblot indicated interaction of FLS1^{WT} and SUMO1. The FLS2-GFP fusion protein with 1 to 5 SUMO conjugations would produce bands in the range of 171.9kDa to 236.3kDa (Figure 5.3). This sample acts as a positive control for SUMO1 co-immunoprecipitation, because FLS2 has been previously shown to be SUMOylated by Orosa and colleagues (Orosa et al. 2018). Upon longer exposure of the x-ray paper to this blot, a band of approximately 130kDa was visualized in the CERK1^{WT} negative control lane and a band of approximately 230kDa was visualized in the FLS2^{WT} negative control lane (Figure 5.4). The negative control lanes should not contain any bands because *CERK1^{WT}* p103 and *FLS2^{WT}* p103 constructs were infiltrated individually into plant samples, purified with anti-GFP microbeads, and immunoblotted with anti-HA. There should be no interacting proteins visualized in these control lanes. Despite the presence of the contaminating band at 130kDa, this blot still shows evidence of SUMOylation of CERK1^{WT} because of the correct sized bands present in the

CERK1^{WT} + SUMO1 IP lane, and the contaminating band is likely a result of technical error. This

will be covered later in the discussion in section 5.3.5.

Co-immunoprecipitation of CERK1^{WT} + SUMO1 and CERK1^{2KR} + SUMO1 immunoblotted

with anti-HA is shown in Figure 5.5, B. A band of approximately 130kDa was visualized in the

CERK1^{WT} + SUMO IP sample and in the CERK1^{2KR} + SUMO IP sample, representing the CERK1-

GFP fusion protein and 3 SUMO1 conjugations. It was predicted that SUMOylation would be

reduced in the CERK1^{2KR} mutant, having only one functional SUMO-site left, and that it would

produce a smaller band at approximately 110kDa. This does not seem to be the case as a band

at approximately 130kDa was visualized in the CERK1^{2KR} + SUMO IP sample lane. This is

potentially because the SUMO-sites predicted by the software in Yate's unpublished thesis

were in fact just predictions using computer algorithms and are therefore not guaranteed to be

true SUMO sites (Yates 2018). In addition, only two out of the three predicted SUMO-sites are

mutated in this construct, and it is possible that most or all SUMOylation occurs in the K495

residue which lies within the kinase domain. The kinase domain is responsible for

phosphorylating and activating downstream signalling RLCK proteins such as PBL27 and BIK1, so

it is possible that only this region is modified by SUMO to regulate immune signalling. In the

study by Orosa and colleagues, they showed reduced SUMOylation of FLS2 by mutating the

predicted SUMO-site within the kinase domain, suggesting that this site is most heavily

modified by SUMO upon bacterial infection (Orosa et al. 2018). In future research, the single

CERK1^{K495R} mutant and the triple CERK1^{3KR} mutant should be tested for SUMOylation. Upon

further analysis of this blot, like the previous immunoblot in figure 5.4, there appeared to be faint contaminating bands at 130kDa in the CERK1^{WT} and CERK1^{2KR} negative control lanes. These lanes should not contain any bands because *CERK1^{WT}* p103 and *CERK1^{2KR}* p103 constructs were infiltrated into plant tissue individually and should not contain any HA-tagged interacting protein. This blot still shows evidence of SUMOylation of CERK1^{2KR} and the bands are most likely due to technical error.

5.3.5. Possible Explanations for Contaminating Bands

When the contaminating bands at 130kDa in the negative control CERK1^{WT} and CERK1^{2KR} IP sample lanes as well as the 230kDa band in the negative control FLS2^{WT} IP sample lane were observed, the most obvious first troubleshooting step was to redo the experiments. Conscious effort was made to prevent mixing of samples during the infiltration, protein extraction, immunoprecipitation, and protein gel loading steps. The same result was produced after multiple attempts to produce images with clear negative control bands. Despite this effort, it is still a possibility this issue was a result of mixing of samples, or spillage of samples into adjacent wells while gel loading, because the contaminating bands are the exact same size as the co-immunoprecipitation bands in the co-infiltrated samples. In the event that this issue was not due to technical error and mixing of samples, a possible explanation for the extra bands is SUMO1-HA contamination in the *Agrobacteria* glycerol stocks containing *CERK1^{WT}* p103, *CERK1^{2KR}* p103 and *FLS2^{WT}* p103 constructs. This would mean that the negative control samples that were infiltrated individually actually did contain some SUMO1-HA which would explain the presence of the same-sized band as the co-infiltrated samples in the negative control lanes.

Since the contaminating bands were consistently present in all repeats of this experiment, it is more likely that the contamination occurred in the glycerol stocks and not by mixing samples in each experimental repeat. Another possible explanation for these bands is a potential endogenous interacting protein of CERK1 and FLS2 that has a very similar structure to HA. If this protein interacts with CERK1 and FLS2 *in vivo*, it would be purified along with CERK1 and FLS2 during immunoprecipitation. If it had a similar enough protein structure to HA, then anti-HA primary antibody would bind to it, and it would be present on the immunoblot. This explanation seems less likely however, because an endogenous protein in *N. benthamiana* would be less likely to bind to *Arabidopsis* CERK1 and FLS2 due to protein structure differences in the different plant species. As well, endogenous proteins would rarely show up in immunoprecipitation because expression levels would be much lower compared to the infiltrated overexpressed proteins CERK1, FLS2 and SUMO1. The next troubleshooting steps for this research would be to re-transform the *CERK1^{WT}* p103, *CERK1^{2KR}* p103 and *FLS2^{WT}* p103 constructs into *Agrobacteria* and carry out the experiment again with the newly transformed cultures. This would determine if the problem had to do with SUMO1 contamination in the *Agrobacteria* glycerol stocks. Another troubleshooting step to consider is using anti-SUMO1 primary antibody instead of anti-HA. Anti-SUMO requires high SUMO-protein concentration, but it would have higher specificity to SUMO1 and would be less likely to bind endogenous protein. These trouble shooting steps were not conducted during this project due to time constraints but are recommended for future investigations on this topic.

5.3.6. Limitations of This Research and Suggested Next Steps

A lot of time was consumed dealing with the initial issues isolating and showing CERK1 expression on immunoblots, re-cloning of CERK1, site-directed mutagenesis and then troubleshooting the contaminating band. Since this project was only a year in duration, time constraints prevented further troubleshooting of the contaminating band and continued investigation of CERK1^{WT} and CERK1^{2KR} interaction with SUMO1, as well as the interaction of CERK1^{2KR} with the co-signalling protein LYK5 and downstream signalling protein PBL27. Co-immunoprecipitation of CERK1^{WT} and CERK1^{2KR} with LYK5 and PBL27 were not performed because time was prioritized to determining the interaction of CERK1^{WT} and CERK1^{2KR} with SUMO1 and troubleshooting the contaminating band problem. The results presented in this project show evidence that CERK1 is SUMOylated upon chitin elicitation, however, re-running the experiment with uncontaminated samples to obtain a blot without bands in the negative control lane would be ideal to confirm this data. In further research, it would be worth investigating the SUMOylation of CERK1^{K495R} single SUMO-site mutant since this mutation occurs within the kinase domain. If SUMOylation is reduced or inhibited in the CERK1^{K495R} mutant, then it is likely to impact the interaction of CERK1 with PBL27, since the kinase domain is responsible for phosphorylating PBL27 to transmit the immune signal. Finally, generating the CERK^{3KR} triple SUMO-site mutant would be necessary to get a full picture of SUMOylation of CERK1 and to better determine whether SUMOylation is a required PTM during fungal PTI signalling.

6.0. *Botrytis cinerea* Infection Assay Analysis

6.1. Introduction

Botrytis cinerea is among the most widespread and damaging pathogenic fungi in the world and causes disease in various crop tissues pre-and post-harvest, making infection surveillance difficult (WILLIAMSON et al. 2007; Shah et al. 2012; Sarven et al. 2020; Shao et al. 2021). A favourable and long-lasting disease management method is the production of genetically resistant crop species, so an understanding of molecular interactions and immune signalling during *B. cinerea* infection is vital (Fones et al. 2020). It is well-established based on previous literature that CERK1 is essential to initiate a response to chitin, the main PAMP molecule present during fungal infection. Many studies have shown a reduction in MAPK signalling, lower ROS production and lower defence gene expression in CERK1 K/O mutants upon chitin treatment (Miya et al. 2007; Wan et al. 2008a; Petutschnig et al. 2010). However, the importance of CERK1 in immunity upon fungal infection has been shown to be dependent on the species of fungus, and no previous literature has analysed the importance of CERK1 for immunity upon *B. cinerea* infection (Miya et al. 2007; Wan et al. 2008a; Petutschnig et al. 2010). Post-translational modification by SUMOylation has been proven to play a key role during necrotrophic fungal infection, and specifically during *B. cinerea* infection. However, the specific protein targets and mechanisms of SUMO-mediated defence is unknown (Fraire-Velázquez and Lozoya-Gloria 2003; Li et al. 2013, 2019; Castaño-Miquel et al. 2017; Stocks et al. 2019). It has been shown that SUMOylation of the PRR protein FLS2 during bacterial infection is essential for initiation of signalling cascades and immune responses (Orosa et al. 2018). The specificity of the SUMO system is predicted to be governed by de-conjugating SUMO-proteases,

since there are more of these proteins than there are SUMO, SUMO activating enzymes, SUMO-conjugating enzymes and SUMO ligating enzymes (Morrell and Sadanandom 2019). One SUMO-protease in particular, DeSI3a, has been shown to localize to the cell membrane and interact with FLS2 (Orosa et al. 2018; Morrell and Sadanandom 2019). DeSI3a cleaves SUMO from target substrates and is a negative regulator of defence upon bacterial infection, as DeSI3a K/O transgenic *Arabidopsis* had enhanced resistance to bacterial infection and showed higher expression of defence genes upon flagellin elicitation (Orosa et al. 2018; Yates 2018). In addition, DeSI3a K/O *Arabidopsis* showed higher expression of defence genes upon chitin elicitation, suggesting it may have similar functions in the fungal PTI pathway (Yates 2018). The original plan for this research was to analyse the importance of SUMOylation during the fungal PTI response by conducting *B. cinerea* infection assays on *cerk1-3KR* transgenic *Arabidopsis* and compare lesion size development with *cerk1-2* K/O and the Col-0. However, it was discovered in section 3.2.1. that the transgenic *Arabidopsis* lines received were not transgenic and did not contain a version of the *CERK1* CDS with SUMO-sites mutated, so these assays could not be completed. The *desi3a-1* K/O *Arabidopsis* line presented an additional way to determine the role of SUMOylation in the fungal PTI pathway. Since SUMOylation confers resistance during bacterial infection, de-SUMOylation by DeSI3a SUMO-protease confers susceptibility. Therefore, the *desi3a-1* K/O transgenic *Arabidopsis* has enhanced resistance to bacterial infection due to lack of or reduced SUMO de-conjugation, also known as hyper-SUMOylation. Since *desi3a-1* K/O *Arabidopsis* indicated the role of SUMOylation in bacterial PTI, it is likely that *desi3a-1* K/O *Arabidopsis* can also help deduce the role of SUMOylation in fungal PTI by analysing plant resistance or susceptibility during *B. cinerea* infection assays. It was predicted

that *cerk1-2* K/O transgenic *Arabidopsis* would have decreased immunity upon *B. cinerea* infection, measured by larger lesions and higher accumulation of fungal DNA, compared to Col-0. *Desi3a-1* K/O transgenic *Arabidopsis* was predicted to have enhanced immunity to infection by *B. cinerea,* measured by smaller lesions and lower fungal DNA accumulation, compared to Col-0.

6.2. Results

6.2.1. Lesion Size Analysis Following *B. cinerea* Infection

   B. cinerea strain H/A5 grown for 2-3 weeks on petri dishes containing potato dextrose agar (PDA) in the dark was used for spore suspension preparation. *B. cinerea* infection assays were carried out on 4–5-week-old *Arabidopsis* grown in long-day conditions. Col-0 as well as *cerk1-2* K/O and *desi3a-1* K/O transgenic lines were used. Biological replicates consisted of 3 agar plates containing 5 leaves of each genotype each (15 leaves per each genotype total). Spore suspension was pipetted onto each leaf, and plates were stored in the dark at 23°C. Photographs taken at 5 DPI were used for analysis, and leaf and lesion size were measured using ImageJ software. Lesion % of total leaf area was calculated and used for comparison between the genotypes. The average lesion % of total leaf area at 5 DPI was 14.16% in Col-0, 22.85% in *cerk1-2* K/O and 16.7% in *desi3a-1* K/O. Lesion % of total leaf area in the *cerk1-2* K/O line was significantly higher than Col-0 and *desi3a-1* K/O (P<0.001). There was no significant difference between the lesion % of total leaf area in Col-0 and *desi3a-1* K/O (Figure 6.1).
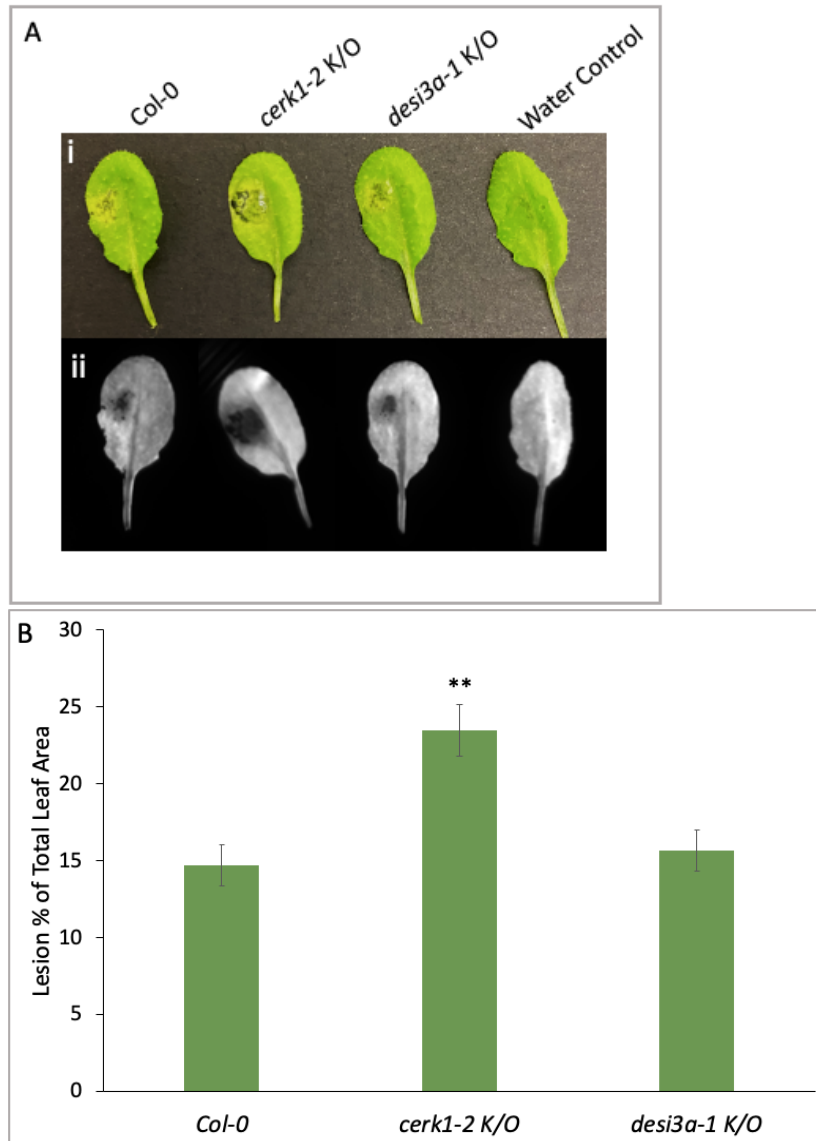
Figure 6.1. Lesion % of total leaf area at 5 DPI. **(A, i)** photograph of a single leaf from each genotype. Leaves selected for visual representation of data. **(A, ii)** Red light imaging of the leaves pictured in (i). Black colouration on leaves under red light indicates necrotrophy due to *B. cinerea* infection. **(B)** Graphical representation of lesion % of total leaf area. Values are the average lesion % from 3 independent experiments each consisting of 15 replicates per genotype (60 leaves per genotype total). ** indicates significant difference (P<0.001). Error bars show the standard error calculated from the standard deviation of the dataset. Photographs taken by author and figure generated using Excel.

6.2.2. Fungal DNA Accumulation Analysis Following *B. cinerea* Infection

Leaves subjected to *B. cinerea* infection assays were pooled into 5 leaves per sample

and frozen at 5 DPI. Total DNA was then extracted from each frozen sample. qPCR was

performed on extracted DNA using *B. cinerea Actin* primers to measure fungal DNA

accumulation and *Arabidopsis Ubiquitin* primers as the reference gene to control for differences

in volume of tissue. Take-off values were analysed using the ΔCT method. Figure 6.2 shows the

average relative fungal load of each genotype at 5 DPI. The average relative fungal load was

0.18 in Col-0, 0.81 in *cerk1-2* K/O and 0.50 in *desi3a-1* K/O. Although the highest relative fungal

load was in the *cerk1-2* K/O sample, there was no significant difference between the genotypes.

The single peak in the melt curve graphs of both *B. cinerea Actin* and *Arabidopsis Ubiquitin*

show that a single product was amplified in each reaction, and therefore Ct values produced

from the qPCR were specific to *B. cinerea Actin* and *Arabidopsis Ubiquitin* amplification, and not

some other product due to unspecific primer binding (Figure 6.3)
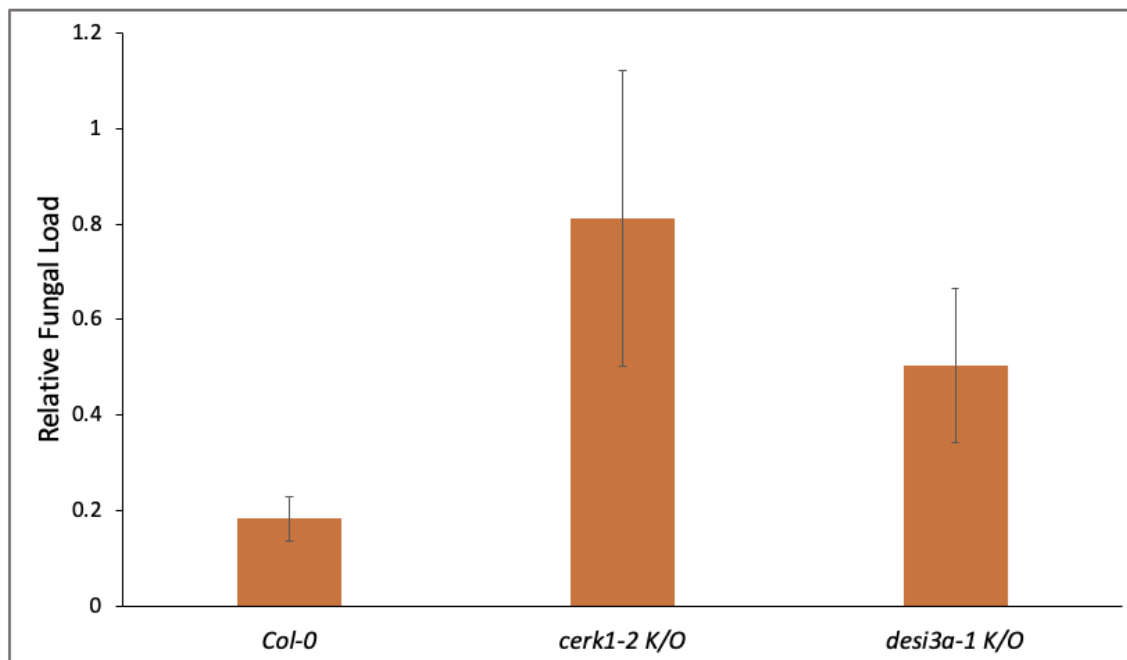
Figure 6.2. Average relative fungal load in leaf samples subjected *B. cinerea* spores at 5 DPI. Relative fungal load was calculated by the formula $2^{-\Delta CT}$, where ΔCT was the average Ct value of *B. cinerea Actin* gene subtracted by the average Ct value of *Arabidopsis Ubiquitin* gene in each sample. Values are the average fungal load in 3 independent experiments consisting of 3 biological replicates for each genotype (9 leaf samples total for each genotype). There was no significant difference between relative fungal load of samples ($P>0.05$). Error bars show the standard error calculated from the standard deviation in the dataset. Figure generated by author using Excel.
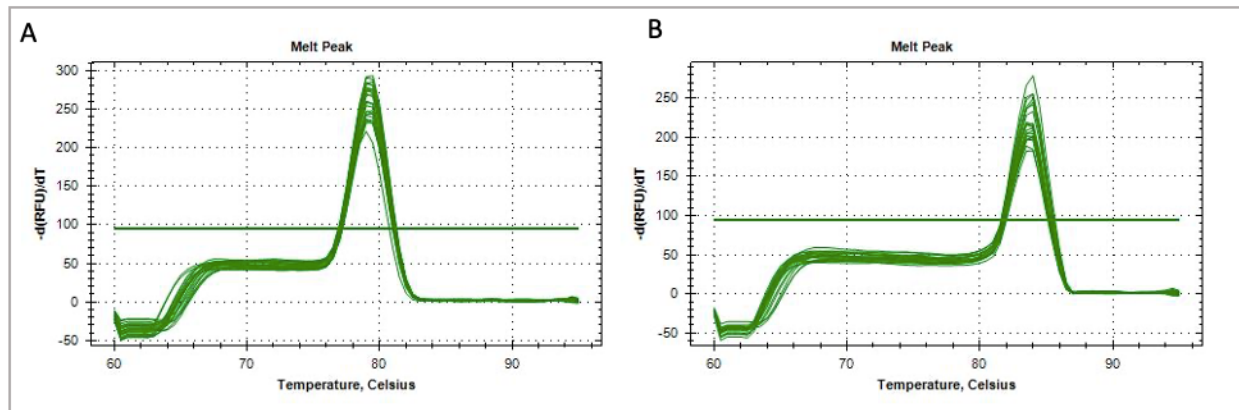
Figure 6.3. Melt curve graphs of one qPCR amplification reaction of **(A)** B. *cinerea Actin* gene and **(B)** *Arabidopsis Ubiquitin* gene. -d(RFU)/dT represents the change in fluorescence divided by the change in temperature, plotted over temperature. The single peak in each graph indicates that each amplification reaction amplified a single gene product and there was no unspecific primer binding and amplification. qPCR experimental repeats had similar melt curves. Figure taken from qPCR results page.

6.3. Discussion

6.3.1. Lesion Development in *cerk1-2* K/O Following *B. cinerea* Infection

On average, lesions caused by *B. cinerea* spores grew the largest compared to total leaf area in the *cerk1-2* K/O transgenic *Arabidopsis* line. Lesion % of total leaf area was significantly higher in this line than in both Col-0 and *desi3a-1* K/O at 5 DPI (P<0.001). This result aligns with previous literature that indicate CERK1 K/O mutants have higher susceptibility to some fungal species because they have lost the ability to respond to chitin elicitors and cannot initiate MAPK signalling, produce ROS or induce the expression of defence genes (Miya et al. 2007; Petutschnig et al. 2014). The *cerk1-2* K/O line contains a T-DNA insertion between exon 10 and exon 11 and was shown to express a version of CERK1 that is truncated in this region, causing it to lose ability to respond to chitin (Figure 6.4, Miya et al. 2007). It is possible that this truncated version of the protein is still able to bind chitin, but it is unable to phosphorylate downstream proteins because most of its kinase domain is missing. CERK1 K/O mutants lacking

the ability to perform PTI will likely have higher susceptibility to fungal infection, which is demonstrated in this scenario during *B. cinerea* infection. However, this is not the case with all species of pathogenic fungi, and the variability in CERK1 K/O susceptibility to infection is demonstrated in the following examples. When CERK1 K/O mutants in one study were infected with the fungus *Alternaria brassicicola*, disease resistance was partially impaired and showed slightly larger lesions in the knockout lines (Miya et al. 2007). In the same study, CERK1 K/O mutants were infected with the fungus *Colletotrichum higginsianum*, and no significant difference was found in lesion size and disease resistance between the CERK1 K/O line and Col-0 (Miya et al. 2007). In another study, *cerk1-2* K/O was infected with the powdery mildew fungal pathogen *Erysiphe cichoracearum,* and was found to have higher and faster production of hyphae and conidiophores than Col-0, suggesting that the knockout plants were more susceptible to the fungus (Wan et al. 2008a). According to these findings, it is predicted that the importance of chitin perception by CERK1 during fungal infection is dependent on the species of fungi and that in some species, CERK1 only partially contributes to resistance. This could be because disease resistance is a multi-layered system, sometimes consisting of multiple PAMP and effector molecules. Some species utilize an array of PAMP and effector molecules so that the interruption of a single component in the system does not cause a drastic change in immunity. In the case of *Colletotrichum higginsianum,* the fungus secretes multiple effector proteins which prevent the function of plant chitinases and compete with host plant PRR proteins, such as CERK1 (Yan et al. 2018). Therefore, R proteins specific to these effector molecules may play a larger role in defence to this particular fungal infection than CERK1. *B. cinerea* does not rely as heavily on host-specific effector molecules. For this reason, plant hosts

don't generally contain single R genes for *B. cinerea* infection, so the ETI defence system is

largely irrelevant (Bi et al. 2022). Plants must rely heavily on PTI defences, so the recognition of

PAMP molecules such as chitin during infection is vital to survival (Bi et al. 2022). This rationale

explains why CERK1 plays a larger role in defence against *B. cinerea* infection and why larger

lesions were able to develop in plants lacking functional CERK1 protein. It should be noted here

that the CERK1 complemented line (transgenic *Arabidopsis* line that contain functional CERK1

re-complemented into the *cerk1-2* K/O line) should be used in future experiments to confirm

that lack of functional CERK1 is the sole reason for the resulting phenotype (larger lesion % of

total leaf area) and that no other factor is affecting susceptibility. The CERK1 complement lines

were not available to use in this experiment (Section 3.2.1) and that is why they were not

included. However, high confidence can still be placed in the results of this experiment based

on the complementary results found in previous literature using the *cerk1-2* K/O and CERK1

complement lines. All previous experiments on *cerk1-2* K/O found that decreased PTI

responses to chitin were the result of non-functioning CERK1, because PTI responses were

restored in the CERK1 complement line (Miya et al. 2007; Wan et al. 2008b).
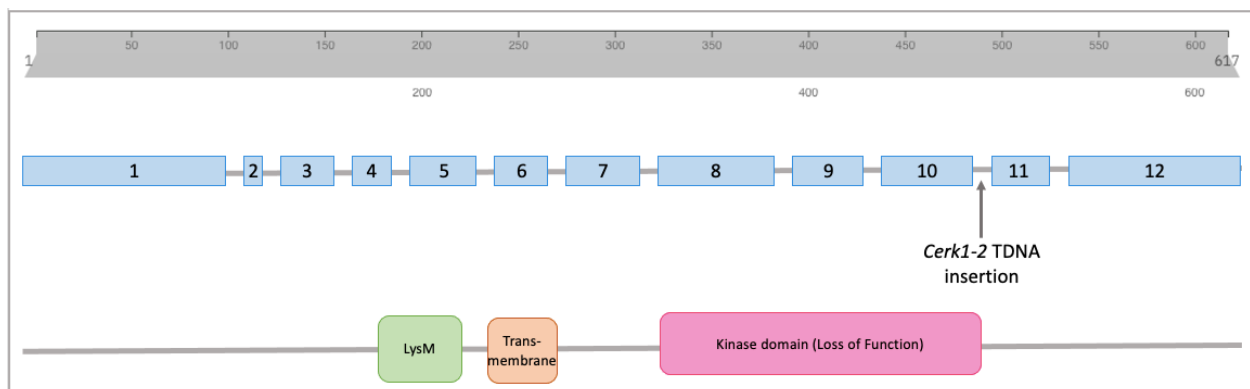
Figure 6.4. T-DNA insertion between exon 10 and exon 11 in *cerk1-2* K/O mutant generates a protein with a non-functional kinase domain and therefore inability to respond to chitin elicitation. Figure generated by author using PowerPoint.

It was predicted that the *desi3a-1* K/O transgenic *Arabidopsis* would have more

resistance to *B. cinerea* infection compared to Col-0. The lesion % of total leaf area was higher

in *desi3a-1* K/O than Col-0, however not significantly. This result contrasts results by Orosa and

colleagues who studied DeSI3a in the bacterial PTI pathway and found that *desi3a-1* K/O lines

had more resistance to infection by *Pseudomonas syringae*, measured by necrosis of leaves and

colony-forming units, at 3 DPI (Orosa et al. 2018). There are a few explanations that help to

explain these results. One explanation is that SUMO plays a different role in fungal defence

systems than in bacterial defence systems and therefore de-SUMOylation by SUMO proteases

play a different role in immunity. The bacterial and fungal PTI immune systems are slightly

different despite many similarities. For example, there are two PRR proteins (CERK1 and LYK5)

in fungal PTI that work together to bind chitin, whereas there is only the single PRR protein

(FLS2) to bind flagellin in bacterial PTI. Secondly, bacterial PTI uses the same RLCK protein

(BIK1) to induce MAPK signalling as well as ROS response, whereas fungal PTI uses two

individual proteins (BIK1 to induce ROS and PBL27 to initiate MAPK signalling) (Cao et al. 2014;

Shinya et al. 2014; Yamada et al. 2016; Liu et al. 2018; Orosa et al. 2018). Since there are

differences in signalling proteins in each pathway, it is possible that SUMOylation plays a

different role in defence in each pathway. However, the many studies of SUMOylation during

fungal infection all indicate that SUMOylation plays a positive role in defence against fungal

infection, and that SUMO proteases negatively regulate defence (Fraire-Velázquez and Lozoya-

Gloria 2003; Li et al. 2013, 2019; Castaño-Miquel et al. 2017; Stocks et al. 2019). In Yates' 2018

unpublished thesis, he showed that the *desi3a-1* K/O line had enhanced ROS production upon

chitin elicitation, indicating more disease resistance when DeSI3a function was removed and therefore more resistance during hyper-SUMOylation. Although this experiment was only repeated once, all other proof on this topic indicate that SUMO plays a positive role in infection, and this explanation can likely be ruled out. The second and more likely explanation is that the experimental conditions weren't set up optimally for this system. It is possible that the resistance conferred by lack of DeSI3a and hyper-SUMOylation of target proteins in the fungal PTI pathway is subtle and was overpowered by the fungal infection. In other words, the spore concentration used in the experiment may have been high enough that the fungus was able to override plant PTI defence mechanisms and establish itself successfully, regardless of the immunity conferred by hyper-SUMOylation in the *desi3a-1* K/O transgenic *Arabidopsis*. To explore this possibility further, additional *B. cinerea* assay analysis should be carried out on *desi3a-1* K/O and Col-0 *Arabidopsis* using serial dilutions of spore suspension and analysing lesion size development. It is likely that with a lower spore suspension, the resistance conferred by hyper-SUMOylation would be visible.

6.3.3. Fungal DNA Accumulation Analysis Following *B. cinerea* Infection

Relative fungal load was higher in the *cerk1-2* K/O (0.81) than in Col-0 (0.18), however this increase was not significantly different. Since lesion % of total leaf area was significantly higher in *cerk1-2* K/O than Col-0, it would make sense that fungal DNA accumulation was also significantly higher. Additionally, *desi3a-1* K/O had a higher relative fungal load at 5 DPI than Col-0, when the lesion % of total leaf area at 5 DPI was very similar to Col-0. The qPCR results depicting relative fungal load in the leaf samples were therefore inconsistent with the lesion

size analysis at 5 DPI. A possible explanation for the highly variable data is the fact that 5 leaves of a single genotype infected with *B. cinerea* spores were accumulated into a single sample for DNA extraction to be used in qPCR analysis. By accumulating biological replicates into a single DNA extraction, the ability to remove outliers from the dataset was eliminated. When measuring lesion size, some leaves contained very large or very small lesions that were removed from the dataset as outliers using the Interquartile Range method. When the same leaf samples were frozen at 5 DPI for DNA extraction, all leaves were accumulated into samples of 5 leaves each. By accumulating samples, the outlier leaves that were removed in the lesion % dataset were included in the qPCR samples. The combination of increased variability of results and decreased number of biological replicates caused the standard error in the dataset to be higher, reducing the confidence of the results. This experiment should be repeated with more replicates, and each individual leaf should be used in a single sample for DNA extraction. This way, outliers in the data can be more accurately removed and the number of biological replicates in the experiment would increase, increasing the confidence level of the results and the correspondence to lesion size.

7.0. Concluding Remarks and Future Perspectives

7.1. Thesis Summary

The goal of this research was to explore the role of SUMOylation in the fungal PTI pathway in the model plant *Arabidopsis* upon *B. cinerea* infection. The original thesis objectives were to determine this role using co-immunoprecipitation assays and *B. cinerea* infection assays. If CERK1^{WT} was able to interact with SUMO1 while the CERK1^{3KR} mutant was not, then the interaction of CERK1^{3KR} with other PTI signalling proteins, LYK5 and PBL27, would be explored to determine if lack of SUMOylation of CERK1 inhibits the initiation of an immune response upon chitin detection. In addition, comparing lesion size development of *cerk1-3KR* and *desi3a-1* K/O transgenic *Arabidopsis* with Col-0 and *cerk1-2* K/O *Arabidopsis* upon *B. cinerea* infection would reveal immunity conferred by SUMOylation during infection. Due to material and experimental challenges, these thesis objectives were transitioned to better reflect the time and resources available.   In chapter 3, the discovery of faulty materials was described. The presence of missense and frameshift mutations in the *CERK1^{WT}* p104 and *CERK1^{3KR}* p104 constructs were likely destabilizing the resulting protein and preventing protein extraction and visualization on immunoblots. Additionally, genotyping analysis of transgenic *Arabidopsis* plants revealed that one of the CERK1 complement lines was just Col-0, and the other CERK1 complement line as well as both CERK1 3KR mutant lines were just *cerk1-2* K/O. Following these discoveries, the additional steps of re-cloning CERK1 and re-generating the SUMO-site mutant constructs were added into the project and were described in chapter 4. *CERK1*, *LYK5* and *PBL27* were successfully cloned. All three single KR SUMO-site mutants were generated using site-directed mutagenesis, and one double KR SUMO-site mutant was

generated (CERK1$^{K74R/K276R}$). The triple KR mutant was not successfully generated, and this was

likely due to technical inefficiency of single-target site-directed mutagenesis. The project

progressed using the CERK1^{2KR} double mutant as a replacement for the triple mutant. In

chapter 5, CERK1^{WT}, CERK1^{2KR}, LYK5 and PBL27 were shown to be expressed and to localize to

the cellular membrane. CERK1 was shown to interact with SUMO1 upon chitin elicitation,

however this data requires validation in future research due to the presence of a contaminating

band in the negative control. CERK1^{2KR} was also shown to interact with SUMO upon chitin

elicitation, so it is predicted that most SUMOylation occurs in the K495 site that resides in the

kinase domain. Again, this data requires validation in future research due to the presence of a

contaminating band in the negative control. This band was most likely caused by a

contamination of SUMO1 in the *Agrobacteria* glycerol stocks of each construct. Finally in

chapter 6, *B. cinerea* infection assays revealed the importance of CERK1 during *B. cinerea*

infection, as the *cerk1*-2 K/O transgenic *Arabidopsis* line developed the largest legions per total

leaf area compared to Col-0. Plant defence against *B. cinerea* infection relies heavily on PTI

defences over ETI defences, so the ability to initiate immune signalling in response to chitin is

vital. The *desi3a-1* K/O however did not show increased immunity as predicted and did not

have significantly smaller lesion development or fungal DNA accumulation than Col-0. All

evidence from previous literature suggests a positive role of SUMOylation in fungal immunity

and therefore a negative role of DesI3a SUMO-protease. It is therefore predicted that the

conditions in this experiment were not optimal for this system, and that the high spore

concentration overrode any immunity conferred by SUMO. Additionally, fungal DNA

accumulation in each genotype was inconsistent with lesion development and it is predicted

that this was because of accumulating samples for DNA extraction and thus increasing the standard error of the data.

7.2. Future Work and Applications

Overall, progress was made during this research project in determining the role of SUMOylation in the fungal PTI system, notably that CERK1^{WT} and CERK1^{2KR} interact with SUMO1 upon chitin elicitation. In addition, materials and methods for further research in this topic were created, validated, and optimized. Suggested future research endeavours in this topic include studying SUMOylation of the single CERK1^{K495R} mutant and the triple CERK1^{3KR} mutant to better understand the role of SUMOylation in the fungal PTI pathway, as well as the interaction of these mutant proteins with other PTI signalling proteins, LYK5 and PBL27, to determine if SUMOylation of CERK1 is essential for the initiation of an immune response. Additional next steps for this research also include regenerating the CERK1 complement and CERK1 3KR transgenic *Arabidopsis* lines and analysing the result of *B. cinerea* infection on lesion size development, fungal DNA accumulation, ROS production and induction of defence gene expression. These experiments will likely give a clear picture of SUMO's role in fungal PTI signalling. If SUMO is found to be essential for initiation of fungal PTI in response to *B. cinerea* infection, then this would present an opportunity for the development of resistant plant crop species via manipulation of SUMO conjugation or de-conjugation machinery by gene editing (Morrell and Sadanandom 2019; Zhang and Zeng 2020). Development of pathogen resistant crops is a desirable method of disease management as the control of *B. cinerea* infection by fungicide application and resistance breeding are insufficient in modern agriculture (Fones et al.

2020; Sarven et al. 2020). As growing food demand and increased spread of pests and disease

pose unique challenges to the future of agriculture, scientific discovery in mechanisms of

pathogen resistance in crops will become critical to food, economic and environmental security.

8.0. Appendix

```
A                      AttB1 primers

CERK1^WT pENTR4    NTCTCGAGAACGGANCAACACTCTCCGTCATCAACCAAAACCTCAATTCTTCAATCGCGC  180
TAIR CERK1^WT CDS  ATCTCGAGAACGGAACAACACTCTCCGTCATCAACCAAAACCTCAATTCTTCAATCGCGC  169
                   **********  *************************************************

CERK1^WT pENTR4    CTTACGATCAAATCAATTTCGATCCAATCCTCAGGTACAACAGTAACATTAAAGACAAAG  240
TAIR CERK1^WT CDS  CTTACGATCAAATCAATTTCGATCCAATCCTCAGGTACAACAGTAACATTAAAGACAAAG  229
                   ************************************************************

CERK1^WT pENTR4    ATAGAATCCAGATGGGCTCTAGGGTTCTTGTACCTTTCCCTTGCGAATGTCAACCTGGTG  300
TAIR CERK1^WT CDS  ATAGAATCCAGATGGGCTCTAGGGTTCTTGTACCTTTCCCTTGCGAATGTCAACCTGGTG  289
                   ************************************************************

CERK1^WT pENTR4    ATTTCCTAGGGCACAATTTCAGCTACAGTGTTCGACAGGAAGATACTTACGAAAGAGTCG  360
TAIR CERK1^WT CDS  ATTTCCTAGGGCACAATTTCAGCTACAGTGTTCGACAGGAAGATACTTACGAAAGAGTCG  349
                   ************************************************************

CERK1^WT pENTR4    CGATTAGTAATTACGCGAATCTCACGACGATGGAGTCGTTACAGGCGAGGAATCCTTTTC  420
TAIR CERK1^WT CDS  CGATTAGTAATTACGCGAATCTCACGACGATGGAGTCGTTACAGGCGAGGAATCCTTTTC  409
                   ************************************************************

CERK1^WT pENTR4    CGGCGACTAACATACCTCTCTCTGCGACGCTTAATGTATTGGTGAATTGTTCTTGTGGTG  480
TAIR CERK1^WT CDS  CGGCGACTAACATACCTCTCTCTGCGACGCTTAATGTATTGGTGAATTGTTCTTGTGGTG  469
                   ************************************************************

CERK1^WT pENTR4    ATGAGAGTGTTTCGAAAGATTTTGGTTTGTTTGTTACGTATCCGCTTCGTCCTGAAGACA  540
TAIR CERK1^WT CDS  ATGAGAGTGTTTCGAAAGATTTTGGTTTGTTTGTTACGTATCCGCTTCGTCCTGAAGACA  529
                   ************************************************************

CERK1^WT pENTR4    GTCTCAGTTCTATTGCGAGATCTTCCGGTGTATCGGCGGATATTCTGCAGAGATATAATC  600
TAIR CERK1^WT CDS  GTCTCAGTTCTATTGCGAGATCTTCCGGTGTATCGGCGGATATTCTGCAGAGATATAATC  589
                   ************************************************************

CERK1^WT pENTR4    CCGGTGTTAATTTTAACTCCGGGAATGGAATCGTTTATGTGCCTGGAAGAGATCCAAATG  660
TAIR CERK1^WT CDS  CCGGTGTTAATTTTAACTCCGGGAATGGAATCGTTTATGTGCCTGGAAGAGATCCAAATG  649
                   ************************************************************

CERK1^WT pENTR4    GTGCATTTCCACCATTCAAATCAAGTAAACAAGATGGTGTTGGTGCTGGAGTTATTGCTG  720
TAIR CERK1^WT CDS  GTGCATTTCCACCATTCAAATCAAGTAAACAAGATGGTGTTGGTGCTGGAGTTATTGCTG  709
                   ************************************************************

CERK1^WT pENTR4    GTATAGTTATAGGAGTGATTGTGGCTTTGTTGTTGATCTTGTTTATCGTATATTATGCTT  780
TAIR CERK1^WT CDS  GTATAGTTATAGGAGTGATTGTGGCTTTGTTGTTGATCTTGTTTATCGTATATTATGCTT  769
                   ************************************************************

CERK1^WT pENTR4    ACCGGAAGAATAAGTCGAAGGGTGATTCGTTTTCTTCTTCTATTCCGTTGTCTACTAAGG  840
TAIR CERK1^WT CDS  ACCGGAAGAATAAGTCGAAGGGTGATTCGTTTTCTTCTTCTATTCCGTTGTCTACTAAGG  829
                   ************************************************************

CERK1^WT pENTR4    CTGATCATGCTTCTTCTACTAGTCTCCAAAGTGGAGGTTTGGGTGGTTGCCGCAGTGTCT  900
TAIR CERK1^WT CDS  CTGATCATGCTTCTTCTACTAGTCTCCAAAGTGGAGGTTTGGGTGG-TGCCGGAGTGTCT  888
                   *************************************************  *****  *******
```

105

```
B          AttB2 primers
CERK1^WT pENTR4  TGCNTCTTCTACTAGTCTCCAAAGTGGAGGTTTGGGTGGTGCCGGAGTGTCTCCTGGCAT  185
TAIR CERK1^WT CDS  TGCTTCTTCTACTAGTCTCCAAAGTGGAGGTTTGGGTGGTGCCGGAGTGTCTCCTGGCAT  896
                   ***.******************************************************

CERK1^WT pENTR4  TGCTGCCATAAGCGTGGACAAATCTGTTGAGTTTTCGTTGGAGGAACTAGCAAAGGCTAC  245
TAIR CERK1^WT CDS  TGCTGCCATAAGCGTGGACAAATCTGTTGAGTTTTCGTTGGAGGAACTAGCAAAGGCTAC  956
                   ************************************************************

CERK1^WT pENTR4  TGATAATTTCAATTTGTCTTTTAAGATTGGGCAAGGTGGTTTTGGGGCTGTTTACTATGC  305
TAIR CERK1^WT CDS  TGATAATTTCAATTTGTCTTTTAAGATTGGGCAAGGTGGTTTTGGGGCTGTTTACTATGC  1016
                   ************************************************************

CERK1^WT pENTR4  AGAGCTGAGAGGAGAAAAAGCTGCGATTAAGAAGATGGACATGGAGGCATCGAAACAGTT  365
TAIR CERK1^WT CDS  AGAGCTGAGAGGAGAAAAAGCTGCGATTAAGAAGATGGACATGGAGGCATCGAAACAGTT  1076
                   ************************************************************

CERK1^WT pENTR4  CTTGGCGGAACTAAAAGTCTTAACGCGTGTACATCATGTCAACCTGGTTCGCCTGATTGG  425
TAIR CERK1^WT CDS  CTTGGCGGAACTAAAAGTCTTAACGCGTGTACATCATGTCAACCTGGTTCGCCTGATTGG  1136
                   ************************************************************

CERK1^WT pENTR4  ATATTGTGTTGAGGGATCACTTTTCTTGGTGTATGAATATGTTGAGAATGGTAACCTTGG  485
TAIR CERK1^WT CDS  ATATTGTGTTGAGGGATCACTTTTCTTGGTGTATGAATATGTTGAGAATGGTAACCTTGG  1196
                   ************************************************************

CERK1^WT pENTR4  ACAACATTTACATGGGTCAGGACGAGAACCATTACCGTGGACTAAGAGAGTGCAGATTGC  545
TAIR CERK1^WT CDS  ACAACATTTACATGGGTCAGGACGAGAACCATTACCGTGGACTAAGAGAGTGCAGATTGC  1256
                   ************************************************************

CERK1^WT pENTR4  ACTAGACTCAGCTAGAGGTTTAGAATATATCCACGAGCACACGGTTCCAGTTTATGTCCA  605
TAIR CERK1^WT CDS  ACTAGACTCAGCTAGAGGTTTAGAATATATCCACGAGCACACGGTTCCAGTTTATGTCCA  1316
                   ************************************************************

CERK1^WT pENTR4  TAGGGACATTAAATCTGCCAATATTTTGATAGACCAGAAAATTCCGAGCAAAGGTAGCAGA  665
TAIR CERK1^WT CDS  TAGGGACATTAAATCTGCCAATATTTTGATAGACCAGAAAATTCCGAGCAAAGGTAGCAGA  1376
                   ************************************************************

CERK1^WT pENTR4  TTTCGGGTTAACAAAACTGACAGAAGTTGGAGGTTCAGCAACTCGGGGTGCAATGGGTAC  725
TAIR CERK1^WT CDS  TTTCGGGTTAACAAAACTGACAGAAGTTGGAGGTTCAGCAACTCGGGGTGCAATGGGTAC  1436
                   ************************************************************

CERK1^WT pENTR4  ATTTGGTTACATGGCACCAGAGACTGTTTATGGAGAAGTGTCTGCAAAAGTAGATGTATA  785
TAIR CERK1^WT CDS  ATTTGGTTACATGGCACCAGAGACTGTTTATGGAGAAGTGTCTGCAAAAGTAGATGTATA  1496
                   ************************************************************

CERK1^WT pENTR4  TGCATTTGGAGTTGTCCTTTACGAATTGATTTCTGCGAAAGGTGCGGTTGTCAAAATGAC  845
TAIR CERK1^WT CDS  TGCATTTGGAGTTGTCCTTTACGAATTGATTTCTGCGAAAGGTGCGGTTGTCAAAATGAC  1556
                   ************************************************************

CERK1^WT pENTR4  AGAAGCCGTTGGTGAATTTAGAGGCCTTGTTGGTGTGTTCGAAGAATCATTCAAGGAAAC  905
TAIR CERK1^WT CDS  AGAAGCCGTTGGTGAATTTAGAGGCCTTGTTGGTGTGTTCGAAGAATCATTCAAGGAAAC  1616
                   ************************************************************

CERK1^WT pENTR4  CGACAAAGAAGAAGCACTACGCAAGATTATAGACCCGAGGCTCGGTGATAGTTACCCGTT  965
TAIR CERK1^WT CDS  CGACAAAGAAGAAGCACTACGCAAGATTATAGACCCGAGGCTCGGTGATAGTTACCCGTT  1676
                   ************************************************************

CERK1^WT pENTR4  TGATTCGGTATACAAGATGGCGGAATTAGGGAAAGCATGTACACAAGAGAATGCGCAGCT  1025
TAIR CERK1^WT CDS  TGATTCGGTATACAAGATGGCGGAATTAGGGAAAGCATGTACACAAGAGAATGCGCAGCT  1736
                   ************************************************************

CERK1^WT pENTR4  ACGTCCGAGTATGAGCCACATTGTGGTTGCNTTATCNNNNNNNNNNNNNNNTCTNCCGNNAA  1085
TAIR CERK1^WT CDS  ACGTCCGAGTATGAGATACATTGTGGTTGCTTTATCCACTCTCTTTTCGTCTACCGGAAA  1796
                   **************.******* *************.*****            *** *** **
```

Figure 8.1. Sequencing data of *CERK1^WT* pENTR4 aligned with CERK1 CDS from TAIR online database. **(A)** sequencing alignment of first half of CDS using AttB1 sequencing primers. **(B)** Sequence alignment of second half of CDS using AttB2 sequencing primers. Yellow highlighted regions indicate where sequences overlap. Figures generated by author using Clustal Omega multiple sequence alignment tool.

A　　　　AttB1 Primers

```
LYK5^WT pENTR4    NNCNCTTTNGGATGCTGAGGTTTTTAGCAAGATGGTACCGAATGGCTGCGTGTACACTTC    60
TAIR LYK5^WT CDS  ----------------------------------------ATGGCTGCGTGTACAC--T    17
                                                          ***************
```

```
LYK5^WT pENTR4    CACGCGCTCTCAGNTCACCTTATTCCTCCTTCTCTTCTTTGCCGTGTCACCGGCGAAAGC   120
TAIR LYK5^WT CDS  CCACGCGCTCTCAGTCACCTTATTCCTCCTTCTCTTCTTTGCCGTGTCACCGGCGAAAGC    77
                  *            **************************************************
```

```
LYK5^WT pENTR4    TCAGCAACCGTACGTCAACAACCACCAGCTCGCCTGCGAGGTCCGTGTCTACGACAACAT   180
TAIR LYK5^WT CDS  TCAGCAACCGTACGTCAACAACCACCAGCTCGCCTGCGAGGTCCGTGTCTACGACAACAT   137
                  ************************************************************
```

```
LYK5^WT pENTR4    AACCAACGGATTCACATGTAACGGCCCACCTTCTTGCCGCTCATACCTCACTTTCTGGTC   240
TAIR LYK5^WT CDS  AACCAACGGATTCACATGTAACGGCCCACCTTCTTGCCGCTCATACCTCACTTTCTGGTC   197
                  ************************************************************
```

```
LYK5^WT pENTR4    TCAACCACCGTACAACACGGCGGACTCAATCGCCAAACTCCTCAACGTCTCCGCCGCAGA   300
TAIR LYK5^WT CDS  TCAACCACCGTACAACACGGCGGACTCAATCGCCAAACTCCTCAACGTCTCCGCCGCAGA   257
                  ************************************************************
```

```
LYK5^WT pENTR4    GATCCAATCAATCAACAACCTCCCCACAGCCACCACCAGAATCCCAACCCGTGAATTAGT   360
TAIR LYK5^WT CDS  GATCCAATCAATCAACAACCTCCCCACAGCCACCACCAGAATCCCAACCCGTGAATTAGT   317
                  ************************************************************
```

```
LYK5^WT pENTR4    CGTGATCCCAGCTAACTGCTCCTGCTCCTCCTCCAGCGGAGGATTTTACCAACACAACGC   420
TAIR LYK5^WT CDS  CGTGATCCCAGCTAACTGCTCCTGCTCCTCCTCCAGCGGAGGATTTTACCAACACAACGC   377
                  ************************************************************
```

```
LYK5^WT pENTR4    CACTTACAATCTCTCCGGTAACAGAGGAGATGAAACCTATTTCTCAGTGGCTAACGATAC   480
TAIR LYK5^WT CDS  CACTTACAATCTCTCCGGTAACAGAGGAGATGAAACCTATTTCTCAGTGGCTAACGATAC   437
                  ************************************************************
```

```
LYK5^WT pENTR4    TTACCAAGCTTTATCCACGTGTCAAGCCATGATGTCACAAAACCGTTACGGCGAGAGACA   540
TAIR LYK5^WT CDS  TTACCAAGCTTTATCCACGTGTCAAGCCATGATGTCACAAAACCGTTACGGCGAGAGACA   497
                  ************************************************************
```

```
LYK5^WT pENTR4    ACTAACCCCCGGCTTAAACCTCCTTGTTCCTCTCCGATGTGCTTGTCCCACCGCCAAACA   600
TAIR LYK5^WT CDS  ACTAACCCCCGGCTTAAACCTCCTTGTTCCTCTCCGATGTGCTTGTCCCACCGCCAAACA   557
                  ************************************************************
```

```
LYK5^WT pENTR4    AACCACCGCCGGGATTTAAATATCTCCTGACTTACTTAGTCGCCATGGGAGATAGTATCTC   660
TAIR LYK5^WT CDS  AACCACCGCCGGGATTTAAATATCTCCTGACTTACTTAGTCGCCATGGGAGATAGTATCTC   617
                  ************************************************************
```

```
LYK5^WT pENTR4    CGGCATCGCCGAGATGTTCAACAGCACATCCGCCGCCATAACCGAAGGTAACGAGCTTAC   720
TAIR LYK5^WT CDS  CGGCATCGCCGAGATGTTCAACAGCACATCCGCCGCCATAACCGAAGGTAACGAGCTTAC   677
                  ************************************************************
```

```
LYK5^WT pENTR4    ATCAGACAATATCTTCTTCTTCACACCGGTTCTAGTTCCTCTCACAACTGAACCTACCAA   780
TAIR LYK5^WT CDS  ATCAGACAATATCTTCTTCTTCACACCGGTTCTAGTTCCTCTCACAACTGAACCTACCAA   737
                  ************************************************************
```

```
LYK5^WT pENTR4    AATCGTTATATCTCCGTCGCCTCCTCCTCCACCCGTTGTTGCTACGCCGCCTCAAACGCC   840
TAIR LYK5^WT CDS  AATCGTTATATCTCCGTCGCCTCCTCCTCCACCCGTTGTTGCTACGCCGCCTCAAACGCC   797
                  ************************************************************
```

```
LYK5^WT pENTR4    AGTTGATCCTCCGGGATCTTCTTCTTCTCACAAATGGATCTACATCGGAATTGGNAATCG   900
TAIR LYK5^WT CDS  AGTTGATCCTCCGGGATCTTCTTCTTCTCACAAATGGATCTACATCGGAATTGG-AATCG   856
                  ****************************************************** *****
```

```
LYK5^WT pENTR4    GAGCTGGNTTGCTTCTCTTACTCTCAATCTTAGCTCTCTGCTTCTACAAACGAAGGTCTA   960
TAIR LYK5^WT CDS  GAGCTGGTTTGCTTCTCTTACTCTCAATCTTAGCTCTCTGCTTCTACAAACGAAGGTCTA   916
                  ******* ****************************************************
```

```
LYK5^WT pENTR4    AGAAGAAGTCATTACCGTCGTCGTTGCCGGAGGANAACAAGCTCTTTGATTCATCAACCA  1020
TAIR LYK5^WT CDS  AGAAGAAGTCATTACCGTCGTCGTTGCCGGAGGAGAACAAGCTCTTTGATTCATCAACCA   976
                  ********************************** ********* ****************
```

B   AttB2 Primers

LYK5^WT pENTR4   TTTGATTCATCANCCAAACCATTCTTTNCCCCCAACAACAACGACTCAATGGTCCATAGA   124
TAIR LYK5^WT CDS TTTGATTCATCAACCAAACAAT-CTATTCCCACAACAACAACGACTCAATGGTCAATAGA   1019
                  ***********.*****.**.**.*.****.***********************.*****

LYK5^WT pENTR4   TTTATCCAATTCATCAGAAGCTTTCGGTTTAAAATCCCCCCATAGAATCTCTAACACTAT   184
TAIR LYK5^WT CDS TTTATCCAATTCATCAGAAGCTTTCGGTTTAAAATCC-GCCATAGAATCTCTAACACTAT   1078
                  ************************************* *********************

LYK5^WT pENTR4   ACAGATTCAACGATCTTTCAATCAGCTACTTCGAATTTCAGCGACGAAAACAGAATCAAA   244
TAIR LYK5^WT CDS ACAGATTCAACGATC-TTCAATCAGCTACTTCGAATTTCAGCGACGAAAACAGAATCAAA   1137
                  ***************.***

LYK5^WT pENTR4   GGCTCTGTTTATCGCGCGACAATCAACGGCGACGATGCCGCTGTGAAAGTGATCAAAGGA   304
TAIR LYK5^WT CDS GGCTCTGTTTATCGCGCGACAATCAACGGCGACGATGCCGCTGTGAAAGTGATCAAAGGA   1197
                  ****

LYK5^WT pENTR4   GATGTTTCTTCCTCTGAGATCAATCTTTTGAAGAAGCTAAATCATTCTAATATCATCCGT   364
TAIR LYK5^WT CDS GATGTTTCTTCCTCTGAGATCAATCTTTTGAAGAAGCTAAATCATTCTAATATCATCCGT   1257
                  ****

LYK5^WT pENTR4   CTCTCAGGTTTCTGTATCCGTGAAGGAACATCGTACCTCGTCTTCGAGTATTCAGAGAAT   424
TAIR LYK5^WT CDS CTCTCAGGTTTCTGTATCCGTGAAGGAACATCGTACCTCGTCTTCGAGTATTCAGAGAAT   1317
                  ****

LYK5^WT pENTR4   GGATCGATCAGTGATTGGCTTCACTCGTCGGGCAAGAAGAGTTTGACATGGAAACAGAGA   484
TAIR LYK5^WT CDS GGATCGATCAGTGATTGGCTTCACTCGTCGGGCAAGAAGAGTTTGACATGGAAACAGAGA   1377
                  ****

LYK5^WT pENTR4   GTTGAAATAGCAAGGGATGTGGCAGAGGCGTTAGATTATCTCCATAACTATATAACTCCA   544
TAIR LYK5^WT CDS GTTGAAATAGCAAGGGATGTGGCAGAGGCGTTAGATTATCTCCATAACTATATAACTCCA   1437
                  ****

LYK5^WT pENTR4   CCTCATATTCATAAGAACTTGGAATCAACAAACATACTTCTGGATTCTAATTTCAGAGCC   604
TAIR LYK5^WT CDS CCTCATATTCATAAGAACTTGGAATCAACAAACATACTTCTGGATTCTAATTTCAGAGCC   1497
                  ****

LYK5^WT pENTR4   AAGATTGCGAATTTCGGTGTTGCGAGGATTCTTGATGAAGGTGATCTTGATCTTCAGTTA   664
TAIR LYK5^WT CDS AAGATTGCGAATTTCGGTGTTGCGAGGATTCTTGATGAAGGTGATCTTGATCTTCAGTTA   1557
                  ****

LYK5^WT pENTR4   ACAAGACATGTTGAAGGAACACAAGGCTACTTAGCTCCAGAGTATGTGGAGAATGGAGTC   724
TAIR LYK5^WT CDS ACAAGACATGTTGAAGGAACACAAGGCTACTTAGCTCCAGAGTATGTGGAGAATGGAGTC   1617
                  ****

LYK5^WT pENTR4   ATTACTTCGAAACTAGACGTGTTTGCTTTTGGAGTTGCGGTTCTTGAGCTTCTTTCGGGG   784
TAIR LYK5^WT CDS ATTACTTCGAAACTAGACGTGTTTGCTTTTGGAGTTGCGGTTCTTGAGCTTCTTTCGGGG   1677
                  ****

LYK5^WT pENTR4   AGAGAAGCAGTAACGATACATAAGAAGAAGGAAGGAGAAGAAGAAGTGGAGATGTTGTGT   844
TAIR LYK5^WT CDS AGAGAAGCAGTAACGATACATAAGAAGAAGGAAGGAGAAGAAGAAGTGGAGATGTTGTGT   1737
                  ****

LYK5^WT pENTR4   AAAGTGATAAACAGTGTGCTTGGAGGAGAGAATGTGAGAGAGAAGTTAAAAGAGTTTATG   904
TAIR LYK5^WT CDS AAAGTGATAAACAGTGTGCTTGGAGGAGAGAATGTGAGAGAGAAGTTAAAAGAGTTTATG   1797
                  ****

LYK5^WT pENTR4   GATCCATCTCTAGGGAATGAGTATCCGTTGGAGCTGGCTTACACCATGGCTCAGCTTGCT   964
TAIR LYK5^WT CDS GATCCATCTCTAGGGAATGAGTATCCGTTGGAGCTGGCTTACACCATGGCTCAGCTTGCT   1857
                  ****

LYK5^WT pENTR4   AAGAGCTGTGTCGCAACTGATCTTAACTCGCGTCCATCTGTCACTCAGGTTCTAACCACG   1024
TAIR LYK5^WT CDS AAGAGCTGTGTCGCAACTGATCTTAACTCGCGTCCATCTGTCACTCAGGTTCTAACCACG   1917
                  ****

LYK5^WT pENTR4   CTCTCAATGATCGTCTCCTCCTCCATCGATTGGGAGCCTTCTGATGACCTTCTTCGTTCC   1084
TAIR LYK5^WT CDS CTCTCAATGATCGTCTCCTCCTCCATCGATTGGGAGCCTTCTGATGACCTTCTTCGTTCC   1977
                  ****

LYK5^WT pENTR4   GGCTCTCTTGGCAACCACTCGAGATCTTCNGAAGTTCCNCATTCG   1129
TAIR LYK5^WT CDS GGCTCTCTTGGCAAC------------------------------ 1992
                  ****

Figure 8.2. Sequencing data of *LYK5^WT* pENTR4 aligned with *LYK5* CDS from TAIR online database. **(A)** sequencing alignment of first half of CDS using AttB1 sequencing primers. **(B)** Sequence alignment of second half of CDS using AttB2 sequencing primers. Yellow highlighted regions indicate where sequences overlap. Figures generated by author using Clustal Omega multiple sequence alignment tool.

A   AttB1 Primers

```
PBL27^WT pENTR4    TCGGAGGCTCGNGTTTTTCAGCNAGATCCATGGGAATGAGTGGGTGTTTGCCTTGTTTTG    60
TAIR PBL27^WT CDS  ------------------------------------ATGAGTGGGTGTTTGCCTTGTTTTG    25
                                                       **************************

PBL27^WT pENTR4    GATCTTCGGCTAAAGACGCTGCTTCTAAAGATTCGGTGAAGAAGGAACTTTCAGCTAAAG   120
TAIR PBL27^WT CDS  GATCTTCGGCTAAAGACGCTGCTTCTAAAGATTCGGTGAAGAAGGAACTTTCAGCTAAAG    85
                   ************************************************************

PBL27^WT pENTR4    ACGGCTCAGTTACTCAGTCTCACCATATCAGCTTAGATAAATCAAAGTCTCGACGAGGTC   180
TAIR PBL27^WT CDS  ACGGCTCAGTTACTCAGTCTCACCATATCAGCTTAGATAAATCAAAGTCTCGACGAGGTC   145
                   ************************************************************

PBL27^WT pENTR4    CTGAACAGAAGAAGGAGCTAACTGCTCCAAAAGAAGGGCCTACTGCGCATATTGCTGCAC   240
TAIR PBL27^WT CDS  CTGAACAGAAGAAGGAGCTAACTGCTCCAAAAGAAGGGCCTACTGCGCATATTGCTGCAC   205
                   ************************************************************

PBL27^WT pENTR4    AAACCTTTACTTTCCGAGAGTTAGCTGCCGCCACTAAAAACTTTCGACCGGAATGTCTTC   300
TAIR PBL27^WT CDS  AAACCTTTACTTTCCGAGAGTTAGCTGCCGCCACTAAAAACTTTCGACCGGAATGTCTTC   265
                   ************************************************************

PBL27^WT pENTR4    TTGGAGAAGGAGGTTTCGGACGTGTTTACAAAGGTCGTCTAGAGACCACAGGACAGATAG   360
TAIR PBL27^WT CDS  TTGGAGAAGGAGGTTTCGGACGTGTTTACAAAGGTCGTCTAGAGACCACAGGACAGATAG   325
                   ************************************************************

PBL27^WT pENTR4    TAGCTGTTAAACAGCTTGATCGAAACGGTCTACAAGGAAACAGAGAGTTTCTTGTAGAGG   420
TAIR PBL27^WT CDS  TAGCTGTTAAACAGCTTGATCGAAACGGTCTACAAGGAAACAGAGAGTTTCTTGTAGAGG   385
                   ************************************************************

PBL27^WT pENTR4    TTCTTATGCTGAGCCTTCTGCATCATCCCAATCTTGTGAATTTGATTGGTTATTGTGCTG   480
TAIR PBL27^WT CDS  TTCTTATGCTGAGCCTTCTGCATCATCCCAATCTTGTGAATTTGATTGGTTATTGTGCTG   445
                   ************************************************************

PBL27^WT pENTR4    ATGGGGACCAGCGTCTTCTTGTGTATGAGTATATGCCACTAGGATCATTGGAGGATCATC   540
TAIR PBL27^WT CDS  ATGGGGACCAGCGTCTTCTTGTGTATGAGTATATGCCACTAGGATCATTGGAGGATCATC   505
                   ************************************************************

PBL27^WT pENTR4    TACACGATCTTCCACCTGATAAAGAGCCTCTAGACTGGAGTACTAGAATGACAATAGCGG   600
TAIR PBL27^WT CDS  TACACGATCTTCCACCTGATAAAGAGCCTCTAGACTGGAGTACTAGAATGACAATAGCGG   565
                   ************************************************************

PBL27^WT pENTR4    CAGGAGCAGCAAAGGGACTGGAGTATCTGCATGATAAAGCGAATCCGCCTGTGATCTACA   660
TAIR PBL27^WT CDS  CAGGAGCAGCAAAGGGACTGGAGTATCTGCATGATAAAGCGAATCCGCCTGTGATCTACA   625
                   ************************************************************

PBL27^WT pENTR4    GAGACCTGAAATCATCCAACATTCTTCTCGGTGATGGCTATCACCCAAAGTTATCTGATT   720
TAIR PBL27^WT CDS  GAGACCTGAAATCATCCAACATTCTTCTCGGTGATGGCTATCACCCAAAGTTATCTGATT   685
                   ************************************************************

PBL27^WT pENTR4    TTGGGTTAGCTAAGTTAGGTCCCGTGGGCGATAAAACACATGTGTCAACTCGTGTGATGG   780
TAIR PBL27^WT CDS  TTGGGTTAGCTAAGTTAGGTCCCGTGGGCGATAAAACACATGTGTCAACTCGTGTGATGG   745
                   ************************************************************

PBL27^WT pENTR4    GCACATATGGTTATTGTGCACCGGAATATGCCATGACAGGGCAACTCACATTGAAATCCG   840
TAIR PBL27^WT CDS  GCACATATGGTTATTGTGCACCGGAATATGCCATGACAGGGCAACTCACATTGAAATCCG   805
                   ************************************************************

PBL27^WT pENTR4    ATGTTTATAGCTTTGGGGGTTGTGTTTCTCGAGCTCATCACGGGTCGAAAAGCTATTGATA   900
TAIR PBL27^WT CDS  ATGTTTATAGCTTTGGGGGTTGTGTTTCTCGAGCTCATCACGGGTCGAAAAGCTATTGATA   865
                   *********************************************************
```

109

Figure 8.3. Sequencing data of *PBL27^WT* pENTR4 aligned with *PBL27* CDS from TAIR online database. **(A)** sequencing alignment of first half of CDS using AttB1 sequencing primers. **(B)** Sequence alignment of second half of CDS using AttB2 sequencing primers. Yellow highlighted regions indicate where sequences overlap. Figures generated by author using Clustal Omega multiple sequence alignment tool.

9.0. References

Araújo, A. E., L. A. Maffia, E. S. G. Mizubuti, A. C. Alfenas, G. de Capdeville, and J. A. S. Grossi. 2005. Survival of Botrytis cinerea as mycelium in rose crop debris and as sclerotia in soil. Fitopatol. Bras. 30:516–521.

Bi, G., Z. Zhou, W. Wang, L. Li, S. Rao, Y. Wu, X. Zhang, F. L. H. Menke, S. Chen, and J. M. Zhou. 2018. Receptor-like cytoplasmic kinases directly link diverse pattern recognition receptors to the activation of mitogen-activated protein kinase cascades in arabidopsis. Plant Cell 30:1543–1561.

Bi, K., Y. Liang, T. Mengiste, and A. Sharon. 2022. Killing softly: a roadmap of Botrytis cinerea pathogenicity. Trends Plant Sci. 28:211–222.

Cao, Y., Y. Liang, K. Tanaka, C. T. Nguyen, R. P. Jedrzejczak, A. Joachimiak, and G. Stacey. 2014. The kinase LYK5 is a major chitin receptor in Arabidopsis and forms a chitin-induced complex with related kinase CERK1. Elife 3:1–19.

Castaño-Miquel, L., A. Mas, I. Teixeira, J. Seguí, A. Perearnau, B. N. Thampi, A. L. Schapire, N. Rodrigo, G. La Verde, S. Manrique, M. Coca, and L. M. Lois. 2017. SUMOylation Inhibition Mediated by Disruption of SUMO E1-E2 Interactions Confers Plant Susceptibility to Necrotrophic Fungal Pathogens. Mol. Plant 10:709–720.

Castaño-Miquel, L., J. Seguí, S. Manrique, I. Teixeira, L. Carretero-Paulet, F. Atencio, and L. M. Lois. 2013. Diversification of SUMO-Activating Enzyme in Arabidopsis: Implications in SUMO Conjugation. Mol. Plant 6:1646–1660.

Cheung, N., L. Tian, X. Liu, and X. Li. 2020. The destructive fungal pathogen Botrytis cinerea—

insights from genes studied with mutant analysis. Pathogens 9:1–46.

Crabill, E., A. Joe, A. Block, J. M. van Rooyen, and J. R. Alfano. 2010. Plant immunity directly or

indirectly restricts the injection of type III effectors by the Pseudomonas syringae type III

secretion system. Plant Physiol. 154:233–244.

Desaki, Y., K. Miyata, M. Suzuki, N. Shibuya, and H. Kaku. 2018. Plant immunity and symbiosis

signaling mediated by LysM receptors. Innate Immun. 24:92–100.

Erwig, J., H. Ghareeb, M. Kopischke, R. Hacke, A. Matei, E. Petutschnig, and V. Lipka. 2017.

Chitin-induced and CHITIN ELICITOR RECEPTOR KINASE1 (CERK1) phosphorylation-

dependent endocytosis of Arabidopsis thaliana LYSIN MOTIF-CONTAINING RECEPTOR-LIKE

KINASE5 (LYK5). New Phytol. 215:382–396. Blackwell Publishing Ltd.

Fausto, A., M. L. Rodrigues, and C. Coelho. 2019. The still underestimated problem of fungal

diseases worldwide. Front. Microbiol. 10:1–5.

Fisher, M. C., D. A. Henk, C. J. Briggs, J. S. Brownstein, L. C. Madoff, S. L. McCraw, and S. J. Gurr.

2012. Emerging fungal threats to animal, plant and ecosystem health. Nature 484:186–

194. Nature Publishing Group.

Fones, H. N., D. P. Bebber, T. M. Chaloner, W. T. Kay, G. Steinberg, and S. J. Gurr. 2020. Threats

to global food security from emerging fungal and oomycete crop pathogens. Nat. Food

1:332–342. Springer US.

Fraire-Velázquez, S., and E. Lozoya-Gloria. 2003. Differential early gene expression in Phaseolus

vulgaris to Mexican isolates of Colletotrichum lindemuthianum in incompatible and

compatible interactions. Physiol. Mol. Plant Pathol. 63:79–89.

Giovannoni, M., D. Lironi, L. Marti, C. Paparella, V. Vecchi, A. A. Gust, G. De Lorenzo, T. Nürnberger, and S. Ferrari. 2021. The Arabidopsis thaliana LysM-containing Receptor-Like Kinase 2 is required for elicitor-induced resistance to pathogens. Plant. Cell Environ. 44:3775–3792.

Jensen, P. H., and D. Weilguny. 2005. Combination primer polymerase chain reaction for multi-site mutagenesis of close proximity sites. J. Biomol. Tech. 16:336–40.

Jones, J. D. G., and J. L. Dangl. 2006. The plant immune system. Nature 444:323–329.

Launay, M., J. Caubel, G. Bourgeois, F. Huard, I. Garcia de Cortazar-Atauri, M. O. Bancal, and N. Brisson. 2014. Climatic indicators for crop infection risk: Application to climate change impacts on five major foliar fungal diseases in Northern France. Agric. Ecosyst. Environ. 197:147–158. Elsevier B.V.

Lewis, J. 1997. The protein protocols handbook. Biochem. Educ. 25:55–56.

Li, S., R. Ji, R. Dudler, M. Yong, Q. Deng, Z. Wang, and D. Hu. 2013. Wheat gene TaS3 contributes to powdery mildew susceptibility. Plant Cell Rep. 32:1891–1901.

Li, S., M. Lin, J. Wang, L. Zhang, M. Lin, Z. Hu, Z. Qi, H. Jiang, Y. Fu, D. Xin, C. Liu, and Q. Chen. 2019. Regulation of soybean SUMOylation system in response to Phytophthora sojae infection and heat shock. Plant Growth Regul. 87:69–82. Springer Netherlands.

Liu, H., and J. H. Naismith. 2008. An efficient one-step site-directed deletion, insertion, single and multiple-site plasmid mutagenesis protocol. BMC Biotechnol. 8:91.

Liu, J., B. Liu, S. Chen, B. Q. Gong, L. Chen, Q. Zhou, F. Xiong, M. Wang, D. Feng, J. F. Li, H. Bin Wang, and J. Wang. 2018. A Tyrosine Phosphorylation Cycle Regulates Fungal Activation of a Plant Receptor Ser/Thr Kinase. Cell Host Microbe 23:241-253.e6. Elsevier Inc.

McNICOL, R. J., B. WILLIAMSON, and A. DOLAN. 1985. Infection of red raspberry styles and

carpels by Botrytis cinerea and its possible role in post-harvest grey mould. Ann. Appl. Biol.

106:49–53.

Mikaelian, I., and A. Sergeant. 1992. A general and fast method to generate multiple site

directed mutations. Nucleic Acids Res. 20:376–376.

Miya, A., P. Albert, T. Shinya, Y. Desaki, K. Ichimura, K. Shirasu, Y. Narusaka, N. Kawakami, H.

Kaku, and N. Shibuya. 2007. CERK1, a LysM receptor kinase, is essential for chitin elicitor

signaling in Arabidopsis. Proc. Natl. Acad. Sci. U. S. A. 104:19613–19618.

Morrell, R., and A. Sadanandom. 2019. Dealing With Stress: A Review of Plant SUMO Proteases.

Front. Plant Sci. 10:1–19.

Neri, F., L. Cappellin, A. Spadoni, I. Cameldi, A. Algarra Alarcon, E. Aprea, A. Romano, F. Gasperi,

and F. Biasioli. 2015. Role of strawberry volatile organic compounds in the development of

Botrytis cinerea infection. Plant Pathol. 64:709–717.

Orosa, B., G. Yates, V. Verma, A. K. Srivastava, M. Srivastava, A. Campanaro, D. De Vega, A.

Fernandes, C. Zhang, J. Lee, M. J. Bennett, and A. Sadanandom. 2018. SUMO conjugation

to the pattern recognition receptor FLS2 triggers intracellular signalling in plant innate

immunity. Nat. Commun. 9:1–12. Springer US.

Petutschnig, E. K., A. M. E. Jones, L. Serazetdinova, U. Lipka, and V. Lipka. 2010. The Lysin Motif

Receptor-like Kinase (LysM-RLK) CERK1 Is a Major Chitin-binding Protein in Arabidopsis

thaliana and Subject to Chitin-induced Phosphorylation. J. Biol. Chem. 285:28902–28911.

Petutschnig, E. K., M. Stolze, U. Lipka, M. Kopischke, J. Horlacher, O. Valerius, W. Rozhon, A. A.

Gust, B. Kemmerling, B. Poppenberger, G. H. Braus, T. Nürnberger, and V. Lipka. 2014. A

novel Arabidopsis CHITIN ELICITOR RECEPTOR KINASE 1 (CERK1) mutant with enhanced pathogen-induced cell death and altered receptor processing. New Phytol. 204:955–967.

Rytz, T. C., M. J. Miller, F. McLoughlin, R. C. Augustine, R. S. Marshall, Y. Juan, Y. Charng, M. Scalf, L. M. Smith, and R. D. Vierstra. 2018. SUMOylome Profiling Reveals a Diverse Array of Nuclear Targets Modified by the SUMO Ligase SIZ1 during Heat Stress. Plant Cell 30:1077– 1099.

Sarven, M. S., Q. Hao, J. Deng, F. Yang, G. Wang, Y. Xiao, and X. Xiao. 2020. Biological Control of Tomato Gray Mold Caused by Botrytis Cinerea with the Entomopathogenic Fungus Metarhizium Anisopliae. Pathogens 9:213.

Shah, P., A. L. T. Powell, R. Orlando, C. Bergmann, and G. Gutierrez-Sanchez. 2012. Proteomic analysis of ripening tomato fruit infected by botrytis cinerea. J. Proteome Res. 11:2178– 2192.

Shao, D., D. L. Smith, M. Kabbage, and M. G. Roth. 2021. Effectors of Plant Necrotrophic Fungi. Front. Plant Sci. 12:1–14.

Sharma, M., D. Fuertes, J. Perez-Gil, and L. M. Lois. 2021. SUMOylation in Phytopathogen Interactions: Balancing Invasion and Resistance. Front. Cell Dev. Biol. 9.

Shinya, T., K. Yamaguchi, Y. Desaki, K. Yamada, T. Narisawa, Y. Kobayashi, K. Maeda, M. Suzuki, T. Tanimoto, J. Takeda, M. Nakashima, R. Funama, M. Narusaka, Y. Narusaka, H. Kaku, T. Kawasaki, and N. Shibuya. 2014. Selective regulation of the chitin-induced defense response by the Arabidopsis receptor-like cytoplasmic kinase PBL27. Plant J. 79:56–66.

Stocks, J. J., C. L. Metheringham, W. J. Plumb, S. J. Lee, L. J. Kelly, R. A. Nichols, and R. J. A. Buggs. 2019. Genomic basis of European ash tree resistance to ash dieback fungus. Nat.

Ecol. Evol. 3:1686–1696. Springer US.

Wan, J., X.-C. Zhang, D. Neece, K. M. Ramonell, S. Clough, S. Kim, M. G. Stacey, and G. Stacey. 2008a. A LysM Receptor-Like Kinase Plays a Critical Role in Chitin Signaling and Fungal Resistance in Arabidopsis. Plant Cell 20:471–481.

Wan, J., X. C. Zhang, and G. Stacey. 2008b. Chitin signaling and plant disease resistance. Plant Signal. Behav. 3:831–833.

Wang, Y., X. Li, B. Fan, C. Zhu, and Z. Chen. 2021. Regulation and Function of Defense-Related Callose Deposition in Plants. Int. J. Mol. Sci. 22:2393.

WILLIAMSON, B., B. TUDZYNSKI, P. TUDZYNSKI, and J. A. L. VAN KAN. 2007. Botrytis cinerea: the cause of grey mould disease. Mol. Plant Pathol. 8:561–580.

Xiao, C. L. 2006. Postharvest Fruit Rots in d'Anjou Pears Caused by Botrytis cinerea, Potebniamyces pyri , and Sphaeropsis pyriputrescens. Plant Heal. Prog. 7.

Yamada, K., K. Yamaguchi, T. Shirakawa, H. Nakagami, A. Mine, K. Ishikawa, M. Fujiwara, M. Narusaka, Y. Narusaka, K. Ichimura, Y. Kobayashi, H. Matsui, Y. Nomura, M. Nomoto, Y. Tada, Y. Fukao, T. Fukamizo, K. Tsuda, K. Shirasu, N. Shibuya, and T. Kawasaki. 2016. The Arabidopsis CERK 1-associated kinase PBL 27 connects chitin perception to MAPK activation. EMBO J. 35:2468–2483.

Yamaguchi, K., and T. Kawasaki. 2021. Pathogen- and plant-derived peptides trigger plant immunity. Peptides 144:170611. Elsevier Inc.

Yan, Y., Q. Yuan, J. Tang, J. Huang, T. Hsiang, Y. Wei, and L. Zheng. 2018. Colletotrichum higginsianum as a Model for Understanding Host–Pathogen Interactions: A Review. Int. J. Mol. Sci. 19:2142.

Yates, G. 2018. Identification of a New Class of SUMO Proteases in Plants,and Investigation Into

   The Role of SUMOylation in Pathogen Perception. Doctoral Thesis.

Zeng, F., S. Zhang, Z. Hao, S. Duan, Y. Meng, P. Li, J. Dong, and Y. Lin. 2018. Efficient strategy for

   introducing large and multiple changes in plasmid DNA. Sci. Rep. 8:1714.

Zhang, Y., and L. Zeng. 2020. Crosstalk between Ubiquitination and Other Post-translational

   Protein Modifications in Plant Immunity. Plant Commun. 1:100041. Elsevier Ltd.

2017. Stop neglecting fungi. Nat. Microbiol. 2:17120.